UNIVERSITÀ DEGLI STUDI DI NAPOLI "FEDERICO II"

FACOLTÀ DI INGEGNERIA

Dipartimento di Ingegneria dei Materiali e della Produzione

DOTTORATO DI RICERCA IN

INGEGNERIA DEI MATERIALI E DELLE STRUTTURE

XXIII CICLO

Bioactive composite scaffolds for bone regeneration : from the process to the biological validation

Relatore:
Ch.mo Prof.
Luigi Ambrosio

Tutor:
Prof. Paolo Antonio Netti

Coordinatore:
Prof. Domenico Acierno

Candidato:
Alfredo Ronca

TRIENNIO 2007/2010

		2

Table of Contents

CHAPTER 1

Tissue engineering and Biomaterials

1.1 Introduction

The dream is as old as humankind. Injury, disease, and congenital malformation have always been part of the human experience. If only damaged bodies could be restored, life could go on for loved ones as though tragedy had not intervened. In recorded history, this possibility first was manifested through myth and magic, as in the Greek legend of Prometheus and eternal liver regeneration [1]. With the development of medicine , man started to interfere with the process that occur within the human body as well. The first surgeries took place in ancient Egypt over 4000 years ago, and involved the use of non-viable or 'dead' materials. For example amputated were replaced with wooden toes and linen was used for suturing [2]. Two thousand years later, dental implants made of gold or wrought iron were used by the Romans, Chinese and Aztecs [3]. Nowadays tissue or organ transplantation is a standard therapy to treat these patients, but this is severely limited by donor shortage. Other available therapies including surgical reconstruction, drug therapy, synthetic prostheses, and medical devices are not limited by supply, but they do have other problems. For example, synthetic prostheses and medical devices are not able to replace all the functions of a damaged or lost organ or tissue [4]. The efforts to address these problems and limitations have elicited the development of new biomaterials and alternative therapies. Over the years, various definitions of the term biomaterials have been proposed. For example, a *biomaterial* can be simply defined as a synthetic material used to replace part of a living system or to function in intimate contact with living tissue. The Clemson University Advisory Board for Biomaterials has formally defined a biomaterial to be "*a systemically and pharmacologically inert substance designed for implantation within or incorporation with living systems*" [5]. Black defined biomaterials as "*a nonviable material used in a medical device, intended to interact with biological systems*" [6] Other definitions have included "*materials of synthetic as well as of natural origin in contact with tissue, blood, and biological fluids, and intended for use for prosthetic, diagnostic, therapeutic, and storage applications without adversely affecting the living organism and its components*" and "*any substance (other than drugs) or combination of*

substances, synthetic or natural in origin, which can be used for any period of time, as a whole or as a part of a system which treats, augments, or replaces any tissue, organ, or function of the body" [7]. According to these definitions one must possess knowledge in a number of different disciplines or collaborate with individuals from a wide variety of different specialties in order to properly develop and use biomaterials in medicine. Likewise, advances in materials science, chemical engineering, and bioengineering allow the rational application of engineering principles to living systems.

Tissue engineering has emerged as a promising alternative approach to treat the loss or malfunction of a tissue or organ without the limitations of current therapies [8][9][10][11]. As a field, tissue engineering has been defined only since the mid-1980s and it combines the principles of biology, engineering, and medicine to create biological substitutes for lost or defective native tissues [12].

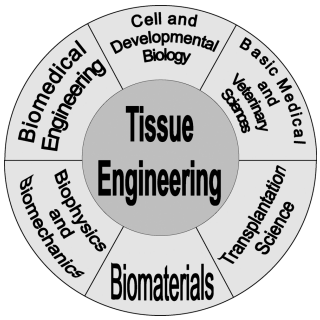

Fig. 1.1: multidisciplinary nature of the tissue engineering field.

The principle of TE is to culture cells into a matrix and incorporate it into the body. The matrices are made of natural materials such as collagen or from synthetic polymers.

The first definition of tissue engineering was provided by Skalak and Fox (1988) who stated it to be "*the application of principles and methods of engineering and life sciences toward the fundamental understanding of structure-function relationships in normal and phatological mammalian tissues and the development of biological substitutes to restore, maintain or improve tissue function"[13]*.

Tissue engineering, through the imitation of nature, has the potential to confront the transplantation crisis caused by the shortage of donor tissues and organs and also to address other important, but yet unmet, patient needs [1]. To engineer living tissues in vitro, cultured cells are coaxed to grow on bioactive degradable scaffolds that provide the physical and chemical cues to guide their differentiation and assembly into three-dimensional (3D) tissues [14].

1.2 Porous scaffold for tissue engineering

The scaffold or three-dimensional (3-D) construct provides the necessary support for cells to proliferate and maintain their differentiated function, and its architecture defines the ultimate shape of the new bone and cartilage [15]. The strategy for Tissue Engineering is divided in six steps (Figure 1). In the first step, cells need to be extracted from the patient. Then, it is necessary to isolate the desired cell type from the crude cell extract. The isolation is essential because this is a selection of cells we want to use and grow for our TE application. In many cases, the population of the desired cells is very low, thus it is essential to growth and expand the population of these cells *in vitro*. This step is very important when working with stem cells because the stem cells need to be maintained in their pluripotent state while their population is increased. Once we have sufficient number of cells, they are implanted in a matrix, called scaffold. The scaffold offers a suitable environment to permit cells to stick, growth, and develop in the right direction. This proliferation is now controlled and catalyzed by the scaffold design and coating. Finally, the scaffold with its inner and outer cells is ready to be implanted into the patient by the surgeon[16].

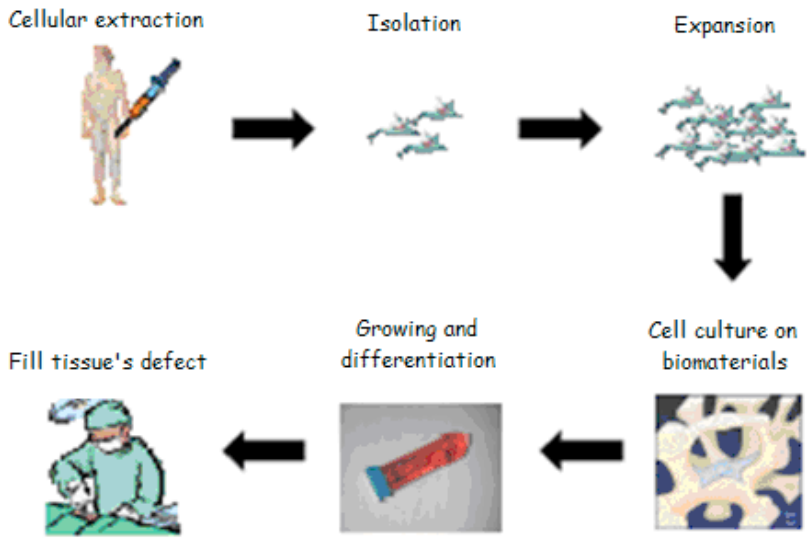

Fig. 1.2: Principle of scaffold-based tissue engineering.

Architectural features , namely pore size and shape, pore wall morphology, porosity, surface area and pore interconnectivity, are probably the most critical parameters as those have been shown to directly impact cell seeding, cell migration tissue

differentiation, transport of oxygen, nutrients and wastes and new tissue formation in three dimensions[17][18]. Approaches in scaffold design must be able to create hierarchical porous structures to attain desired mechanical function and mass transport (that is, permeability and diffusion) properties, and to produce these structures within arbitrary and complex three dimensional (3D) anatomical shapes. Hierarchical refers to the fact that features at scales from the nanometre to millimetre level will determine how well the scaffold meets conflicting mechanical function and mass-transport need. The scaffolds also provide temporary mechanical support to the regenerating tissue. They must degrade into biocompatible products, ideally on a time scale comparable to that of new tissue development. Such scaffolds are typically fabricated with biocompatible polymers, proteins, peptides, and inorganic materials. Today, four types of material have been experimentally and clinically studied as scaffold material: (A) synthetic organic materials; (B) synthetic inorganic materials: hydroxyapatite, tricalciumphosphate; (C) organic materials of natural origin: collagen, hyaluronic acid; (D) inorganic material of natural origin: coralline hydroxyapatite [19]; the intrinsic material properties, such as the mechanical or thermal behaviour of a polymer play a role in the utilization of tissue engineering and also in the embodiment and the morphology of the shaped scaffold body [20]. The scaffold should be fabricated from a highly biocompatible material, which does not have the potential to elicit an immunological, or clinically detectable primary or secondary foreign body reaction. Furthermore, a polymer scaffold material has to be chosen that will degrade and resorb at a controlled rate [21]. Aside from the properties of the raw material, the major factor determining the final scaffold characteristics is the fabrication technique utilized to produce the scaffold [22].

In addition to acting as a bare physical support, scaffolds can be engineered to provide biological functions and actively induce tissue regeneration. Biocompatibility, or tissue tolerance is not enough. A general theory of biomaterials was expressed by henche and Ethridge in 1982 as[23]:

- An ideal implant material perform as if it were equivalent to the host tissue
- The tissue at the interface should be equivalent to the normal host tissue
- The response of the material to physical stimuli should be like that of the tissue replaced

A stable interfacial bond between tissue and implants must be achieved in order to obtain an equivalent physical response, and controlled physical stimuli is necessary for a stable interface to be produced.

The surface of a 3D scaffold, for example, can be functionalized to promote cell adhesion through specific cell–matrix interactions. In fact, the formation of complex tissues from single cells and tissue maintenance needs large amounts of information which must be transported from cell to cell and from cells to ECM.

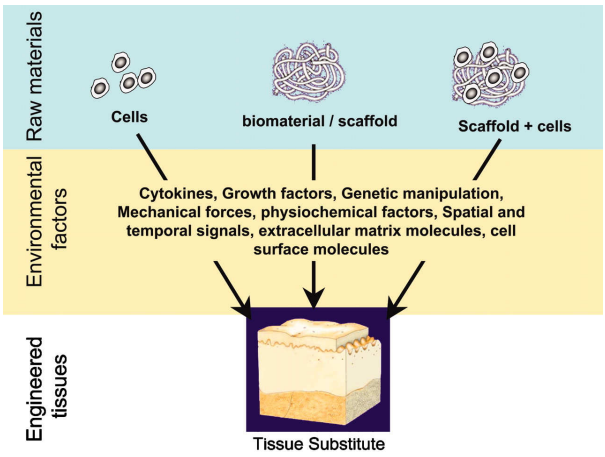

Fig. 1.3: Tissue engineering approaches are classified into three categories: (I) cells alone, (*II*) cells with scaffolds, and (*III*) scaffolds alone.

Since regeneration is an instance of induced *in vivo* synthesis, the activity of scaffolds has been described in terms of the quality of products induced to regenerate in the presence of these scaffolds. Their unique biological activity appears to lie primarily in their ability to regulate cell function through specific cell-matrix interactions involving integrins, mostly those fibroblasts and myofibroblast, and ligand on the matrix surface [24]. Activity is also conferred by chemical composition, which determines the *identity of ligands*; the specific surface of the porous network; the orientation of pore channels, which determines the *spatial configuration of ligands;* and the scaffold degradation rate which depends on the chemical composition as well as the cross-link density of the macromolecular network and determines the *duration of the active surface.*

In bone tissue engineering, the understanding of boneforming behavior of cells must be combined with progress in material science, to achieve guided bone regeneration. The scientific community is taking up this challenge through the employment of insoluble signals integrated with the degradable polymer matrix. These act as reinforcement

agents as well as osteoconductive signals, offering a valid compromise between the mechanical response and bioactivity of the scaffold. Many papers propose the use of calcium phosphates such as hydroxyapatite (HA) to stimulate a biochemical response from living tissues, to obtain a strong bond between the scaffold and the adjacent tissue with positive results[25].

1.3 Aim and structure of the thesis

The aims of this thesis are:

- To develop porous composite scaffold based on polyester and hydroxyapatite for bone regeneration using different techniques
- To charachterise these scaffold from a morphologic, mechanical and biological point of view.
- To design, prepare and characterise porous PDLLA scaffold, obtained by stereolithography.
- To develop new photo-crosslinkable composite resin suitable for stereolithography application.

In **Chapter 2,** a review on scaffold fabrication techniques is described. Their principles of operation are briefly explained underlining main advantages and shortcoming. Most part of the chapter is dedicated to the solid freeform fabrication technique with aprticalu attention to stereolithography and its biomedical application.

In **Chapter 3,** we describe the preparation of PCL and composite PCL/HAP scaffolds obtained with the *phase inversion/salt leaching* technique. The mechanical and morphological properties of the scaffold are determined analyzing also their osteoconductive properties.

In **Chapter 4,** two different technique to produce reinforced bioactive scaffold is compared. PCL composite scaffolds are obtained by incorporating poly(L-lactide) (PLLA) continuous fibers within a PCL matrix through the synergic combination of *phase inversion/salt leaching* technique and the *filament winding* technology. Then the structures are compared from a mechanical and morphological point of view with traditional PCL scaffold reinforced with calcium phosphate particles. Finally an *in vivo* test have been performed by Orthopaedic institute Rizzoli in Boulogne.

Chapter 5 reports the use of methacrylate-functionalised PDLLA oligomers with a non-reactive diluent for stereolithography application. Different porous architecture are prepared and compared from a morphological point of view. Double gyroid network architecture are chosen for the *in vitro* test and are seeded with hMSCs for 21 days.

In **Chapter 6** we describe the preparation of a composite PDLLA/ nano HAP resin for application in stereolithography. Double gyroid structure are prepared and characterized to evaluate the effect of nano-HAP on mechanical and biological properties.

References

[1] R. Lanza, R. Langer, J. Vacanti, *Principles of tissue engineering,* **2007**, Elsevier academic press.

[2] B.D. Ratner, *Advanced in Biomaterial 2008,***2008**, Washington.

[3] D. F. Williams , *The Williams Dictionary of Biomaterials,* **1999**, Liverpool University Press.

[4] G. Chen, T. Ushida, T. Tateishi, *Macromol. Biosci*. **2002**, 2, 67

[5] P.J.S. Bártolo, H. Almeida, *Int. J. Computer Applications in Technology,* **2009,** 36, 1, 1

[6] J.Black, *Biological Performance of Materials,* **1992**, 2nd ed. New York: Marcel Dekker

[7] S.D. Bruck, *Properties of Biomaterials in the Physiological Environment*, **1980**, Boca raton, FL: CRC Press

[8] P. Langer, J. P. Vacanti, *Science*, **1993**, 260, 920

[9] R. M. Nerem, A. Sambanis, *Tissue Eng*. **1995**, 1, 3.

[10] B. D. Boyan, C. H. Lohmann, J. Romero, Z. Schwartz, *Clin. Plast. Surg*. **1999**, 26, 629.

[11] M. S. Chapekar, *J. Biomed. Mater. Res*. **2000**, 53, 617.

[12] G.V. Novakovic, R.I. Greshney, *Culture of cells for tissue engineering,* **2006,** John Wiley & sons publication.

[13] D.F. Williams, *Definition in biomaterials.* In: *Progress in Biomedical Engineering*, Amsterdam Elsveier.

[14] L. G. Griffith, G, Naughton, *Science,* **2002**, 295, 1009.

[15] D. W. Hutmacher, *Biomaterials,* **2000,** 21, 2529.

[16] S. J. Hollister, *Nature Materials,* **2005,** 4, 518.

[17] V. Guarino F. Causa, A.Salerno, L. Ambrosio, *Material Science and Technology,***2008**, 24, 9, 1111.

[18] A. Gloria, T. Russo, R. De Santis, L. Ambrosio, *journal of Apllied Biomaterials & Bioceramics*, **2009**, 3,7, 141.

[19] B.E. Vhaignaud, R. Langer, J.P. Vacanti, *Synthetic Biodegradable Polymer scaffolds,***1997**, A.Atala and D.J. Mooney (Eds).

[20] T. Weigel, G. Shinkel, A. Lendlein, *Expert Rev. Med. Dev.,* **2006**, 3, 6, 835.

[21] D.W. Hutmacher, *J. Biomater. Sci. Polymer Edn*, **2001,** 12, 1, 107.

[22] M. B. Murphy, A. G. Mikos, *Principles of tissue engineering.* **2007,** 22, 318

[23] L.L. Henche, E.C. Ethridge, *Bioamterials: An Intefacial Approach,* **1982**, Academic Press, New York.

[24] I.V Yannas, *Scaffolding in Tissue Engineering,* **2006**, Cap. 1, *Taylor and francis Group.*

[25] V. Guarino, P Taddei, M. Di Foggia, C. Fagnano, G. Ciapetti, L. Ambrosio, *Tissue Engineering*, **2009**, 15, 1

CHAPTER 2

A review of scaffolds fabrication techniques

2.1 Introduction

Since the mid-1980s, researchers have developed many novel techniques to shape polymers into complex architectures that exhibit the desired properties for specific tissue-engineering applications. These fabrication techniques result in reproducible scaffolds for the regeneration of specific tissues. The scaffold should provide to a three-dimensional (3D) template that supports temporary loads driving the growth of the tissue to form its final shape[1]. In order to perform a complex biological and sensititve system such as the human body tissue, the requirements of scaffold materials for tissue engineering are manifold and extremely challenging[2]. First, the main requirement for a scaffold, particularly in bone tissue engineering is a controllable interconnected porosity to direct the cells to grow into the desires physical vascularisation of the ingrown tissue[3][4]. The scaffold morphology is determined by the fabrication method and by varying the component dimensions, scaffolds can be formed with porosity and strengths that are significantly different to their original morphology [5]. These key scaffold characteristics can be tailored to the application by careful selection of the polymers, additional scaffold components, and the fabrication technique [6]. A number of fabrication technologies have been applied to process biodegradable and bioresorbable materials into 3D polymeric scaffolds of high porosity and surface area. From a scaffold design and function viewpoint each processing methodology shows several advantages and shortcomings. In this chapter, different methods for scaffold design and preparation are summarized with specific emphasis on stereolithography (RP) technique. An important part of this thesis will be focused on the architecture of the pore network of tissue engineering scaffolds, on the preparation of scaffolds with different architectures and their functionality in tissue engineering.

2.2 Conventional techniques

The conventional techniques of scaffold fabrication: solvent leaching, gas foaming, vacuum drying, and thermally induced phase separation (TIPS) in combination with salt

leaching produce foam-like structures which are generally classified in the engineering literature as *cellular solids [4]* Porosity and pore size can be controlled by varying the particle/polymer ratio and particle size.

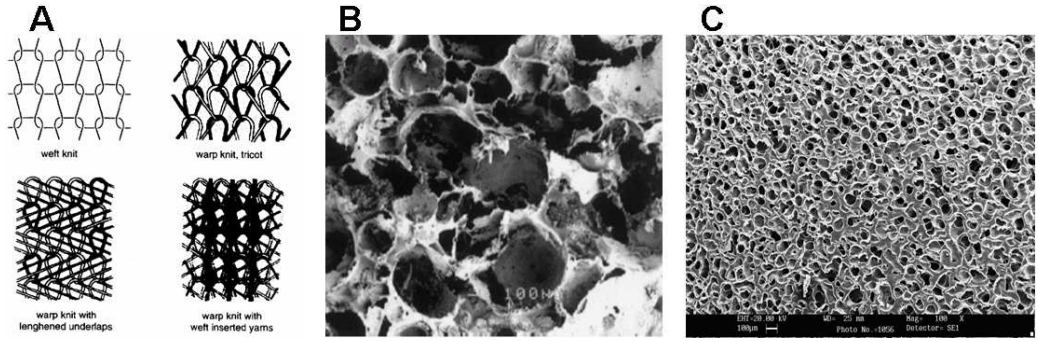

Fig. 2.1: Conventional technique commonly used in tissue engineering: A) textile, B) salt leaching, C) Gas foaming.

2.2.1 Salt Leaching

Particulate leaching method involves the casting of a polymer/porogen composite followed by the dissolution of the porogen. Polymer porous membranes of controlled porosity, surface/volume ratio, and crystallinity were prepared with porogen weight fraction, and the median pore diameter increased as the porogen particle size increased [7].

Fig. 2.2: schematic description of particulate leaching.

It is a simple and user friendly method, suitable with a range of biomaterials and no special equipment is needed.

2.2.2 Gas foaming

It is a technique to fabricate macro-porous sponges from synthetic biodegradable polymer using high pressure carbon dioxide processing at room [7]. Solid discs of polymer were saturated with CO_2 by exposure to high pressure CO_2gas for hours at room temperature. The solubility of the gas in the polymer was then rapidly decreased by reducing the CO_2 gas pressure to atmospheric levels. This created a

thermodynamics instability for the CO_2 dissolved in the matrix. Polymer sponges with large pores (approximately 100μm) and porosities of up to 93% could be fabricated with this technique [9].

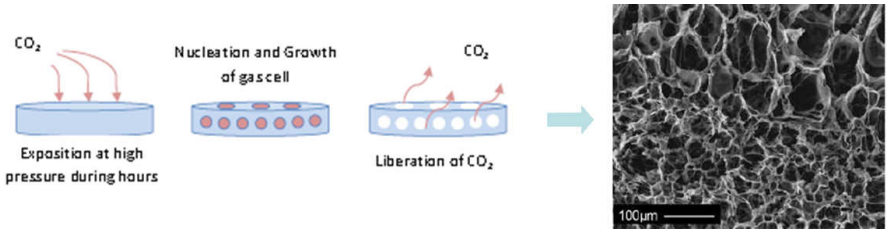

Fig. 2.3: schematic description of gas foaming.

Salerno et all prepared open-pore biodegradable foams with controlled porosity architectures using gas foaming micro-particulate of poly (ε-caprolactone) as is possible to see in figure 5 [10].

2.2.3 Thermal induced phase separation

Thermal-induced phase separation (TIPS) has been show to be an excellent technique to make micro-porous polymeric membranes. After a polymer is dissolved in a solvent at high temperature , phase separation by spinodal decomposition is induced by cooling or quenching the solution [11].

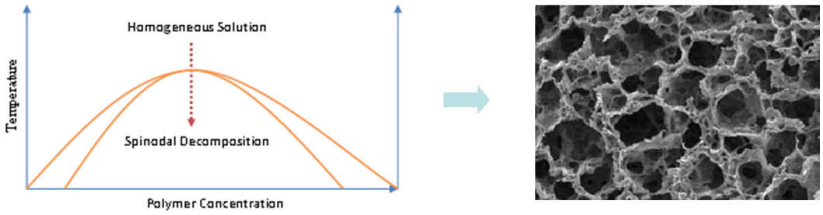

Fig. 2.4: schematic description of spinodal decomposition [7][12].

The TIPS process is classified mainly into two types such as solid-liquid TIPS, where the polymer crystallizes out of the solution, and liquid-liquid TIPS, where the solution separates into a polymer rich continuous phase and a droplet phase. Phase separation continues until the polymer-rich phase becomes immobilized by gelation, glass transition, or crystallization. Once this occurs, the structures is effectively frozen into a place and the solvent can be removed from the film [13]. Fully interconnected pores and large pore interconnections can be fabricated if spinodal decomposition is totally achieved. However, there are numerous drawbacks to applying those techniques for tissue engineering applications. These conventional technique are incapable of precisely and repeatedly controlling the microstructures

of the scaffold in term of pore size, geometry, interconnectivity and spatial distribution of pores. The pores are not fully inter-connected due to the formation of skin layers during solvent evaporation. The pore size varies, as it is difficult to ensure that the porogens are well-dispersed and not agglomerated to form bigger particles. Pore walls thickness, length and edges changes as a function of the solvent evaporation rate. The scaffolds cannot be made with thick sections as deeply embedded porogens become too distant from the surface and residual porogens may be left in the final structure [14]. Moreover organic solvents are used and causes problem of biocompatibility.

2.3 Rapid prototyping

In many scaffold manufacturing techniques, the control of the internal architecture and interconnectivity is limited Conventional scaffold processing techniques are, in fact, incapable of precisely controlling pore size, pore geometry, spatial distribution of pores and construction of internal channels within the scaffold[15]. To overcome the drawbacks of the conventional techniques, rapid Prototyping (RP) methods are attracting the interest of the TE community. The RP techniques allow the fabrication of very complex 3d structure in a layer-wise fashion in a reproducible way [16]. Rapid Prototyping (RP), also termed “solid freeform fabrication (SFF),” is a technology based on the advanced development of computer and manufacturing. All prototypes made with the current evolving RP process have several features in common [17][18]. A solid surface CAD model is electronically sectioned into layers of predetermined thickness. These sections define the shape of the part collectively. Information about each section is then electronically transmitted to the RP machine layer by layer. Subsequent layers are sequentially processed until the part is complete. The RP process basically uses the following steps to make prototypes:

- create a CAD model of the design.
- convert the CAD model to STL file format.
- Slice the STL file into 2D cross-sectional layers.
- Grow the prototype
- Postprocessing

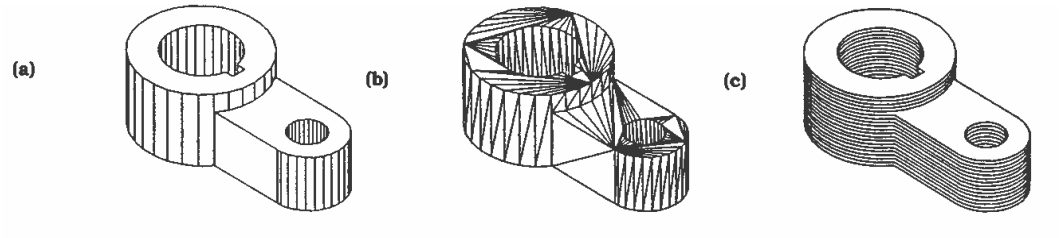

Fig. 2.5: The Solid Models as a: (a) Solid Model, (b) an STL file, and (c) in Sliced Layers

RP has the advantages of being able to build structures with customized shapes and better control over localized pore morphologies, porosities and material composition to suit the requirements of multiple cell types arranged in hierarchical structures.

Over the past two decades, more than 20 RP systems were developed and commercialised [19] with a focus on the rapid manufacturing of prototypes for non-biomedical applications. Very recently, biomaterial scientists used these technologies to fabricate scaffolds for tissue engineering. SFF techniques offer unique ways to precisely control matrix architecture (size, shape, interconnectivity, branching, geometry and orientation) yielding biomimetic structures varying in design and material composition, thereby enhancing control over mechanical properties, biological effects and degradation kinetics of the scaffolds. RP has been used in the medical field primarily as a means of guiding surgical procedures using tactile models derived from patient computerized tomography (CT) data [20].

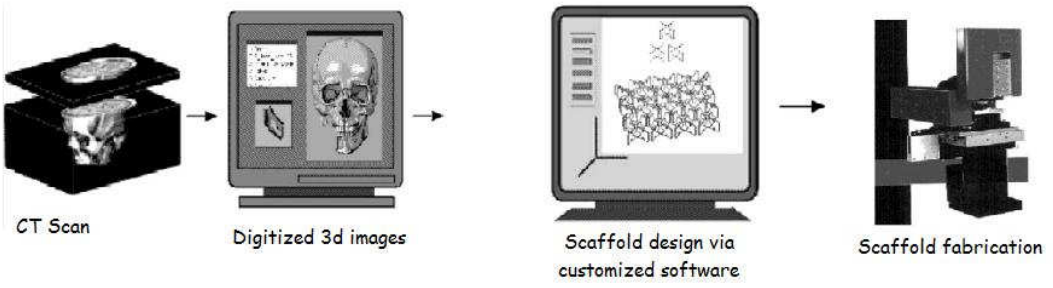

Fig. 2.6: Graphical illustration of a concept to build a customized 3D scaffold via robot supported micro assembly[4].

Direct fabrication of custom implants is promising in offering simpler and more rapid surgical implementations. The potential to intimately control the microstructure of porous channels and the overall macroscopic shape of the implants makes RP an ideal process for fabricating implant and tissue engineering scaffold as well. For the

fabrication of tissue engineering scaffold, SFF techniques have several advantages over conventional techniques:

- Excellent control over (pore network) design and properties;
- Excellent reproducibility
- Improved mechanical properties
- Higher pore interconnectivities
- Better suited for modelling.

The various RP&M technologies for tissue engineering, described in the following sections, include **stereolithography** processes, laser sintering, extrusion and 3D printing.

2.3.1 3D printing (3DP)

Basically the 3DP is a layered fabrication process, in which the sliced 2D profile of a computer model is printed on a fresh layer of powder via deposition of a suitable binder. Successive 2D profiles are then printed on a freshly laid layer of powder until the whole model is completed. The specimen is completed upon removal of the unbound powder and suitable post-processing [21].

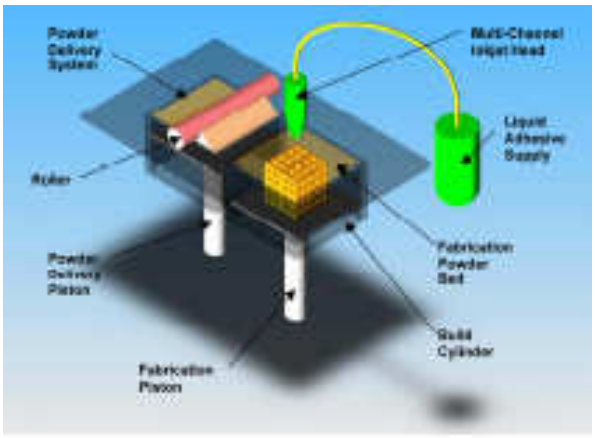

Fig. 2.7: Schematic overview of 3D printing method [22].

Recently the capability of creating complex 3D structures attracted tissue engineers to apply the technology to design and fabricate scaffolds [23]. With this method it is possible to obtain porosity of 45-60% with pore size in the range of 45 - 1600μm. The layer-by-layer process allowed fabrication of complex architectures with excellent resolution. Moreover, significant times are required to manufacture scaffold with suitable techniques [24].

2.3.2 Selective laser sintering (SLS)

SLS uses a fine powder of material which is heated with CO_2 laser of power in the range of 25-50 W such that the surface tension of the grain are overcome and they fuse together. Before the powder is sintered, the entire bed is heated to just below the melting point of the material in order to minimize thermal distortion and facilitate fusion to the previous layer.

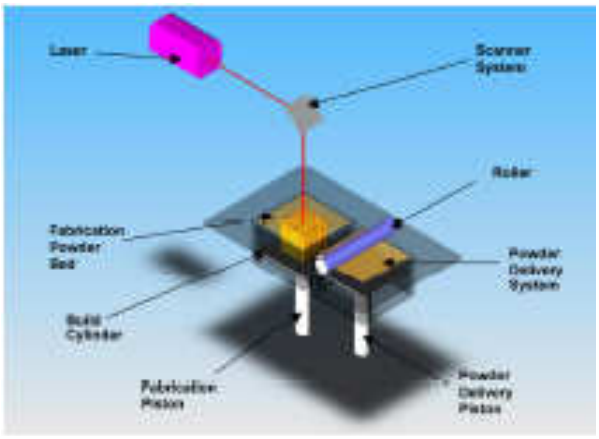

Fig. 2.8: schematic view of the selective laser sintering techniques [22].

Each layer is drawn in the powder bed using the laser to sinter the material. Then the bed is lowered and a powder-feed chamber raised. A new layer of powder is deposited and spread by a counter rotating roller. The sintered material forms the desired structure while the undesired powder remains in place to support the structure and may be cleaned away and recycled once the process is completed.

Only porosity up to 40% could be obtained, with pore size in the range of 30-2500μm. Once again, an accurate control over pore size and interconnectivity can be achieved and the layer-by-layer process allowed fabrication of complex and anatomically-shaped structures.

2.3.3 Fused Deposition Modelling

Fused deposition modeling (FDM) (Crump 1992) is a process whereby a molten material is extruded through a nozzle and deposited as a layer on a surface. At the completion of the layer deposition, the sample stage is lowered and a new layer is deposited. In this fashion, the technique fabricates a 3D structure. A benefit of this method is the absence of organic solvents in the fabrication process. The computer-aided process is controlled by the use of CAD data in the design of the scaffold.

The technique has been used to prepare porous scaffolds from polymers such as PCL [25], PEG-PCL-PLA [26], and PCL/HA composite [27].

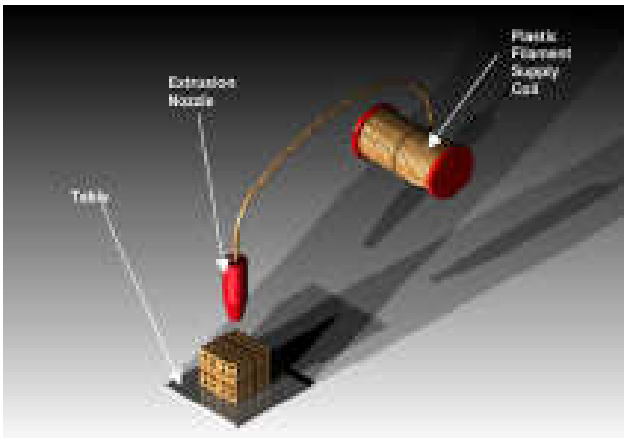

Fig. 2.9: Schematic description of fused deposition modelling [22].

Large porosity up to 80% can be achieved, with pore size in the range of 100-2000 μm. The exact control of pore size and interconnectivity can also be obtained [28][29].

2.4 Stereolithography

Stereolithography is an additive fabrication process using a liquid UV-curable photopolymer and a UV laser to build structures a layer at a time. Stereolithographic processes produce 3D solid objects in a multi-layer procedure through the selective photo-initiated cure reaction of a polymer (Bártolo and Mitchell, 2003). These processes usually employ two distinct methods of irradiation. The first method is the mask-based method in which an image is transferred to a liquid polymer by irradiating through a patterned mask. The irradiated part of the liquid polymer is then solidified. These systems generally require the generation of a lot of masks with precise mask alignments. In the second method, a direct writing process using a focused UV beam produces polymer structures[22].

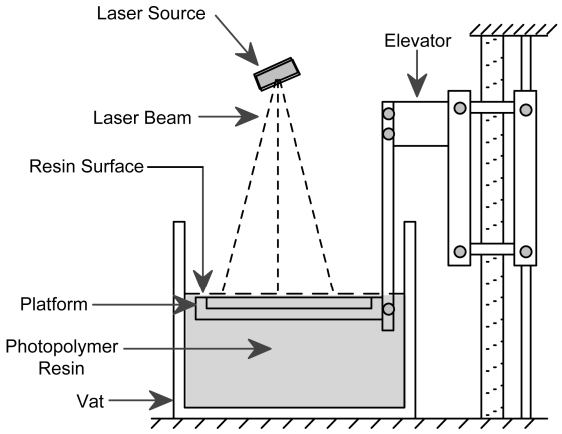

Fig. 2.10: **Conventional Stereolithography system[22]**.

Generally, SL is considered to provide the greatest accuracy and best surface finish of any RP technology. The model material is robust, slightly brittle, and relatively light, although it is hydroscopic and may physically warp over time (a few months) if exposed to high humidity [30]. Although fine structures can be produced by the laser SL technique, the process is usually slow because of the nature of point-by-point laser scanning. This prevents the incorporation of cells within the scaffold walls during the fabrication process and could also lead to denaturation and inactivation of biological molecules during the prolonged fabrication period [31]. One solution for this problem is the use of a Liquid Crystal Display (LCD) or a digital processing projection system as a flexible mask. Microstereolithography is a relatively recent development, similar to conventional stereolithography. There are three methods of microstereolithography and they have differences in the laminate on and solidification processes. The first is free-surface method that is the subject of this study [32]. In this method, UV curable resin is exposed to UV laser beam above the free-surface of the resin and the resin at the surface is solidified. The second is fixed-surface method. In this method, UV curable resin is exposed to UV beam toward flatly transparent window that is immersed in the resin and the resin at the surface formed by this window is solidified [33]. This method has a higher resolution than free-surface method. However, the yield of this method is low because adhesion between the resin and the window causes destruction of a solidified structure. The third is inside-solidification method [34]. Unlike the two methods described above, in this method resin is solidified at not the surface, but a point inside the UV curable resin.

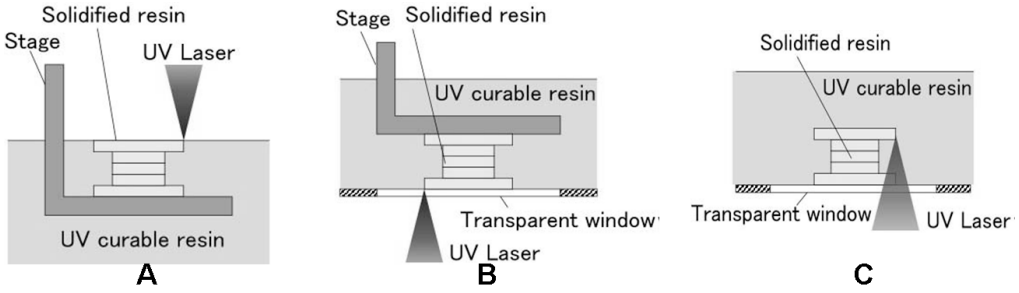

Fig. 2.11: The methods of microstereolithography

This method presents an high resolution of submicron order, and can fabricate movable microstructures without the support. However, the size of a structure is restricted to several tens of micrometers because this method must use objective lens with high numerical aperture [33]. Bertsch and colleagues reported a μSL process employing a liquid crystal display (LCD) as a dynamic mask to photopolymerize an entire layer [35]. However, LCD as a dynamic mask has limited optical efficiency [36]. A new technology, Digital Micro-mirror Device™ (DMD, Texas Instruments, Dallas, TX), offers better performance in terms of optical fill factor (85% with DMD vs. 64% with LCD) and light transmission (71% with DMD vs. 21% with LCD)[31].

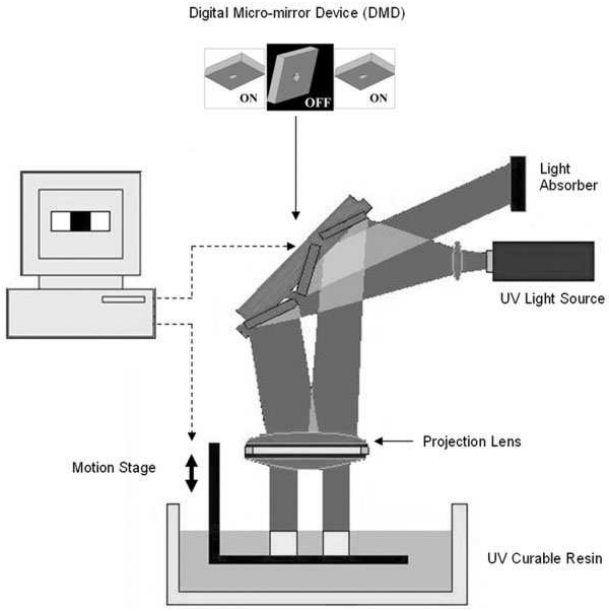

Fig. 2.12: Schematic of the Digital Micro-mirror Device Micro-stereolithography (DMD-μSL) set-up [31].

The shapes of these constructed layers are determined by slicing the design CAD model with a series of closely spaced horizontal planes. By taking the sliced layer patterns in the electronic format, the mask patterns are dynamically generated as bitmap images on

a computer-programmable array of digital micro-mirrors on the DMD chip. The arrays of aluminium micro-mirrors are anchored on top of addressable SRAM CMOS circuitries, and two positions are permitted for the mirror to tilt at +10◦ or −10◦ along its diagonal [36]. By toggling the voltage applied to the individual micro-mirror, the mirror can be switched between stable positions with the light reflecting “on” and “off” directions. Large porosity could be obtained with this method (~90%), with pore size in the range of 20-1000 μm. The light illuminated on the DMD chip is shaped according to the defined mask pattern, and then, the modulated light is transferred through a reduction lens. Hence, an image is formed on curable resin surface with a reduced feature size. In each layer, the illuminated area is solidified simultaneously under one exposure, while the dark regions remain liquid. After the fabrication of one layer, the substrate is immersed into the UV curable resin and the new layer is fabricated on top of the existing structure. A complex, geometrically shaped microstructure can be fabricated by building all the layers sequentially and stacking them from bottom to top. The dynamic mask is the core component of the μ-SL system that determines the shape of the fabricated microstructure. As the dynamic mask, the DMD modulates the light by collectively controlling the micro-mirror arrays to switch the light on and off on each individual pixel. An accurate control over pore size and interconnectivity can be achieved. The layer-wise fashioned process allowed fabrication of complex and anatomically-shaped structures [37][37].

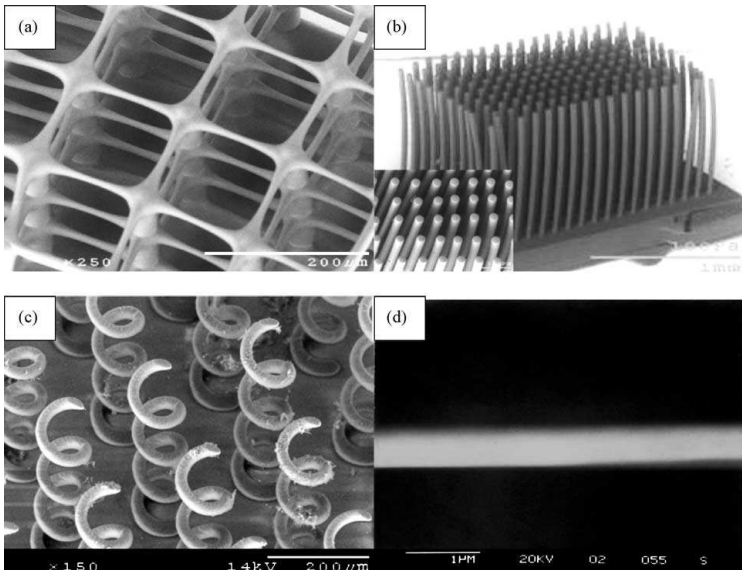

Fig. 2.13: 3D complex microstructures fabricated by μ-SL process[36]

.

However, the machinery required are very expensive and only polymers compatible with UV curing can be used. The development of new biodegradable resin would allow the preparation of well-defined tissue engineering scaffolds for a wide range of tissues.

In SLA, control of thickness of the layer that is cured is essential. For a given resin, the cure depth is determined by the energy of the light to which the resin is exposed. This energy can be controlled by adjusting the power of the light source, and the scanning speed (laser system) or the exposure time (projection system). Upon laser exposure, the photopolymer obeys the Beer–Lambert law of absorption. Earlier macro-scale experiments suggested that the photopolymer has a threshold exposure and curing depth, can be expressed in the following working curve as:

$$\mathbf{C_d = D_p \ln \frac{E}{E_c}}$$

where C_d is the curing depth, D_p is the penetration depth of the resin defined as $D = (2.3*\varepsilon[J])$ (ε is the molar extinction coefficient of the initiator, [J] is the initiator concentration), and E and E_c are the laser exposure on the resin surface and critical exposure of the resin at the laser wavelength, respectively [38]. A plot of the determined cure depth (or cured layer thickness) versus the applied irradiation dose is termed a working curve, and is constructed to determine the correct settings for stereolithography fabrication. As the applied irradiation dose (E) exceeds the critical energy required to reach the gel point (E_c), a solidified layer forms from the resin surface. The value of E_c depends, among on the concentration of photo-initiator, and of dissolved oxygen and other inhibiting species. To ensure chemical and mechanical bonding between the layers during building , the macromers conversion at the interface between layers should be slightly higher than the gel point [39]. A high extinction coefficient of the resin corresponds to a low light penetration depth (D_p), and will allow most accurate control of the polymerisation process and minimal over-cure. The penetration depth can be decreased by increasing the photo-initiator concentration, or by including a dye in the resin. This non reactive component competes with the photo-initiator in absorbing light.

As shown in Fig. 14, the experimental measurements of working curves of UV curable resins are obtained by measuring the curing depth under various UV exposures. The curing depth is linearly proportional to the natural logarithm of UV exposure, which is

in good agreement with the numerical mode. Under the same UV exposure, the resin with 0.3% UV doping has a smaller curing depth [36].

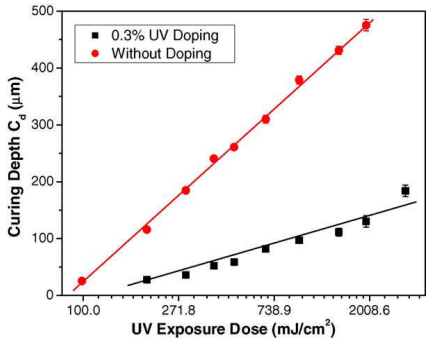

Fig. 2.14: Measured curing depth vs. incident UV light exposure at different doping level

2.4.1 Photopolymer used in stereolithography

In stereolithography, parts are built from a photosensitive polymer fluid that cures under the exposure to a laser beam. Photopolymers are solidified (cured) when exposed to electromagnetic radiation with a specific wavelength including γ rays, X-rays, UV, visible light and infrared. Photopolymerizations also offer improved temporal control of the initiation process when compared to methods such as redox initiation systems, as they are controlled by the presence of light [40]. The polymerizations are complete in a minimal amount of time, making them ideal for a surgical setting. The rate can be adjusted by altering the polymerization conditions, including the choice and concentration of the photoinitiator, the concentration of reactive double bonds in the formulation, the wavelength of the light source (UV or visible), as well as the light intensity. Perhaps the limited number of resin that are commercial available for processing by stereolithography has often been considered the main limitation of the technique. The resin should be a liquid that rapidly solidifies upon illumination with light. Acrilate-based photopolymers are the most widely used resin system developed for stereolithography [41]. Only few resin have been described that allow the preparation of elastomeric object by stereolithography. It has been shown [42] that poly(propylene fumarate) (PPF) mixed with a photoinitiator can be crosslinked by exposing it to a concentrated flood of UV light through a translucent mold. It requires a reactive diluent such as diethyl fumarate to obtain an appropriate reaction rate and viscosity of the resin [43]. Matsuda et al. reported use of a custom-built SLA device to 3D-print a structure

from ε-caprolactone [44]. This resin formulations include macromers with low glass transition temperature and relatively high molecular weights (1-5 kg/mol), often in combination with non-reactive diluents such as N-methylpyrollidone (NMP) or water to reduce the viscosity of the resin. To create polymer-ceramic composite objects ceramic particles (Hydroxyapatite) are homogeneously suspended in the resin and photo-polymerised in the SLA [45][46]. The ceramic powder is used because it elicit osteconductive and osteoinductive properties and decreases the penetration depth of the incident light improving the vertical resolution of the process. Moreover, the mechanical properties of the manufactured parts are also increased [47][48], and become sufficient to allow the manufactured microparts to be directly used as microcomponent. Popov et al prepared non-resorbable polyacrylate and hydroxyapatite composite parts, and implanted them into the femurs of rats for time periods of up to 8 weeks [49]. This show that anatomically shaped implants, compatible with cells and surrounding tissues can be manufactured using stereolithography.

2.5 Medical application of rapid prototyping

One area in which rapid prototyping is having a great impact is the medical field. Some of the application include surgical planning and the fabrication of prosthetic. The field of medicine gratly benefits from the development and improvement of rapid prototyping technology. The number of medical applications of rapid prototyping are increasing everyday, making the future of RP more and more promising. The creation of medical models requires a number of steps: the acquisition of high-quality volumetric (3D) image data of the anatomy to be modelled, 3D image processing to extract the region of interest from surrounding tissues, mathematical surface modelling of the anatomic surfaces, formatting of data for RP (this includes the creation of model support structures that support the model during building and are subsequently manually removed), model building, and quality assurance of model quality and dimensional accuracy. These steps require significant expertise and knowledge in medical imaging, 3D medical image processing, computer-assisted design, and manufacturing software and engineering processes [30]. With the progress in computer-aided design and manufacturing technologies, it is now possible to make use of this information in

conducting the surgery itself by making use of patient-specific models of parts of the body fabricated by stereolithography [50]. Noteworthy, biodegradability is essential in the fabrication of medical implants such as tissue engineering scaffolds. A degradable photo-polymerisable system can be obtained by chain-crosslinking hydrolysable oligomers with reactive end-groups [51][52]. To be able to apply PDLLA macromers in stereolithography, the macromer must be in the liquid state. This can be achieved by heating or diluting. Reactive diluents such as methyl methacrylate, butane-dimethacrylate and N-methyl-2-pyrrolidone have been used in regular photo-polymerisation reactions [53] and in stereolithography [51].

2.6 Design and fabrication of biomorphic scaffolds by stereolithography

The scaffolds suitable for tissue engineering, apart from being biocompatible and biodegradable, should present highly interconnected pores; have sufficient mechanical properties; and, provide a suitable substrate for cell attachment, migration and proliferation [54]. However, the majority of existing approaches under-utilize SFF by producing CAD based scaffolds with straight edges and sharp turns or those derived from Boolean intersections of geometric primitives such as spheres and cylinders. Neither of these partitions provides a biomorphic environment suitable for cell attachment, migration and proliferation [55]. The biomorphic geometry that best mimics this structural configuration would be surfaces that are continuous through space and divided into two (pore and non-pore) not-necessarily-equal sub-spaces by a nonintersecting two-sided surface. Minimal surfaces are ideal to describe such a space. TPMS are minimal surfaces periodic in three independent directions, extending infinitely and, in the absence of self-intersections, partitioning the space into two labyrinths. Figure 1 shows the TPMS Primitive (P) surface, the Diamond (D) surface discovered by Schwarz [6] and the Gyroid (G) surface discovered by Schoen [56].

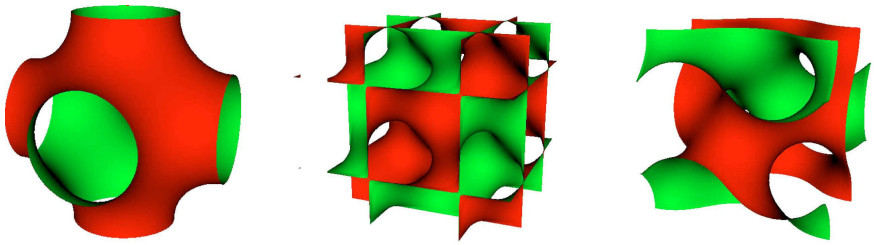

Fig. 2.15: 3-Dimensional tessellations of Schwarz's Primitive (left), and Diamond (centre) and Schoen's Gyroid (right) Triply Periodic Minimal Surfaces.

Surfaces whose mean curvature H is everywhere zero are *minimal surfaces* – any sufficiently small patch cut from a minimal surface has the least area of all surface patches with the same boundary. The triply periodic minimal surfaces (TPMS) are particularly fascinating because they are without self intersections and partitionate the space into two labyrinths [56][57]. This viable morphology, when replicated at macro (tissue) level may also have profound influence on cell migration and tissue growth and may provide an optimal biomorphic tissue analogue [55].

Conclusion

Tissue engineering is based on the concept that cells seeded onto 3D bioresorbable scaffolds can build native tissues under suitable *in vitro* and *in vivo* conditions. Ideally, a scaffold material should permit the application of a solid free form fabrication technology, so that a porous scaffold with any desired three-dimensional morphology as well as shape could be designed and fabricated. Several techniques have been developed to process synthetic and natural scaffold materials into porous structures. The conventional techniques for scaffold fabrication (textile technologies, solvent casting, particulate leaching) are defined as processes that create scaffolds having a continuous, uninterrupted pore structure which lacks any long-range channelling microarchitecture. Solid freeform fabrication systems provide a solution to this problem by creating scaffolds with controlled internal microarchitecture, which should increase the mass transport of oxygen and nutrients deep into the scaffold. Several systems have been successfully adapted to produce synthetic and natural biodegradable polymer, bioceramic and hydrogel scaffolds. in particular stereolithography is a SFF technique that is particularly versatile with respect to the freedom of design of the structures that are to be built. Moreover the development of new resin has enabled to fabricate biodegradable devices with open architectures for biomedical engineering purpose.

References

[1] V.J Chen, P.X. Ma, *BiomaterialsI,* **2004**, 25, 2065

[2] K. Rezwan, Q.Z. Chen, J.J. Blaker, A.R. Boccaccini, *Bioamterials*, **2006**, 27, 3413.

[3] V.Guarino, F. Causa, L. Ambrosio *Journal of Applied Biomaterials & Biomechanics*, **2007,** 5, 3

[4] D.W. Hutmacher, *J. Biomater. Sci. Polymer Edn*, **2001,** 12, 1, 107.

[5] K. Yayaraman, M. Kotaki, Y. Zhang, X. Mo, *J. Nanosci. Nanotech.,* **2004,** 4, 52

[6] R. C. Thomson, M. J. Yaszemski and A. G. Mikos, *Principles of Tissue Engineering*, **1997**, R. P. Lanza, R. Langer and W. L. Chick (Eds), p. 263.

[7] P.D. Dalton, T. Woodfield, D.W. Hutmacher. *Porous scaffold design for tissue engineering*, **2005,** 4.

[8] C.B. Park, D.F. Baldwin, N.P. Suh, *Polymer engineering Science*, **1995**, 35, 432

[9] D.J. Mooney, D.F. Baldwin, N.P Suh, J.P. Vacanti, R. Langer, *Biomaterials*, **1996,** 17, 417.

[10] A. Salerno, S. Iannace, P.A. Netti, *Bioscience*, **2008**, 8, 655.

[11] H. Matsuyama, T. Iwatani, Y. Kitamura, M. Tearamoto, N. Sugoh, *Journal of Applied Polymer Science,* **2001**, 79, 2449.

[12] Y.X. Huang, J. Ren, C. Chen, T.B. Ren, X.Y. Zhou, *Journal Biomaterials Applications*, **2008**, 22, 409.

[13] P.D. Graham, A.J. Pervan, A.J. McHugh, *Macromolecules*, **1997**, 30, 1651.

[14] L. J. Gibson, M. F. Ashby, *Cellular Solids: Structure and Properties*, **1997** 2nd edn. Cambridge, University Press.

[15] A. Gloria, T. Russo, R. De Santis, L. Ambrosio, *journal of Apllied Biomaterials & Bioceramics*, **2009**, 3,7, 141.

[16] A. Armillotta, R. Peltzer, *Journal of Advance Manufacturing Technology,* **2008**, 39, 501.

[17] P. Jacobs, *Rapid prototyping and manufacturing & fundamentals of stereolithography*, **1992,** SME Publications, Hong Kong.

[18] S. Ashley, *Mechanical Engineering,* **1991**, 34.

[19] K.F. Leong, et all, *Rapid Prototyping, Principles and Applications*, **2003**, 19

[20] S. Yang, K.F. Leong, Z. Du, C.K. Chua, *Tissue engineering,* **2002**, 8, 1

[21] J.J. Lee, E. Sachs, M. Cima, *Rapid prototyping journal,* **1995**, 4, 24.

[22] P.J.S. Bártolo, H. Almeida, *Int. J. Computer Applications in Technology,* **2009,** 36,1,1.

[23] C.F.X. Lam, X.M. Mo, S.H. Teoh, D.W. Hutmacher, *Materials science and Engineering,* **2002**, 20, 49.

[24] H. Seitz, W. Rieder, S. Irsen, B. Leukers, C. Tille, *Journal Biomedical Material Research B Applied Biomaterials*, **2005**, 74B, 782.

[25] D.W. Hutmacher, T. Schantz, I. Zein, K.W. Ng, S.H. Teoh, K.C. Tan, *J Biomed Mater Res,* **2001**, 55, 2, 203.

[26] M.E. Hoque, D.W. Hutmacher, W. Feng, S. Li, M.H. Huang, M. Vert, Y.S. Wong, *J Biomater Sci Polym Ed* **2005**, 16, 12, 1595.

[27] J.J. Sun, C.J. Bae, Y.H. Koh, H.E. Kim, H.W. Kim, *J. Mater. Science Mater Med,* **2007**, 18, 6, 1017.

[28] L. Moroni, J.R. de Wijn, C.A. van Blitterswijk, *Bioamterials*, **2006**, 27, 974.

[29] T.B.F. Woodfield, J. Malda, J. Wijn, F. Péters, J. Riesle, C.A. van Blitterswijk, *Biomaterials*, **2007**, 25, 4149.

[30] J. Winder, R. Bibb *Journal of Oral and Maxillofacial Surgery*, **2005**, 63, 7 1006.

[31] Y. Lu, G. Mapili, G. Suhali, S. Chen, K. Roy, *J Biomed Mater Res,* **2006**, 77A, 396.

[32] K.Ikuta, S.Maruo, T.Fujisawa and A.Yamada, *Proc. of IEEE International Conference on Micro Electro Mechanical Systems MEMS'99*, **1999**, 376.

[33] K Kobayashi, K. Ikuta,

[34] S. Maruo, Koji Ikuta, *Sensors and Actuators A*, **2002**, 100, 70.

[35] A. Bertsch, H. Lorenz, P. Renaud, *Sensor and actuator*, **1999**, 73,14.

[36] C. Sun, N. Fang, D.M. Wu, X. Zhang, *Sensor and Actuator,* **2005**, 121, 113.

[37] R. Sodian, M. Loebe, A. Hein, D.P. Martin, S.P. Hoerstrup, E.V. Potapov, H. Hausmann, T. Lueth, R. Hetzer, **2002**, *ASAIO Journal*, 48, 234.

[38] X. Zhang , X.N. Jiang, C. Sun, *Sensors and Actuators* , **1999,** 77, 149.

[39] F. P. W. Melchels, J. Feijen , D.W. Grijpma, *Biomaterials,* **2010**, 31, 6121.

[40] K.A. Davisa, J.A. Burdick, K.S. Anseth, *Biomaterials*, **2003**, 24, 2485.

[41] S.J. Lee, H.W. Kang, J.K. Park , J.W. Rhie, S.K. Hah, D.W. Cho, *Biomedical Microdevices,* **2008**, 10, 233.

[42] J.P. Fisher, D. Dean, P.S. Engel, A.G. Mikos, *Annu Rev Mater Sci* **2001**, 31,171.

[43] K.W Lee , S.F. Wang ,B.C. Fox, E.L. Ritman, M.J. Yaszemski, L.C. Lu, *Biomacromolecules*, **2007**, 8, 1077.

[44] T. Matsuda, M. Mizutani, S.C. Arnold, *Macromolecules,* **2000**, 33, 795

[45] C. Provin, S. Monneret, *Ieee Transactions On Electronics Packaging Manufacturing*, **2002,** 25, 1, 59

[46] C.Provin, S. Monneret, H. le Galle, S. Corbel, *Advanced Materials*, 15, 12, 994.

[47] A. Lungu, A. Mejiritski, and D. C. Neckers, *Polymer*, 1998, 39, 4757.

[48] S. N. Goyanes, J. D. Marconi, P. G. König, M. D. Martin, I. Mondragon, *J. Alloys Compounds*, **2000**, 310, 374.

[49] V.K. popov, A.v. evseev, A.l. Ivanov, V.V. Roginski, A.I. Volozhin, S.M. Howdle, *Journal of Materials Science-Materials in Medicine,* **2004**, 15, 123.

[50] D.P. Sarment, K. AL-Shammari, C.E. Kazor, *International journal of periodontics & Restorative Dentistry*, **2003**, 23, 287.

[51] F.P.W. Melchels , J. Feijen , D.W. Grijpma, *Bioamterials*, **2009,** 30, 3801.

[52] J. Ericsson, A. Hult, *Makromol Chem*, **1991**, 192, 7, 1609.

[53] R.F. Storey, S.C. Warren, C.J. Allison, J.S. Wiggins, A.D. Puckett, *Polymer*, **1993**, 30, 3801.

[54] D.W. Hutmacher, M. Sittinger, M.V. Risbud, *Trends in Biotechnology*, **2004,** 22, 7, 354.

[55] S. Rajagopalan, R. A. Robb, *Medical image Analysis*, **2006**, 10, 5, 693.

[56] E.A. Lord , A.L. Mackay, *Science*, **2003**, 85, 3, 346.

[57] H. Karcher, K. Poltier, *construction of triply periodic minimal surface.*

CHAPTER 3

Bioactivation of PCL matrices by calcium phosphate solid signals.

3.1 Introduction

Critical step of all tissue engineering techniques is the use of a tridimensional structure which, mimicking the extracellular matrix (ECM), serves as scaffold which is able to promote and guide actively the tissue regeneration process [1]. *In vitro* and *in vivo* tissue engineering strategies generally include signalling molecules, which should try to reproduce the natural sequence of signals guiding spontaneous tissue repair, cells, in case tissue is not able to regenerate by itself, and if necessary a scaffold, which provides a mechanical support to the development of neotissue [2]. Bone tissue engineering is a promising fields that aims to fabricating biological alternatives for harvested tissue and organ for transplantation without the limitations of current therapies [3]. In contrast to traditional surgical methods of bone-defects management, this approach relies on three-dimensional structures for temporary replacement of damage tissue, mimicking its morphology and physiological function [4]. The scaffold or three-dimensional construct provides the necessary support for cells to proliferate and maintain their differentiated functions, and its architecture defines the ultimate shape of the new bone and cartilage [5]. Furthermore the selection of the most appropriate material to produce a scaffold is a primary aspect for the construction of a final tissue engineered product [4]. It is possible to distinguish four types of biomaterials, according to their natural or synthetic origin, and organic or inorganic nature [5]: (A) natural based materials from animal or vegetal source (starch[6], alginate) (B) Synthetic organic materials, such as polyester (e.g. polyglicolide, polylactide [7], polydioxane [8], polycaprolactone, and polyhanydrides [9]), (C) synthetic and (D) natural inorganic materials such as hydroxyapatite (HA)[10], calcium phosphate composites [11], glass and coralline HA [11][12]. Several scaffold material have been investigated for tissue engineering including hydroxyapatite (HA), poly(α-hydroxyesters), and natural polymers such as collagen and chitin [14]. Polycaprolactone (PCL) is a semicrystalline linear resorbable polyester widely used for biomedical application. It is subjected to biodegradation because of the susceptibility of

its aliphatic ester linkage to hydrolysis [15][16]. In vitro and in vivo biocompatibility studies have been performed on this polymer, resulting in U.S. Food and Drug Administration approval of a number of medical and drug devices [17][18]. On the other hand polyester represent some limitation due to the inflammatory response and the inhibition of tissue formation [5]. Biocompatibility does not solely imply a lack of toxicity or the ability to be chemically compatible with the host tissue. The term has been used to describe the ability of a material not to elicit a response from the host tissue on implantation: a biocompatible material is one which should perform 'appropriately and in concert with a certain host response in a specific application'[19].

From this point of view Bioactivation represent the main strategy in modern biomaterial development, addressing the adequate direction of the response of the implant to external stimuli. Its goal is the development of new types of materials that stimulate a biochemical response from living tissue in order to obtain a strong bond between the scaffold and the tissue [20]. Osteocoductive and osteoinductive stimuli may be induced by using insoluble signals, via calcium phosphate and, in particular, HA [14] inside the implant or by soluble signals represented by proteins, such as growth factor [21] and peptide sequence [22].

Another common belief among many scientists trying to develop new biocompatible biodegradable polymers has been that these should be natural molecules or, alternatively, analogues of natural polymers, which should release degradation products that enter the normal metabolic pathways, rather than being xenobiotic. One first approach considered polymers which undergo hydrolytical degradation producing metabolites normally present in the physiological environment [23]. Analogs of the extracellular matrix have been produced from collagen and glycosaminoglycans which are widely and abundantly distributed in the body, but in order to achieve a certain stability of the device, it has often been necessary to modify these natural molecules chemically. However, in a number of cases concern has been expressed for the potential toxicity of some of the crosslinking agents utilized, such as glutaraldehyde, formaldehyde and isocyanates [24]. An alternative solution to produce insoluble molecules starting from natural components was explored in the mid 1980s and led to the development of hyaluronan esters [25]. These novel hyaluronan-based materials were obtained by the esterification of the free carboxyl groups of glucuronic acid

present along the chain backbone. The current work is aimed at the study of some PCL-based composites, conceived as substitutes for bone regeneration. Macroporous structure were prepared with the salt leaching technique and were analyzed from a morphological and mechanical point of view analyzing also their osteoconductive properties.

3.2 Materials

3.2.1 Polycaprolactone (PCL)

Poly(ε-caprolactone) (PCL) is a biocompatible and biodegradable polyester, widely used for biomedical applications. PCL is prepared by ring opening polymerization of ε-caprolactone using a catalyst such as stannous octanoate.

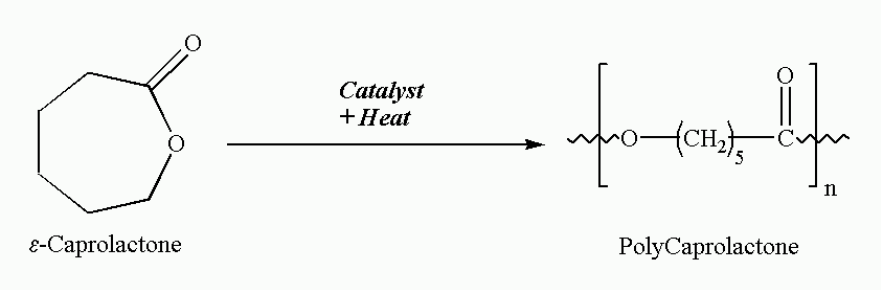

Fig. 3.1:Synthesis of PCL by ring opening polymerization of ε-caprolactone using a catalyst such as stannous octanoate.

PCL is a semi-crystalline polymer having glass transition temperature of −60 ◦C and melting point ranging between 59 and 64 ◦C, depending upon its crystalline nature of PCL [16]. It is soluble in chloroform, dichloromethane, carbon tetrachloride, benzene, toluene, cyclohexanone and 2-nitropropane at room temperature.

Properties	Units	Conditions	Value
Molecular conformation	-	-	Nearly planar
Molecular weight (of repeat unit)	g mol^{-1}	-	114
Weight average molecular weight	g mol^{-1}	GPC	74000
Number average molecular weight	g mol^{-1}	GPC	25000
Intrinsic viscosity	Cm^3 g^{-1}	Dilute solution viscosimetry	0.9
Solvents	-	-	DMAc – MDc – Thf – benzene
Entalpy of polymerization	kj mol^{-1}	25°C – 1 atm	-28.8
Entropy of polymerization	kj mol^{-1}	25°C – 1 atm	-53.9
Gibbs free Energy of pol.	kj mol^{-1}	25°C – 1 atm	-12.8
Physical state	-	semycristalline	
Degree of cristallinity	%	DSC	69
Unit cell	-	X-ray difraction	Orthorhombic
Number of repeating units per unit cell	-	-	4
Measured density	g cm^{-3}	X-ray diffraction	1.094 – 1.200
Elongation	%	-	700
Glass transitino temperature	K	DSC	201
Meltign temperature	K	DSC	331
Heat of fusion	kj mol^{-1}	DSC	8.9

Tab. 3.1 : Physio-chemical PCL properties of special interest.

PCL can be blended with other polymers to improve stress crack resistance, dyeability and adhesion [26]. Degradation of PCL in comparison to polyglycolic acid and other polymers is slow making it suitable for long-term delivery extending over a period of more than one year. Degradation process is a bulk process that can be divided into two phases: (A) molecular weight loss due to chain scission, (B) onset of weight loss. No weight loss is observed during the initial phase of the biodegradation process, which covers a molecular weight (*Mn*) range of 200,000 to 5000. The second phase of polymer degradation is characterized by a decrease in the rate of chain scission and the onset of weight loss. Extensive *in vitro* and *in vivo* biocompatibility and efficacy studies have been performed, resulting in US Food and Drug Administration approval of a number of medical drug delivery system [27]. At the present PCL is regarded as a soft- and hard –tissue compatible bioresorbable material. Although application of PCL might be limited due to its

poor mechanical properties, depending on the preparation technique and molecular weight.

	σ (MPa)	E (Gpa)	ρ (g/cm^3)
PCL	30	0.35	1.13
Cortical Bone	30 - 160	4 - 27	1.8 – 2.2
Trabecular Bone	7 – 130	1 – 11	1.5 – 1.9

Tab. 3.2 : Comparison between typical mechanical properties of PCL and Bone tissue.

Therefore, strategies to improve mechanical performance of PCL-based scaffold are needed. Calcium phosphates such as HAP or tricalcium phosphate have been employed as bone implant in various form.

3.2.2 Calcium phosphates

The ability to bond to bone tissue is a unique property of bioactive ceramics. Analyses of the bone-implant interface revealed that the presence of hydroxyapatite is one of the key features in the bonding zone. Figure 2 schematically summarized a variety of events that were reported to occur at the bioactive ceramic-tissue interface [28]: (1) dissolution from the ceramic; (2) precipitation from solution onto the ceramic; (3) ion exchange and structural rearrangement at the ceramic-tissue interface; (4) interdiffusion from the surface boundary layer into the ceramic; (5) solution-mediated effects on cellular activity; (6) deposition of either the mineral phase (a), or the organic phase (b), without integration into the ceramic surface; (7) deposition with integration into the ceramic; (8) chemotaxis to the ceramic surface; (9) cell attachment and proliferation; (10) cell differentiation; and (11) extracellular matrix formation

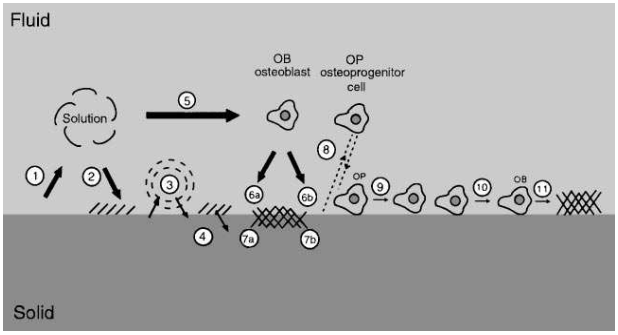

Fig. 3.2: Schematic diagram representing the events which take place at the interface between bioactive ceramics and the surrounding biological environment [28]

An important aspect of the overall reaction sequence between these materials and tissues is that, in the absence of a biologically equivalent, calcium deficient, carbonate containing hydroxyapatite (c-Ap) surface upon implantation, dissolution, precipitation and ion exchange reactions lead to a biologically equivalent apatitic surface on the implanted material. This reaction does not proceed by itself, but is accompanied by parallel reactions, such as adsorption and incorporation of biological molecules and attachment of surrounding cells.

Bioceramics can be divided into three broad classification: near-inert, bioactive and resorbable. The different tissues reactions elicited by the implant material can be partly explained by considering the surface reactions which occur *in vivo* [19].

Near-inert ceramics trigger the formation of a thin 1-3µm thick 'protective' layer absorbed to the surface of the implant. Even if there is no aggressive foreign body response, there is no bonding between implant and host tissue.

Bioactive materials possess the ability to undergo continuing surface reactions with the host tissue, acting in amore natural away. In fact these materials form a chemical bond s rapidly with the host tissue and no fibrous layer is formed . Materials that exhibit this behaviour are calcium phosphate.

Resorbable ceramics present a composition that can be degraded chemically by body fluids or digested by macrophages. Really important is that degradation products are non-toxicand should be easily disposed of by the cells. Example of such materials is tricalcium phosphate that I rapidly resorbed into the body when placed in bony defects. This classification is summarized in the table 2:

Classification	**Tissue response**	**Examples**
Near inert	Formation of non-adherent fibrous membrane	Alluminia Zirconia
Bioactive	Formation of an interfacial bond	Hydroxyapatite
Resorbable	Tissue replaces implant as it degrades	Tricalcium phosphate

Tab. 3.3: Bioceramic classification

Calcium phosphates, specifically hydroxyapatite ceramics, have generated a great deal of interest in relation to hard tissue applications due to their bioactivity. Calcium phosphate ceramics, such as Hydroxyapatite (HAP) $Ca_{10}(PO_4)_6(OH)_2$ with an atomic ratio of calcium phosphate (Ca/P) of 1.67 or β-tricalcium phosphate (β-

TCP) β-$Ca_3(PO_4)_2$, are used for cavity filling applications and work via the colonization of the implant by new bone tissue [29]. From a crystallographic point of view HAP is more similar to natural bone tissue apatite than β-TCP and so it represent a better structural material for bone growth, but the resorption rate of HAP is extremely slow as compared with β-TCP [29]. However, due to the poor mechanical performance of these materials, clinical usage has been limited to applications where calcium phosphate are used either to confer bioactivity or in the form of low density ceramic foams, where mechanical performance is not an issue. In order to improve the mechanical properties of CPCs, a number of researchers have blended polymers with CP cements with promising results.

3.2.3 Composite materials

Composite materials often show an excellent balance between strength and toughness and usually show improved characteristic compared to their separate components. Previous studies have shown that blends of calcium phosphate and polymers is a suitable combination to reach high degree of elasticity and a good biocompatibility [14][32]. Different ways were realized to bring these two components together into a potential implant, like simple mechanical mixing or co-precipitation. By special techniques, it is also possible to introduce porosity into the implant which is advantageous for most applications as bone substitution material [33].

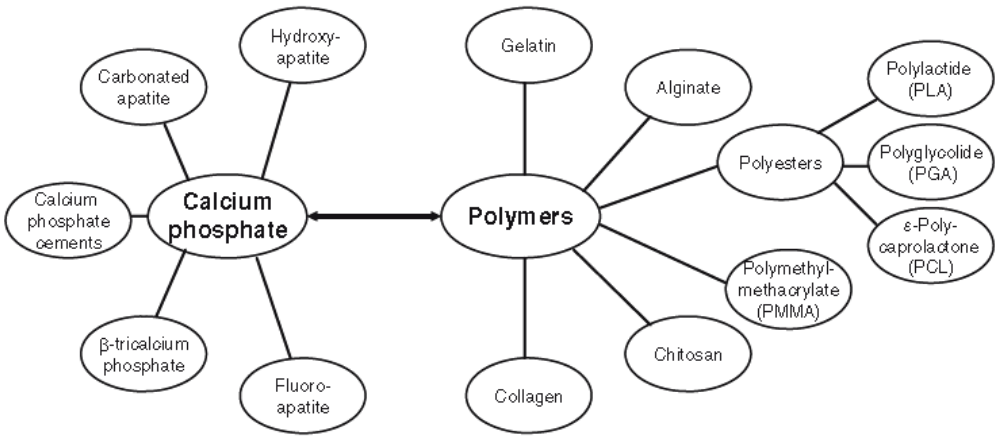

Fig. 3.3: Some possible combination of calcium phosphates and polymers

So a possible strategies to enhance mechanical properties is to reinforce PCL by adding hydroxyapatite HAP particles inside the polymer matrix: the presence of bioactive solid signals such as HAP in the polymer matrix may improve bone formation by osteoblasts mimicking the natural bone mineral phase. Beside the osteoconductive enhancement, the inclusion within PCL matrix of rigid bone-like particles may improve the mechanical properties of the polymer .

As well as bioactivation several studies demonstrates that the micro-architecture of the porous scaffold may guide cell function by regulating the interactions between cell, and the diffusion of nutrient and metabolic wastes throughout the three-dimensional construct. To mimic the topological and microstructural characteristic of the ECM, a scaffold has to present high degree of porosity, high surface to volume ratio, fully interconnected porosity, appropriate pore size and geometry control. So , in this context, the design and processing of a porous scaffold with a suitable morphological characteristic with an appropriate pore size and specific surface for cell seeding becomes crucial for the success of these materials as scaffolds for orthopaedic applications [4].

In this chapter porous PCL/HA networks were prepared through phase inversion/salt leaching method using NaCl crystal as porogen agent. Stoichiometric HAP micrometric particles were chosen for their higher chemically stability. The porosity, pore interconnection, and specific surface area, as well as, the mechanical properties of the scaffolds, were investigated as a function of the amount of HAP particles. Preliminary cellular studies have been carried out using mesenchymal stem cells from adult human synovial to assess the potential of the proposed scaffold as bone substitutes.

3.3 Methods

3.3.1 Scaffolds fabrication

Poly-ε-caprolactone pellets (Sigma Aldrich M_w 65 kDa) were dissolved in a 80wt% tetrahydrofuran (Sigma Aldrich, anhydrous >99,9%) solution (5g polymer in 20 ml tetrahydrofuran) by stirring for about 3h at room temperature. Sodium chloride crystals, sieved to a specific range (212-300μm), were homogeneously mixed to the polymer solution with a volume ratio of about 9/1. Therefore the mixture was pured

in the mold in order to obtain cylindrical specimen with controlled size. Samples were dipped in ethanol (20 minutes for 3 times) at room temperature and, finally, washed in bidistilled H_2O for 7 days. For the hydroxyapatite reinforced scaffolds, the HA powder was added to the PCL solution 20 wt% before solvent extraction.

3.3.2 Scaffold morphology analysis: SEM and µCT

Scaffold microstructure was investigated by scanning electron microscopy (Leica 420). Samples were gold-coated using a sputter coater set at 15 mA for 20 min in order to perform a qualitative analysis about pore size, distribution and interconnection. Furthermore structures have been analyzed from a structural point of view using a micro-computed tomography (µCT), (Skyscan 1072 at 10µm resolution). Scanning was done at an X-ray tube voltage of 54 kV, a current of 136 µA and a rotation angle of 180 °C. After reconstruction using the Skyscan software thresholded isosurfaces images were obtained. The software was also used to generate pore size distribution maps of the structures.

3.3.3 Thermogravimetric analysis

Thermogravimetric analysis (TGA) was performed to verify the effective weight percentage of HAP in the composite scaffold using a TA instrument TGA model 5000. A nitrogen atmosphere was used with a temperature range from 25 to 700°C.

3.3.4 Mechanical testing

Compressive mechanical properties were evaluated at room temperature on dynamometric machine (Instron) equipped with a 100N load cell and a crosshead speed of 1mm/min. Cylindrical specimen with 2:1 height/diameter ratio (diameter 7 mm, height 14) were fabricated according to the ASTM 695/2a standard. The elastic modulus E was calculated by the initial slope of the stress-strain curve before the plateau region. Dynamic-mechanical studies were performed by Bose electroforce biodynamic system by superimposing a sinusoidal stress to the specimen and recording the related strain.

Dynamic mechanical Analysis (DMA) can be simply described as applying an oscillating force to a sample and analyzing the material's response to that force [34].

The modulus measured in DMA is, however, not exactly the same as the Young's modulus of the classic stress–strain curve. Porous cylindrical specimen were stimulated under sinusoidal stimulation spanning the frequency from 0.1 to 9 Hz., where a pre-load of 0.05 N was initially applied followed by a dynamic load of 1N. From these data we can calculate the storage or elastic modulus E' and the loss modulus E'' as follow:

- $E' = (\sigma_0/\varepsilon_0)\cos\delta$
- $E'' = (\sigma_0/\varepsilon_0)\sin\delta$

3.3.5 Preliminary biological evaluation

Multipotent mesenchymal stem cells from human synovial membrane were used for biological evaluation of PCL/HAP composite macroporous scaffolds. Random biopsies of SM (wet weight 10–50 mg) were obtained aseptically from the knee joints of one human donors (16 years old). As comparison HMSc from a male donor (4 years old) were obtained to test the difference in cell capability to express the osteoblastic phenotype. Synovial sample was diluted 1:1 with OptiMem (Invitrogen) culture medium supplemented with 10% FBS, antibiotic (100 µg /ml penicillin, 100 µg /ml streptomycin) and fungizone (250 µg/ml) as antimycotic. Following overnight incubation at 37°C in humidified atmosphere 5% CO_2, cells were collected by centrifugation 800 r.p.m for 15 min, washed twice. Plated in a culture flask and allowed to attach for 48 hours. Non adherent cells were removed and cellular suspension were centrifuged for 10 min at 800 r.p.m to recover the culture medium. The medium was replaced every 3 days. After 2-3 weeks of primary culture, when the sparsely attached cells reached confluence, they were washed twice with calcium and magnesium–free phosphate buffered saline (PBS), harvested by treatment with trypsin and replated at a 1:4 dilution for the first subculture. Cell passages were continued in the same way with a 1:4 dilution when cells reached confluence. The next step was to verify cells capability to express markers of different phenotype like adipocytic and osteoblastic. The in vitro adipogenesis assay was performed as described elsewhere (2). SM-derived cells were allowed to become confluent and were cultured for an additional 5 days. Adipogenic induction medium was then added, consisting of growth medium

supplemented with 1 m*M* dexamethasone, 0.5 m*M* methyl-isobutylxanthine and 10 mg/ml insulin, (all from Sigma). Cells were treated 4 times with adipogenic induction medium. The cultures were then maintained in adipogenic maintenance medium for 21 days before fixation, and microscopic observation.

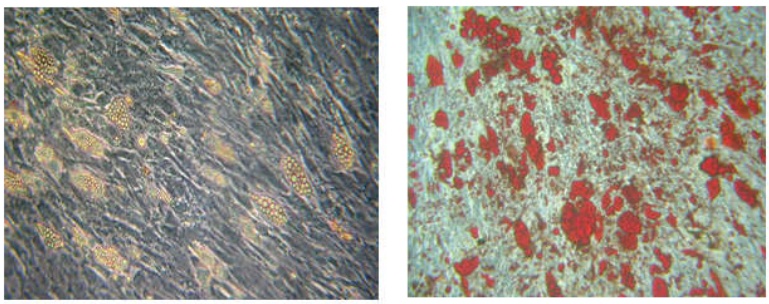

A B

Fig. 3.4: microscopic images of SM-derived cells cultured for 21 days with adipipogenic induction medium (A) and after treatment with Sudan III

To verify the in vitro osteogenic expression SM-derived cells were cultured for 21 days with growth medium supplemented with 100 n*M* dexamethasone, 10 m*M* b-glycerophosphate, and 50 m*M* ascorbic acid.

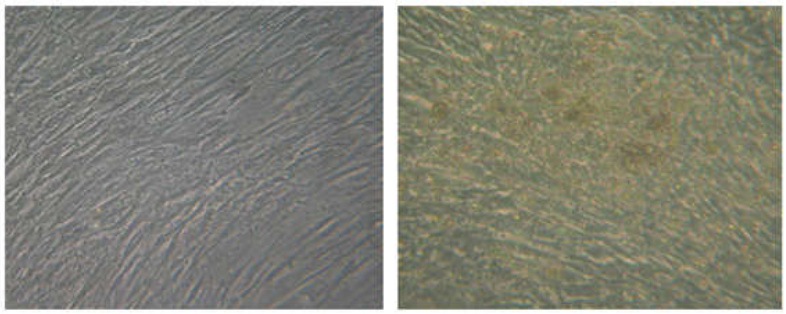

A B

Fig. 3.5: micrographic images of SM-derived cells after 21 days treatment with normal medium (A) and osteogenic medium (B)

As control part of the SM-derived cells were cultured in normal growth medium as we can see in figure

3.4 Results and discussions

3.4.1 Scaffold morphology analysis: SEM and µ-CT

Porous PCL/HAP scaffolds obtained by phase inversion/salt leaching method were characterized by SEM micrographs of the surface. A typical topology of PCL/HAP scaffold was outlined in figure :

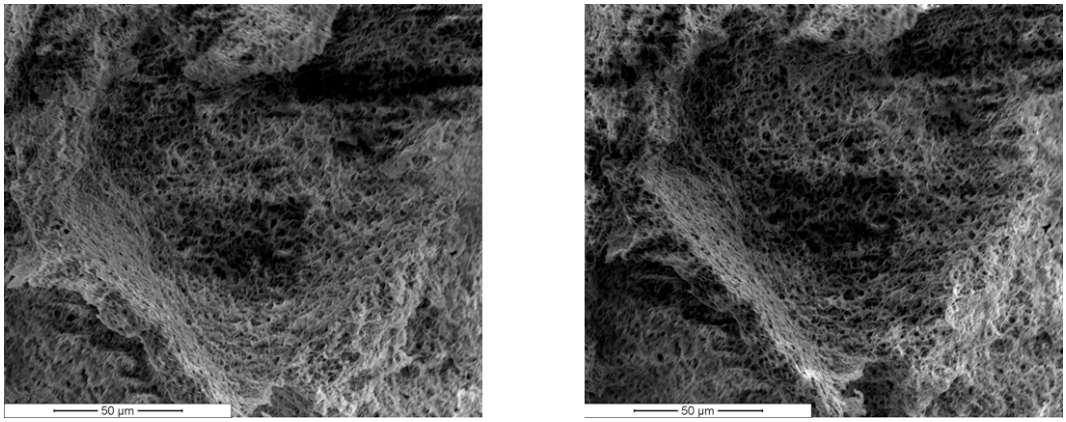

Fig. 3.6: Microporosity of PCL/HAP -based composite scaffolds by SEM analysis. Micropores along section surface.

As a consequence of the dispersion of NaCl crystals with well-controlled size inside the PCL matrix and an intimate contacts between crystals, the proposed technique guarantees an adequate pore size range and a high degree of interconnection of pores. Indeed, as evidenced by SEM observations, the obtained scaffolds were characterized by a regular structural porosity with homogeneously distributed and well-interconnected pores. It can be clearly seen that all scaffolds have the two distribution peaks of the smaller and bigger pores at around 5–20 µm and 200–400 µm, respectively. Phase inversion process led to the formation of small pores (smaller then 20µm), while the removal of NaCl led to the formation of big pores (bigger than 100 µm). Figure 6 shows the surface topography of the pore wall in PCL/HAP scaffolds. It was also necessary to have a quantitative information about the different elements present inside the scaffold. This is accomplished by using the "built-in" spectrometer called an Energy Dispersive X-ray Spectrometer. Energy dispersive X-ray analysis, also known as EDS, EDX or EDAX, is a technique used to identify the elemental composition of a sample or small area of interest on the

sample. To explain further, when the sample is bombarded by the electron beam of the SEM, electrons are ejected from the atoms on the specimens surface.

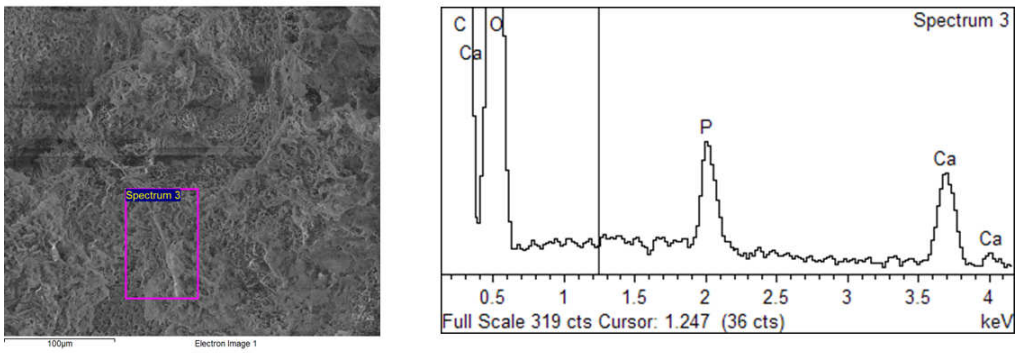

Fig. 3.7: Qualitative evaluation of P and Ca peaks by energy dispersive spectroscopy analysis on the cross section.

Element	Weight (%)	Atomic (%)
C	59.35	68.39
O	33.34	28.85
P	2.30	1.03
Ca	5.01	1.73

Tab. 3.4: elemental composition of the cross section area.

The EDS x-ray detector measures the number of emitted x-rays versus their energy. The energy of the x-ray is characteristic of the element from which the x-ray was emitted. A spectrum of the energy versus relative counts of the detected x-rays is obtained and evaluated for qualitative and quantitative determinations of the elements present. The energy dispersive spectroscopy analysis performed on the cross section of HAP-loaded scaffolds (Fig. 6) confirmed the presence of the apatitic phase: two large peaks due to Ca and P elements were observed, and a Ca=P atomic ratio about 1.66, that is, very close to the theoretical value of stoichiometric HAP (Ca=P¼1.67), was calculated. Because the completely unpredictable structure inside the scaffold pores and pore inteconnectivity can be difficult to assess, but the use of micro-computed tomography (µCT) allows for a more precise definition and better assessment of scaffold characteristic. Structures were analyzed from a quantitative point of view using a micro-computed scanning (µCT) to observe the microstructure of materials in 3D. Three-dimensional (3d) image analysis techniques are used to quantify distribution properties of the 3d microstructure of such partly scaffolds. After

reconstruction using the Skyscan software thresholded isosurfaces images were obtained.

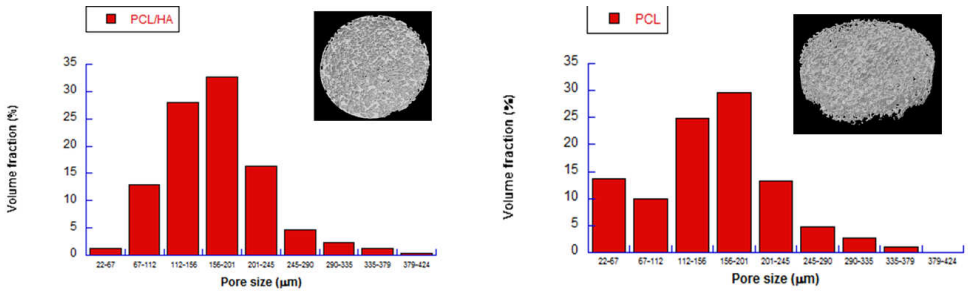

Fig. 3.8:pore size distribution of PCL/HAP scaffold from µ-CT analysis. The bars in the histogram correspond to volume fraction of pores with specific diameters

From the µCT data, the structural parameters of the built scaffold were determined and summarized in table :

Sample	**Porosity** (%)	**Specific surface area** (mm^{-1})	**Pore size (µm)**
PCL	74,6 ± 3,2	49,5 ± 6,7	181 ± 18
PCL/HAP	72,5 ± 4,3	41,3 ± 3,18	172 ± 15

Tab. 3.5: Parameters of the built porous structures as determined by µ-CT

The results indicate that the scaffold porosities are around 70–75%, which is considered to be beneficial for cell in-growth. Porosity seems to be unaffected from the HAP particles as it is to recognize from the comparison between PCL and PCL/HAP scaffolds. Among the morphological characteristics, a crucial aspect for cell adhesion and then proliferation is represented by the specific area of the substrate. In particular, since the surface area could modify important functional features such as the mechanism of cell adhesion and the rate of degradation, the surface/volume ratio (S/V) was investigated. It was obtained from the µCT-data and a high value of 37.9 mm^2/mm^3 was determined for this scaffolds.

3.4.2 Thermogravimetric analysis

Essential statement regarding the thermal stability of a composite are obtained from the thermogravimetric (TGA) and analyses. Thermogravimetric curves (TGA) of PCL and PCL composite are given in Figure . Thermal decomposition of each sample takes place in a programmed temperature range of 30-700ºC. In the case of

PCL we have only one weight loss between 350 and 425 ºC due to the polymer degradation. For the composite material it is possible to recognize the same weight losses seen for the previous sample but also there are a certain percentage of material that doesn't degrades over 700 ºC. This mass retain over 700 ºC is due to the presence of HAP that is the mineral phase and doesn't degrade until 1000 ºC.

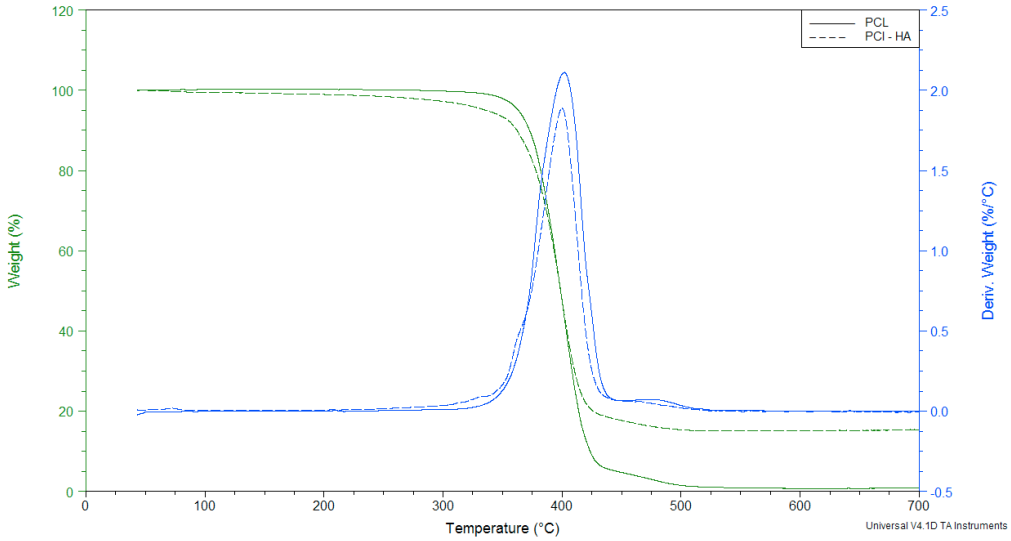

Fig. 3.9:TGA of PCL and PCL/HAP composite scaffold.

3.4.3 Mechanical testing

The mechanical properties of porous scaffolds are evaluated by compressive tests. The mechanical properties of PCL, PCL/HAP scaffolds are shown in Figure . Compared with the pure PCL scaffold, composite scaffolds exhibit higher compressive modulus. The compressive modulus of PCL/HAP scaffold increases from 0.075 to 0.20 MPa while the compressive strength increases from 25 to 52 Pa as the filler content increases from 0 to 20 wt%. The improvement in elastic modulus and strength could be attributed to the enhancement of the interaction between filler and matrix and a better dispersion of filler in the matrix. The static compression tests enabled to obtain the stress/strain curve of composite scaffolds. Firstly, it describes the mechanical behaviour of porous systems under static conditions: it shows a linear elasticity at low stresses followed by a long collapse plateau truncated by a regime of densification in which the stress rises steeply. The elastic modulus E was calculated by the initial slope of the stress-strain curve before the plateau region.

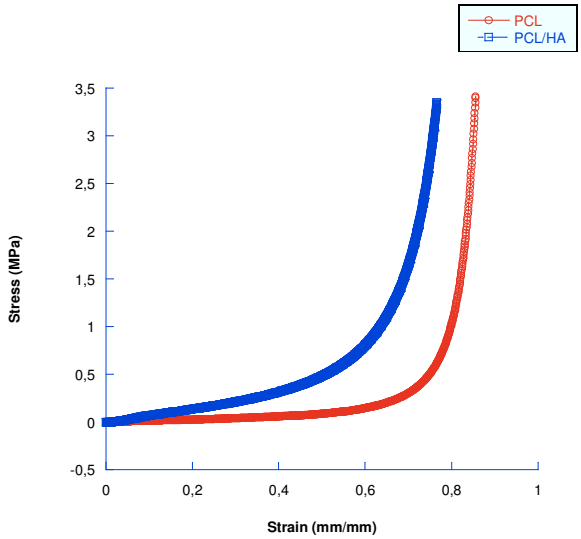

Fig. 3.10: stress/strain curve for PCL and PCL/HA scaffolds. Composite scaffold shows an high elastic modulus .

Sample	σ_{max} (elastic region) (MPa)	E (Gpa)	ε_{max} (elastic region) (MPa)
PCL	0,13±0,003	0,075±0,004	0,421±0,02
PCL/HAP	0,30±0,003	0,20±0,024	0,405±0,03

Tab. 3.6 : Static compression test evidence the difference in mechanical response between PCL and PCL-HAP composite scaffold.

The definition of the elastic range allowed to establish the average load and amplitude to apply for the cyclic stimulation. Specimens were tested under the stress control mode, where a pre-load of 0.05 N was initially applied followed by a dynamic load of 1N. The evolution of elastic moduli was evaluated varying the frequency from 0.1 to 9 Hz.

Dynamic tests confirm the result obtained by static compressive test, showing an higher value of E' for the PCL/HAP samples. Moreover the test highlights a certain viscoelastic behaviour of the samples showing that E' increases with frequency, while loss modulus E'' is not significantly affected as frequency varies.

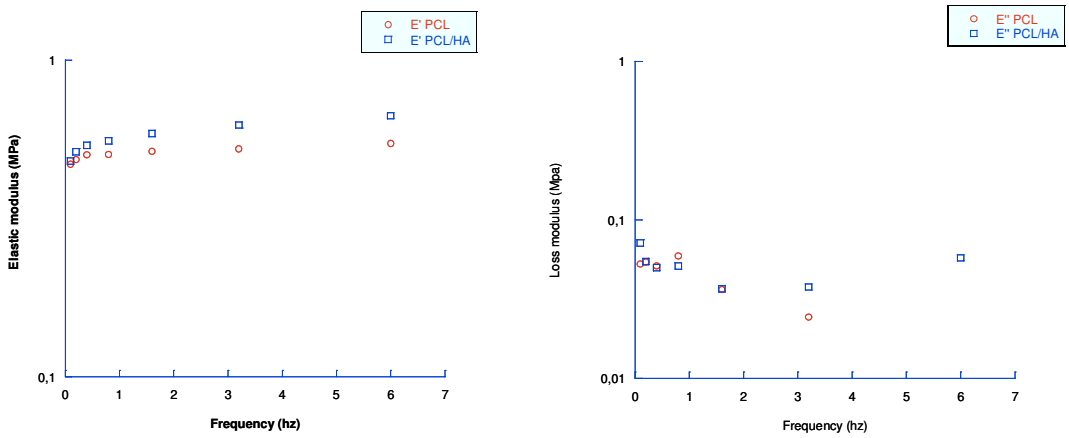

Fig. 3.11:evaluation of Storage modulus (E') and loss modulus (E'') through DMA for PCL and PCL-HA porous structure

3.4.4 Biological evaluation

Scaffolds were prepared to cell seeding with two different methods: one part were sterilized by ethylene oxide and the others washed with antibiotic/antymicotic PBS solution. Ethylene oxide acts more strongly against bacteria, especially gram-positive bacteria, than against yeast and fungi. The disinfectant effect of ethylene oxide is similar to that of sterilization by heat, but because of limited penetration, it affects only the surface. The Sterility Assurance Level, after a certain specified exposure to ethylene oxide is 10^{-6}, meaning that the chance of finding a single bacterium is below 1 per million. The remaining part of the scaffolds were soaking in ethanol overnight and then 1% antibiotic/antimycotic in PBS for 2 days. After they were extracted from the solution and washed in PBS for 1 day to remove antibiotic/antimycotic traces and prewetting in medium for 3 days. Human synovium MSCs were seeded dropwise 15 x 10^4 per sample on 12 samples and allowed to settle on the surface for 30 min; 3 scaffolds were soaked in osteogenic medium without cells as control. Then 200 µl of medium were added to the wells. The seeded scaffolds were cultured in osteogenic medium for 14 days, with media exchange every three days. After 3 days culturing, scaffolds were assayed for cell viability using MTT assay alkaline phospahatase content was measured every 7 days using the alkaline phosphatise kit and observed by SEM as detailed elsewhere.

The MTT assay is a colorimetric assays that allows to assess the viability (cell counting) and the proliferation of cells (cell culture assays). The MTT calorimetric

assay determines the ability of viable cells to convert a soluble tetrazolium salt 3–(4,5-dimethylthiazol-2l)-2,5-diphenyltetrazolium bromide (MTT) into an insoluble formazan precipitate. Tetrazolium salts accept electrons from oxidized substrates or appropriate enzymes, such as NADH and NADPH. In particular, MTT is reduced at the ubiquinone and cytochrome b and c sites of the mitochondrial electron transport system and is the result of succinate dehydrogenase activity. This reaction converts the yellow salts to blue-colored formazan crystals that can be dissolved in an organic solvent whose concentration can be spectrophotometrically determined by optical density at 570 nm.

Culture medium were removed from the well and cells were washed with PBS (Sodium phosphate 10 mM, pH 7.4, NaCl 120 mM – KCl 2.7 mM).

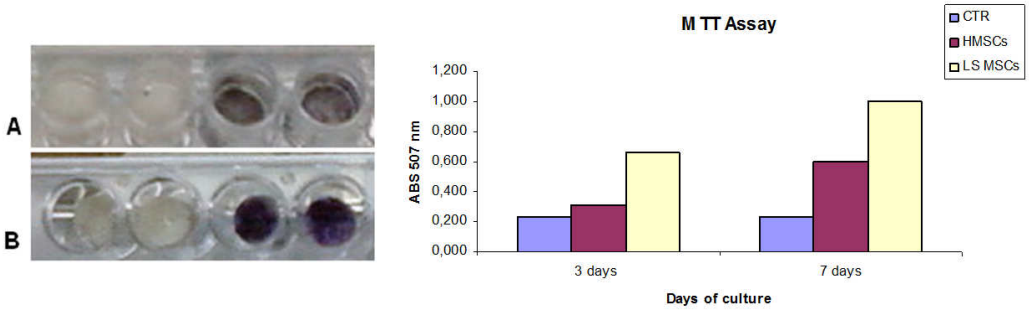

Fig. 3.12:MTT assay at 3 (A) and 7 (B) days after seeding, with relative absorbance value

Absorbance shows an high increase between 3 and 7 days if compared with the control peak, this would suggest that 3D matrices are colonized by a very high number of proliferating cells, moreover synovial liquid MSC show higher value of absorbance if compared with HMSc.

ALP (Alkaline phosphatase) activity through colorimetric assay (Roche kit) was used as an indirect measure of the capacity to hydrolyze inorganic phosphate. The enzyme assay kit is based on the alkaline phosphatase (ALP)-mediated conversion of p-nitrophenol phosphate to nitrophenol in an alkaline buffer. P-nitrophenyl phosphate is colourless while *p*-nitrophenol shows a yellow colouring in alkaline environment and it exhibits an absorption maximum at 405-415 nm. The is used to examine cell differentiation such as osteogenesis, which is associated with increased expression of ALP. The production of p-nitrophenol in the presence of ALP was measured by monitoring light absorbance by the solution at 405 nm. Results are expressed as u/(mg protein).

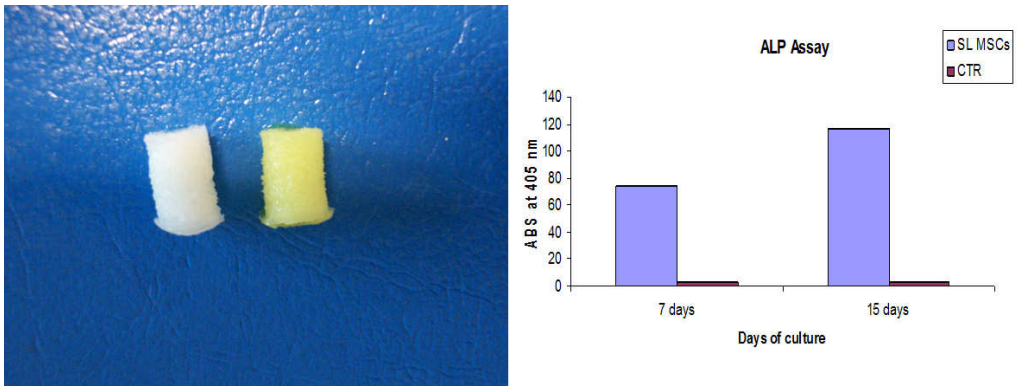

Fig. 3.13: ALP release by cells grown onto PCL-HA samples for different time periods.

Preliminary results at 14 days shows an increase in ALP activity suggesting an increased osteoblast differentiation. High-resolution morphological techniques, SEM imaging, led us to observe the spreading and growth of cells onto materials.

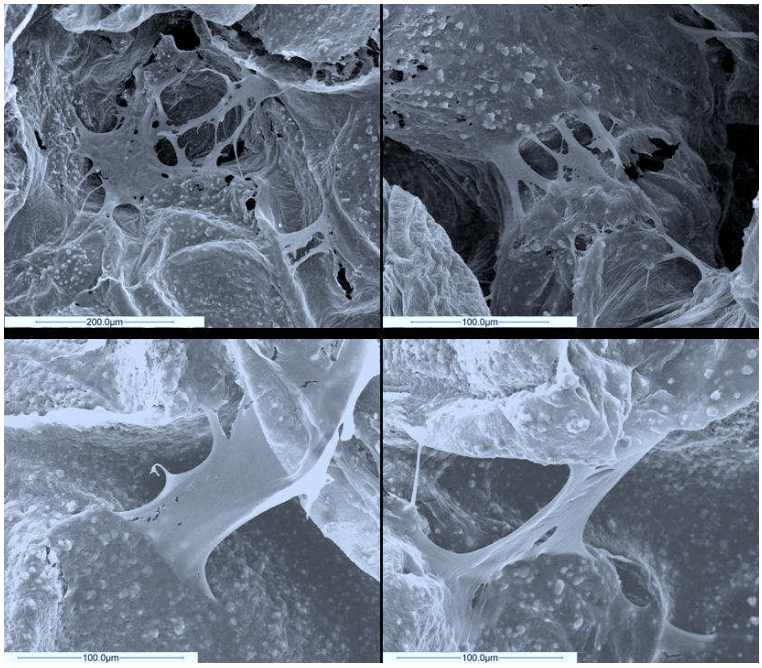

Fig. 3.14: SM-derived cells spreading onto micro/macroporous PCL at 2 weeks: cells are elongated, connected to each other and a few enter the macropores

At 2 weeks Cells were multilayered with evident cytoplasmic filopodia providing intercellular communication, and a consistent extracellular network underneath. SEM images reveal that many anchoring processes were observed extending from cells to the biomaterial surface, as well to other cells. Cytoplasmic prolongations going deeper in the pores of the polymeric matrix are observed.

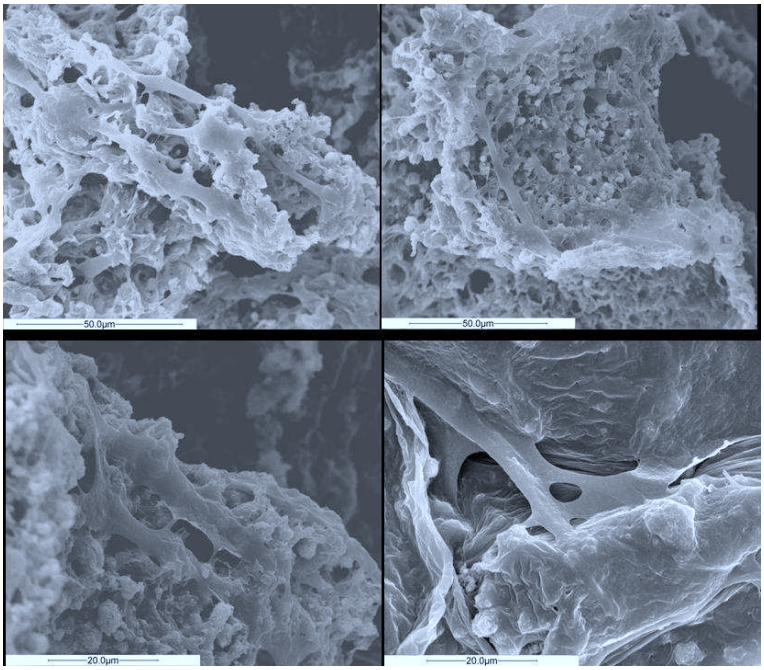

Fig. 3.15: for higher magnification it's possible to seethe formation of cell layer on Scaffold's surface.

At higher magnification it's possible to notice the formation of a cell layer on PCL evidences a significant proliferation of adhered cells up to 2 weeks, and the release of alkaline phosphatase, is consistent with osteoblastic maturation on the scaffolds.

3.5 Conclusions

We have developed a method of producing three dimensional, open-cell, composite foams of PCL and hydroxyapatite particles. The composite scaffolds with porosity 80% were fabricated using PI/SL (phase inversion/salt leaching) method. This method allows efficient exposure of HAP at the surface of polymer/bioceramics composite scaffold as Sem analysis show. So PI/SL scaffolds can increase the chances of osteogenic cells to make contact with the bioactive ceramics, which enhances osteoblast differentiation and growth. Moreover composite scaffolds exhibit enhanced mechanical properties showing higher compressive moduli as compared to the PCL scaffolds. It was found that by incorporating 20 wt% HAP in the scaffold, the compressive modulus increased from 0.07 of the PCL sample to 0.2 MPa. So the mechanical strength was found to be dependent on the filler in the scaffold while porosity and thermal property of the scaffolds seem to be not much affected from HAP particles as SEM images and µ-CT

analysis demonstrate. Although the PCL/HAP composite scaffolds showed higher mechanical properties, as compared with the PCL scaffolds, the measured compressive moduli of the prepared scaffolds is rather low compared to that of human bone. This might be due to the highly porous structure of the fabricated scaffolds and the poor mechanical properties of the PCL itself, even after reinforcement with HA. Therefore, the fabricated scaffold could be applied in non load-bearing parts. More importantly, the composite was developed not only to improve enhance the mechanical properties but also to improve the overall biological response to the scaffold by creating a bioactive substrate that could ultimately integrate with bone tissue. Cellular response and bioactive potential of the 3-D, porous composite were evaluated *in vitro* by culturing the scaffold with human sinovium-derived MSCs for to 2 weeks. It was found that the PCL/HAP composite scaffolds supported the synthesis of alkaline phosphatase, in addition to the adhesion and proliferation of Human Sinovium-derived MSCs. Furthermore, encouraging results are reached in the comparison between human bone marrow MSCs and MSCs from human-sinovial membrane. SM-derived cells treated with osteogenic medium underwent a change in their morphology from spindle shaped to cuboidal, (Figure 4A and 4B) and formed large nodules after 21 days and increased over time. Furthermore they were found more active on the composite, due to a higher value of absorbance in the MTT assay.

Acknowledgments

We would like to acknowledge Prof. D. Ronca and Prof. A. Oliva (Second University of Naples) for providing the Human Sinovium-derived MSCs and for all the biological evaluation and the DIMP (Department of Material Engineering and Production) for funding.

References

[1]. F. Ungaro, M. Biondi, L. Indolfi, G. De Rosa, M.I. La Rotonda, F. Quaglia, P. Netti, *Topic in Tissue Engineering*, **2005**, 2.

[2]. F. Quaglia, *International Journal of Pharmaceutics*, **2008**, 364, 281.

[3]. R, Langer, J.P. Vacanti, *Science*, **1993**, 260, 920.

[4]. V. Guarino, F. Causa, P.A. Netti, G. Ciapetti, S. Pagani, D. Martini, N. Baldini, L.Ambrosio, *Journal of biom. Mat. Res. Part B: Applied Biom.* **2008**, 86B, 2, 548.

[5]. V. Guarino, F. Causa, L. Ambrosio, *Expert review of medical devices*, **2007**, 4, 3, 405.

[6]. P.B. Malafaya, F. Sappers, R.L. Reis, *J. Mater. Res. Mater. Med.,***2006**, 17, 4, 371.

[7]. V.J. Chen, L.A. Smith, P.X. Ma, *Biomaterials*, **2006**, 27, 3973.

[8]. F. Burkersroda, L. Schdl, A. Gopferich, *Biomaterials*, **2002**, 23, 4221.

[9]. D.S. Katti, S. Lakshmi, R. Langer, C:T. Laurencin, *Adv. Drug Deliv. Rev.*, **2002**, 54, 933.

[10]. M. Navarro, D. della Valle, S. Martinez, *Biomaterials*, **2004**, 25, 4233.

[11]. H.K. Hu, M.D. Weir, E.F. Burguera, A.M. Fraser, *Biomaterials*, **2006**, 27, 4279.

[12]. E. Damien, P.A. Revell, *J. Appl. Biometer. Biomech.,* **2004**, 2, 65.

[13]. D.W. Hutmacher, *Biomaterials,* **2000**, 21, 2519.

[14]. F. Causa, P.A. Netti, L. Ambrosio, G. Ciapetti, N. Baldini, S. Pagani, D. Martini, A. Giunti. *J. Of biom. Mat. Res. : Part A:* **2006**, 76, 1, 151.

[15]. J.M. Williams, A.A Dewunmi, R.M. Scheka, C.L. Flanagana, P.H. Krebsbacha, S.E. Feinbergd, S. J. Hollistera, S. Das, *Biomaterials*, **2005**, 26, 4817.

[16]. H.Y. Kweon, M.K. Yoo, I.K. Park, T.H. Kim, H.C. Lee, Hyun-Sook Lee, Jong-Suk Oh, T. Akaike, Chong-Su Cho, *Biomaterials*, **2003,** 24, 801.

[17]. R.S. Bexwada, D.D. Jamiolkowski, I. Lee, A. Vishvaroop, J. Persivale, S. Treka-Benthin, M. Erneta, J. Suryadevara, A. Yang, S. Liu, *Biomaterials,* **1995**, 16, 1141.

[18]. D. Rohner, D.W. Hutmacher, T.K. Cheng, M. Oberholzer, B. Hammer, *J.*

Biomed. Mat. Res. Part B, **2003**, 66, 574.

[19]. K.A. King, S.M . Best, K.E. Tanner, P.A. Revell, W.Bonfield, *Proc. Instn. Mech,* **1998**, 212,6,437

[20]. S.F. Elbert, J.A. Hubbel, *Annu. Rev. Mater. Res. ,* **2001**, 31, 183.

[21]. H.W. Kim, J.C. Knowles, H.E. Kim, *Biomaterials*, **2004**, 25, 1279.

[22]. J.A. Hubbell, *Biotechnology*, **1995**, 13, 565.

[23]. D. Campoccia, P. Doherty, M. Radice, P. Brun, G. Abatangelo, D. F. Williams, *Biomaterials*, **1998**, 19, 2101.

[24]. P.B. Van Wachem , M.J.A. Van Luyn, P. Nieuwenhuis , H.K. Koerten, L. Olde Damink, H. Ten Hoopen, J. Feijen. *Biomaterials*, **1991**, 12, 215.

[25]. A. Rastrelli ,M. Beccaro , F. Biviano ,G. Calderini , A. Pastorello, *Clin. Implant Mat.*, **1990**, 9, 199.

[26]. V.R. Sinha, K. Bansal, R. Kaushik, R. Kumria, A. Trehan, *International Journal of Pharmaceutics*, **2004**, 278, 1.

[27]. D.W. Hutmacher, T. Schantz, I. Zein, K.W. Ng, S.H. Teoh, K.C. Tan, *Jornal of Biomedical Material Research*, **2001**, 55,2, 203.

[28]. P. Ducheyne, Q. Qiu, *Biomaterials*, **1999**, 20, 2287.

[29]. E. Fernandez, F.J. Gil, M.P. Ginebra, F.C.M Driessens, J.A. Planell, , *J. of Mat. Sci. Mat. In Med*, **1999**, 10, 169.

[30]. M.P. Ginebra, E. Fernandez, F.C.M Driessens, M.G. Boltong, J. Muntasell, J. Font, J.A. Planell, *J. of Mat. Sci. Mat. In Med. ,* **1995**, 6, 857

[31]. P.W. Brown, N.Hocker, S. Hoyle, *J. Amer. Ceram. Soc.,* **1991**, 74, 1848.

[32]. H. Chim, D.W.Hutmacher, A.M. Chou, A.L.Oliverira, R.L. Reis, T.C. Lim, J.T. Schantz, *Int. J. Oral. Maxillofac. Surg.,* **2006**, 35, 928.

[33]. M. Neumann, M. Epple, *European journal of Trauma,* **2006**, 32,2 125.

[34]. J.F. Mano, C.M. Vaz, S.C. Mendes, R.L. Reis, A. M. Cunha, *journal of Materials Science: Mat. In Med,* **1999**, 10, 857.

CHAPTER 4

HYAFF11® loaded scaffolds for Bone regeneration.

4.1 Introduction

4.1.1 Design of multifunctional scaffolds

Permanent implants into tissue almost always elicit a chronic inflammation called a foreign body response. This response is characterized by formation of a poorly vascularised fibrous layer analogous to a scar at the material tissue interface. The foreign body response is typically benign and sometimes desirable to anchor devices into host tissue, but leads to enough clinical complications (e.g. infection, tissue contraction) that it is considered a risk to be avoided if possible in many applications [1][2]. It is obvious from the recent literature on clinical engineering that there is an increasing interest in resorbable biomaterials with specific biological properties and good biocompatibility profiles that resorb or degrade in body fluids so that the device ultimately disappear with no ill effects [3][4]. Much of this interest has been stimulated by recent breakthroughs in tissue-engineering techniques, where resorbable scaffold materials are used as a support matrix or as a substrate for the delivery of cultured cells or for three-dimensional tissue reconstruction [5]. In this context the syncronization of polymer degradation with its replacement by natural tissue produced from cells would be desiderable [6]. The influence of several factors on degradation kinetics may be considered, including molecular factors (e.g. chain orientation, molecular weight, and polydispersity), supramolecular factors (cristallinity, the spatial distribution of chemically reactive filler) and environmental factors (mechanical stimuli) to potentially generate wide range of resorbable properties for custom-made system. So the degradation properties of a scaffold are relevant both to the biomaterial design and to the long-term success of a tissue engineered construct [7]. Biodegradable synthetic polymers offer a number of advantages over other materials for developing scaffolds in tissue engineering [8] and they have been used in a number of clinical application. Among the families of synthetic polymers, the polyesters have been attractive for these applications because of their ease of degradation by hydrolysis of ester linkage,

degradation products being resorbed through the metabolic pathways in some cases and the potential to tailor the structure to alter degradation rates. Over the last two decades, biodegradable polyesters, such as poly(lactic acid) PLA, poly(glycolic acid) PGA and poly(ε-caprolactone) PCL, have emerged as a class of biomaterials of growing interest for application in surgery, drug delivery and tissue engineering [9][10]. They exhibit predictable and reproducible mechanical and physical properties, such as tensile strength, elastic modulus and degradation rate under controlled conditions [11]. A key consideration in scaffold design is that the complex composition and structural organization of hard mineralized tissues, such as bone, cannot be replicated using a single material offering a limited range of properties [12]. In particular, scaffolds for bone regeneration have to provide a highly interconnected porous structure to guide cell in growth for tissue formation, whereas maintaining a sufficient mechanical strength to supply the structural requirement of the substituted tissue [13]. To date, the employment of composite materials may be a good solution, achieving the ideal balance between strength and toughness due to the improvement of specific characteristics of the composite compared to its separate components [14]. However, the need of scaffold materials to be porous, biocompatible and biodegradable, and to exhibit a degradation or resorption rate similar to the rate of tissue replacement, is often in conflict with the possession of adequate mechanical properties able to match those of the tissues at the site of implantation [15]. To date, several studies have examined the use of bioceramic particles such as silica, HA or other calcium phosphates in combination with biodegradable polymers like poly ε-caprolactone (PCL) to produce bone substitutes [14]. However, most results taken from previous studies reveal that, while the incorporation of a ceramic phase improved the bioactivity of the polymeric scaffold, this advantage is not usually combined with a commensurate enhancement of the mechanical properties of the composite [16]. Recently, Guarino et al. [12] proposed an alternative composite tubular structure. This is obtained by the merging of a PCL matrix with continuous fibres of PLLA helically wound by the filament winding technique. By applying the basic theory of continuous fiber-reinforced composites to the scaffold design, a composite material has been

developed with an optimal spatial organization of fibers within the polymer matrix, able to mimic the structural organization and performance of the living tissue.

One common belief among many scientists trying to develop new biocompatible biodegradable polymers has been that these should be natural molecules or, alternatively, analogues of natural polymers, which should release degradation products that enter the normal metabolic pathways, rather than being xenobiotic. One first approach considered polymers which undergo hydrolytical degradation producing metabolites normally present in the physiological environment [23]. Analogs of the extracellular matrix have been produced from collagen and glycosaminoglycans which are widely and abundantly distributed in the body, but in order to achieve a certain stability of the device, it has often been necessary to modify these natural molecules chemically. However, in a number of cases concern has been expressed for the potential toxicity of some of the crosslinking agents utilized, such as glutaraldehyde, formaldehyde and isocyanates [24]. An alternative solution to produce insoluble molecules starting from natural components was explored in the mid 1980s and led to the development of hyaluronan esters [19]. Hyaluronan-based polymers applied to tissue defects provide an appropriate scaffolding and favourable microenvironment for the regeneration process. the integration of highly degradable materials, obtained by chemical modification of purified hyaluronan (HA) namely HYAFF11®, formed by the partial or totally esterification of carboxyl group of glucuronic acid provides the opportunity to affect directly the cell activities, favouring the adhesion of certain cell types [23][20][21]. Here, partially esterified HYAFF11® (esterification degree 75%) has been selected for its optimal hydrophilic/hydrophobic character which confers an adequate biological recognition and it has been used in combination with a composite scaffold obtained by incorporating poly(L-lactide) (PLLA) continuous fibers within a PCL matrix through the synergic combination of phase inversion/salt leaching technique and the filament winding technology. The combination of phase inversion with salt leaching assures highly porous structures with a pore volume fraction exceeding 80% of total volume and a bimodal pore distribution [22] , while filament winding technology is a powerful instrument to produce composite polymers with improved mechanical response in compression and tailored degradation kinetics

[6]. In addition to fibre reinforced scaffolds polymeric composite structure of PCL and ester of hyaluronic acid have been prepared with the salt leaching/phase inversion technique encouraging by the biological result which similar system have exhibited as *in vivo* scaffold for tissue regeneration.

A morphological investigation involving the porosity assessment was performed by using scanning electron microscopy, and micro computer tomography analysis (μ-CT), whereas the degradation kinetics was investigated by thermogravimetry (TGA). Mechanical properties were assessed trough static and dynamic mechanical tests while *in vivo* tests were performed in collaboration with Orthopaedic institute Rizzoli in Boulogne as preliminary studies of material-tissue interactions.

4.1.2 Biodegradable polymers

Degradable polyesters derived from three monomers lactide, glycolide, and caprolactone are in common clinical use and are characterized by degradation times ranging from days to years depending on formulation and initial Mw. Over the last two decades biodegradable polymers, such as poly(lactic acid) PLA, poly(glycolic acid) PGA and poly(ε-caprolactone) PCL, belonging to the family of poly(α-hydroxyesters), have emerged as a class of biomaterials of growing interest for application in tissue engineering. With the exception of polyglycolide (PGA), the polymers in this family are soluble in many common organic solvents and thus can be processed by a variety of thermal and solvent-based methods [23]. They are insoluble in water but degrade by hydrolytic attack of the ester bond. Many studies suggests that these polymer are sufficiently biocompatible, non toxic and non-inflammatory. Because of their chemical and structural similarities, they degrade in similar way through ester hydrolysis processes and decarboxylation from the chain ends, assuring their complete removal from the body.

PLA is present in three isomeric forms d(-), l(+) and racimic (d,l) and the polymers are usually abbreviated to indicate the chirality. Poly(l)LA and poly(d)LA are semi-crystalline solids, with similar rates of hydrolytic degradation. For most application the (l) isomer of lactic acid is chosen because it is preferentially metabolized in the body. PLA degrades through random hydrolysis of their ester bonds to form lactic acid which is normally present in the body. This acid then enters tricarbolxylic acid

cycle and is excreted as water and carbondioxide. The rate of degradation however is determined by factors such as configurational structure, copolymer ratio, cristallinity, molecular weight, morphology, stresses, amount of residual monomer, porosity and site of implantation [24][25]. PCL is a semycristalline polymer with a glass transition temperature of about -60°C. The polymer has a low melting temperature (59 to 64°C) and is compatible with a range of other polymers. PCL shows a remarkably slow degradation rate – from 6 months up to 3 years for its complete removal form the host body – as a function of the starting molecular weight [26][27]. The long-term degradation follows a two-step mechanism: a random hydrolytic ester cleavage and weight loss through the diffusion of oligomeric species from the bulk Firstly this preserve mechanical integrity over the degradation lifetime of the devices, so allowing adequate mechanical support during the post-implantation period. Secondly the absence of toxic response assures bone ingrowth into the porous scaffold [6]. In the recent history of biompolymers, different molecular engineering have led to the development of a variety of modified natural polymers aimed at reaching the highest level of compatibility in the physiological environment [28]. HA could certainly find additional uses, particularly in the biomaterials field, but some physical and biological characteristics of hyaluronan in its purified form, such as water solubility, rapid resorption and short residence time in the tissue, limit its possible applications. For this reason, several attempts have been made to modify its molecular structure to obtain a more stable solid material. An alternative solution to produce molecules starting from natural component was explored in the 1980 and led to the development of hyaluronan ester [29][23]. Cross linking and coupling reaction were two of the ways considered to obtain a modified stable form of HA. In particular our attention has been focused on HYAFF®, another class of hyaluronan derivate polymers obtained by a coupling reaction. This esterification reaction improve the stability of the polymer without altering so much its biological characteristic [30]. This chemical modification acts both by reducing the hydrophilic, negatively charged, carboxyl groups and increasing its hydrophobic components.

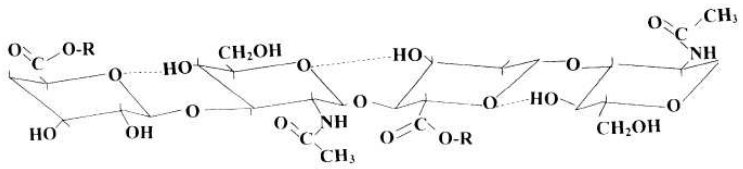

Fig. 4.1: The structure of the total benzylic hyaluronan ester Hyaff®11. [30]

It was found that the higher the percentage of esterification of hyaluronan, the lower its solubility in water. Examining in detail the properties of benzyl and ethyl HA, the derivatives where 100% of the carboxyl groups are esterified (benzyl and ethyl total esters), it emerges that they are insoluble transparent materials which can be extruded into thin membranes [31]. Examining the materials behaviour in aqueous solution, the total benzyl ester (HYAFF®11) showed only slight hydration when placed in buffered phosphate saline solution. In the case of 75% hyaluronan benzyl and ethyl esters (respectively HYAFFA' 11p75 and HYAFF' 7p75) hydration was even greater, reaching up to 1250% of weight increase with respect to the dry conditions [23]. In this work partially esterified HYAFF®11p75 (esterification degree equal to75%) has been used for its optimal hydrophilic/hydrophobic character which confers an adequate biological recognition, without drastically penalizing the structural integrity of the composite scaffold.

4.2 Materials and Methods

4.2.1Materials

Poly(ε-caprolactone) (PCL, MW 65 kDa) and PLLA fibres (75 D-tex) were purchased, respectively, from Sigma–Aldrich and Sofradim companies. A benzyl ester of hyaluronic acid with 75% of esterification degree (HYAFF11®-75p) supplied by Fidia Advanced Biopolymers in powder form. Tetrahydrofurane (THF) and dimethylsulfoxide (DMSO) have been purchased from Sigma Aldrich . Sodium chloride crystal (Fluka AT>99.9%) were sieved in specific size range depending on scaffold type (212-300μm and 300-500 μm). A mixture of $Ca_2NaK(PO_4)_2$ (CSPP) and, monocalcium phosphate monohydrate (MCPM) were supplied by Technical Univeristy of Catalunia (UPC) under the name of R-cem.

4.2.2 Fibres reinforced scaffold preparation

Poly ε-caprolactone pellets (MW 65 kDa) were dissolved in a solvent mixture to form a solution by stirring for 3 h at room temperature using a PCL/solvents ratio equal to 12/88 wt/wt. Two different solvents were used, respectively, tetrahydrofurane and dimethylsulfoxide by 80/20 weight ratio. HYAFF11 was then mixed to the polymer solution imposing a PCL/HYAFF11 weight ratio equal to 80/20. NaCl crystals with specific size ranges (300-500μm) were employed as templating agents and the PCL/NaCl volume ratio(32/64 v/v) was selected in order to optimize the fibre/matrix adhesion. Finally fiber reinforced composite scaffold (PHF) were obtained by combining the phase inversion/salt leaching and filament winding technology. Briefly, PLA fibres impregnated through the PCL/HYAFF11 solution, were wound on a polypropylene tubing coated stainless steel mandrel with 1 mm diameters by using a specific winding parameters set (winding angle WA = 45°, winding pitch WP = 500 μm). In order to improve the surface finishing and to give a more regular shape to the scaffold, a teflon round mold has been employed as showed in figure 2.

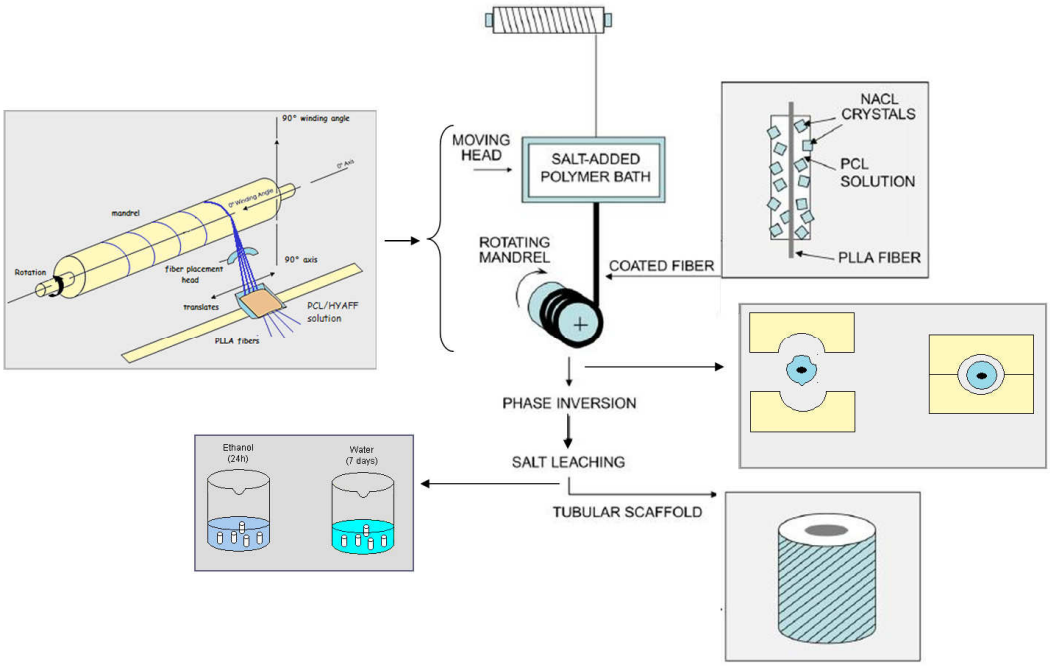

Fig. 4.2: Scheme of the filament winding procedure used to prepare PLLA fibre-reinforced scaffolds

Once tubular shaped scaffold was obtained, conventional procedures involving ethanol and water washings, for 24 h and 7 days, samples with 5 mm as outer diameter and 10 mm as height were employed for morphological and mechanical characterization. For the *in vivo* test PHF samples have been employed with the following dimension: 16 mm as outer diameter, 4 mm as inner diameter and 20 mm as height taking care to the external surface finishing.

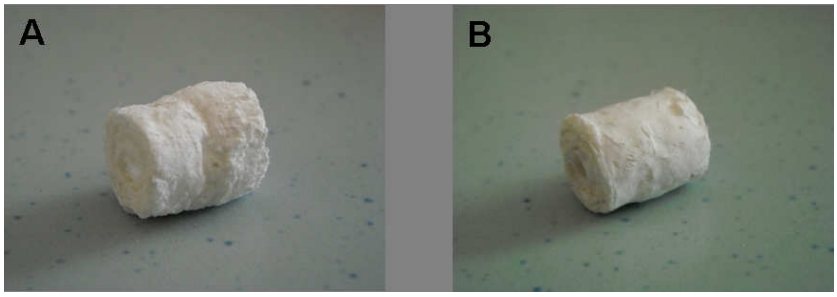

Fig. 4.3: comparison of unrefined (A) and refined (B) surfaces of PCL/PLLA scaffolds.

4.2.3 Calcium phosphate composite scaffolds preparation.

Poly ε-caprolactonepellets (MW 65 kDa) were dissolved in a THF/DMSO (80/20 wt/wt) solution by stirring for 3 h at room temperature. The benzyl ester of hyaluronic acid (HYAFF11 - 75p) in powder form was then mixed to the polymer solution imposing a PCL/HAYFF11 weight ratio equal to 80/20 (wt/wt). NaCl crystal with specific size ranges (212-300μm)were employed as templating agent by using a PCL/NaCl weight ratio equal to (1/9 wt/wt). Furthermore, a mixture of of $Ca_2NaK(PO_4)_2$ (CSPP) and, monocalcium phosphate monohydrate (MCPM) under the name of R-Cem have been used as reinforcing agent.

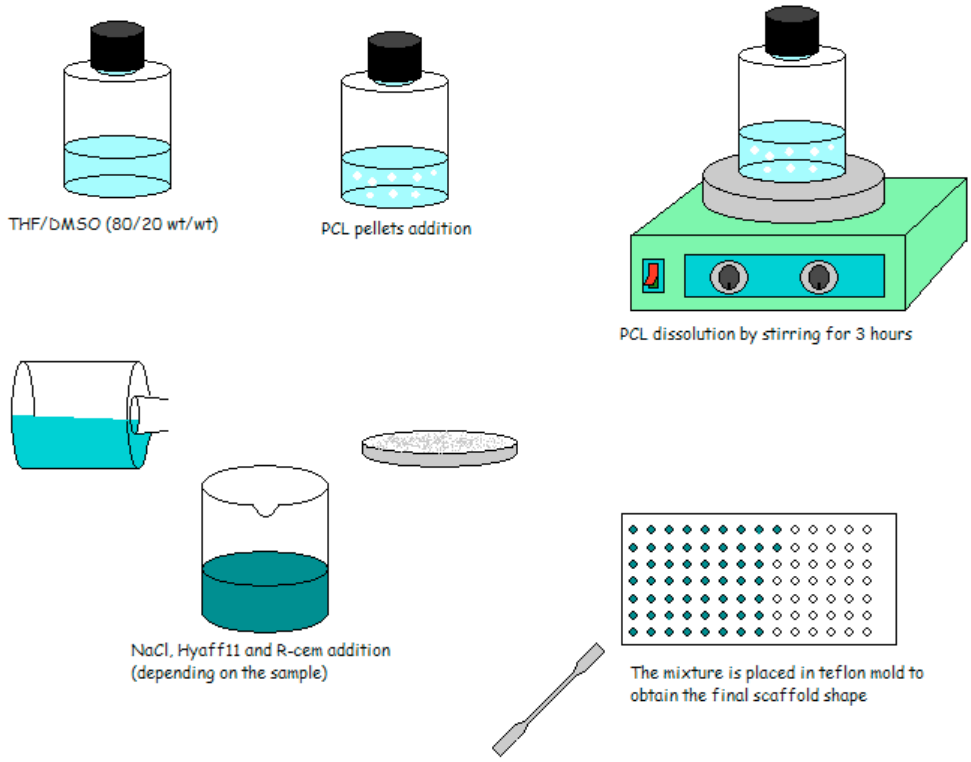

Fig. 4.4: scheme of the salt leaching/phase inversion tecnnique used to prepare PCL/HYAFF11/R-Cem composite scaffolds. preparation

Two different PCL and HYAFF11 scaffold based composite have been prepared with the salt leaching/phase inversion technique, labelled respectively as PHS and PHRS. The PHS type was developed from the PCL/HYAFF11 solution described above. After NaCl crystal incorporation the mixture was placed into Teflon moulds reproducing the final cylindrical shape, 5 mm as diameter and 10 mm as height, of the scaffold. Finally, ethanol washing for 24 h at room temperature were performed to completely extract the used solvents whereas daily washing in bi-distilled water for 7 days were used to leach out NaCl crystals as well to remove other contaminants.

4.2.4 Morphological investigation by SEM and μ-CT analysis

Scaffold morphology was investigated via Scanning Electron Microscopy using a scanning electron microscope (Stereoscan 440, Leica, UK). Briefly, specimens were cut using a razor blade along preferential directions, parallel and perpendicular to the surface, respectively. The resulting transverse and longitudinal sections were gold-coated under vacuum by using an automatic coating sputter set at 15 mA for

about 20 min (Emiscope SC500, Italy). The porosity was assessed in terms of pore size, shape and spatial distribution by images at different magnifications. Structural analysis waas performed by micro-computed tomography (μCT) using a Skyscan 1072 scanner at 11.1 μm resolution . Scanning was done at X-ray tube voltage of 54 kV and a current of 136 μA.

After reconstruction using Skyscan CT-analyser and CT-Volume software, thresholded isosurfaces images were obtained. The software was also used to generate pore size distribution maps of the structures. The maps were used to calculate porosities and pore size distribution.

4.2.5 Thermal analisys

The DSC thermograms were performed by a DSC Q20 (TA Instruments) equipped with a nitrogen cooling unit. All measurements were performed in a helium atmosphere using standard crimped aluminum pans. Samples, with average weights of 2 mg, were scanned at a heating rate of 10 °C min till 250°C. Four type of samples were analyzed: PS, PHS, PHRS, PHF. The melting temperature, Tm,and the enthalpy of fusion were determined from the peak value of the endotherms peak. Thermal gravimetric analysis (TGA) was performed on a TA Instrument Q 5000 under nitrogen atmosphere, from room temperature up to 700 °C, with a heating rate of 10 °C/min.

4.2.6 Mechanical properties of porous structures

Mechanical test in compression was done using a dynamometric machine (Instron 4204) equipped with a load cell of 1 kN and requiring a crosshead speed of 1mm/min. Porous cylindrical specimens characterized by a height of 10 mm and a diameter of 5 mm were fabricated according to the ASTM 695/2a standard. The stress and modulus response to strain were recorded. The elastic modulus E' has been calculated as the slope of the tangent to the initial linear portion of the deformation curve. Dynamic mechanical analysis (DMA) was performed using a Bose Electroforce Biodynamic system applying a sinusoidal stimulation on the test specimen. The DMA results are presented in terms of three main parameters: storage modulus (*E'*), loss modulus (*E''*), and mechanical loss tangent (tan δ). The

cyclic stimulation was originated by a sinusoidal stress with dynamic amplitude of 0.5 N spanning the frequency from 0.1 to 6 Hz in order to simulate the native microenvironment of bone tissue.

4.2.7 In vivo test

Three different sample typologies have been used for the *in vivo* test PHRF (PCL/hyaff/R-Cem + PLLA fibres) , PHRF with PRP (Platelet rich Plasma) and BMSCs (Bone marrow mesenchimal stem cells), PHRF with BMP7. Implants were cut in cylindrical shape with the following dimension: 20mm length, 16 mm external diameter and 4 mm internal diameter and were sterilized with ethylene oxide.

Fig. 4.5: Shape and sterilization procedure for the PHF scaffolds used in the *in vivo* test.

A 20mm critical-size bone defect was created in the sheep metatarsal bone and scaffold was impanted. An osteosynthesis stainless plate to stabilize the site of fracture. Rabbits were anesthetized by intramuscular injection of a mixture of ketamine hydrochloride and xylazine. The metatarsal bone was exposed any bleeding was carefully controlled. All debris was removed from the defect with a curette, and the edges were carefully refined. The implants were then pressfit into the defect and the fracture site was stabilized by the stainless steel plate. The skin was closed with double with a continuous 4-0 dexon suture.

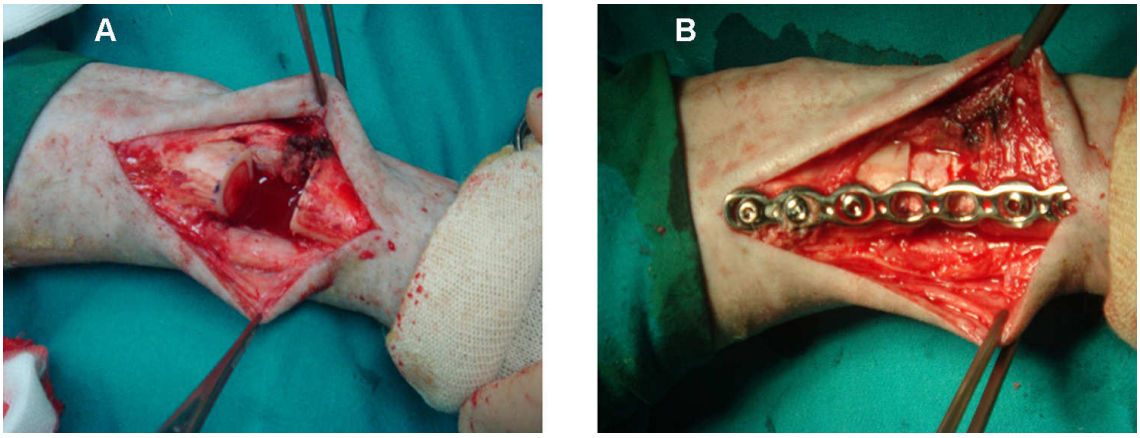

Fig. 4.6: PHF scaffold's implantation in a 20mm critical-size bone defect in the sheep metatarsal.

Ships were euthanized at 12 weeks after surgery by intravenous overdose of sodium pentobarbital. The implants were removed and they were then dehydrated in graded series of alcohols until the absolute was reached. They were stained with Fast Green and acid fuchsin and were processed for routine histological and histomorphometric analyses by using a transmission and polarized light Microscope at various different magnification. To determine bony ingrowth within a certain frame of time, all animals received a polychrome sequential labeling with 2 different spectrophotometric methods. Alizarin red and Xylenol in order to confirm the osteogenic activity.

4.3 Results and discussion

4.3.1 Scaffold morphology

The preliminary investigation of the structural architecture of composite scaffolds was made by SEM. In each case, high structural porosity, characterized by a bimodal pore size distribution, was observed. In the case of PHS and PHRS, cross-section images indicate a homogeneous spatial distribution of macropores of undefined shape and with sizes ranging from 150 to 400 μm.

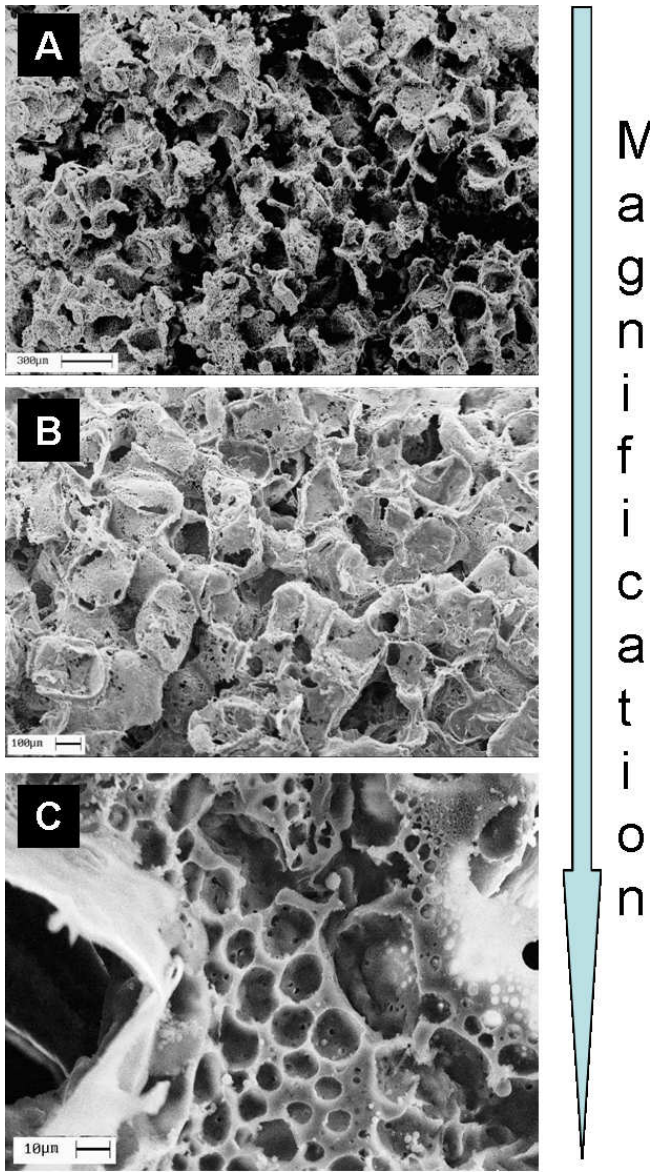

Fig. 4.7: Microporosity of PCL/HYAFF11/R-Cem-based composite scaffolds by SEM analysis at different magnification: A) 100X, B) 150X, C)1000X

A more accurate investigation of scaffold morphology by FE-SEM allowed investigation of the distribution of different polymeric and ceramic phases into the scaffold matrix as a function of the chemical and physical properties highlighting the presence of the HYAFF11 hydrophilic phases (dark gray) embedded in the PCL hydrophobic matrix (light gray).

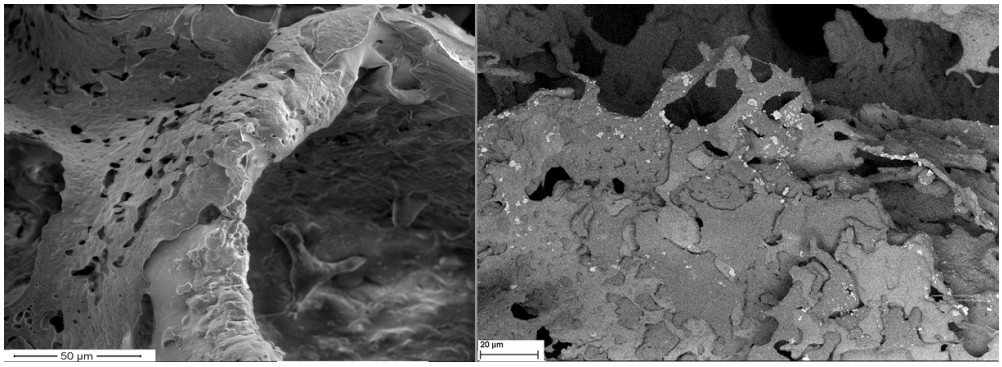

Fig. 4.8: Morphology of PCL/HYAFF11®-based composite scaffolds by FE-SEM analyses. Detection of hydrophilic HYAFF11® (dark gray) patches onto the hydrophobic PCL (light gray)

For the fibre reinforced samples a more ordered structural organization is observed with PLLA fibres were well integrated into the PCL matrix without any significant alteration of pore morphology. PHF samples show a bimodal porosity characterized by two different pore size: a microporosity with small pore sizes ranging 1–10 µm and a macro-porosity with 100–400 µm pore size have been distinguished. Marked differences in micro - and macropore morphology are also apparent on comparing scaffolds with and without fibres. More specifically, a reduction in macroporosity as well as concomitant increase in microporosity have been revealed in the case of PHF, ascribable to the different amount of templating agent and polymer solution concentration used during the preparation.

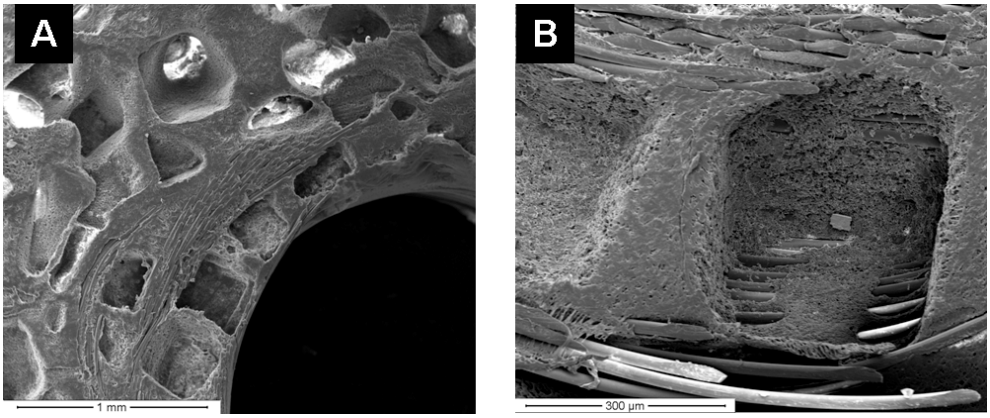

Fig. 4.9: SEM analysis of fibre-reinforced composite scaffolds at different magnification: (A) pore morphology (120X) and (B) organization of PLLA fibres inside porous PCL matrix(420X)

As support of the qualitative investigation on scaffold morphology, a quantitative evaluation of porosity, pore size distribution and specific surface area was measured by µ-tomographic analysis. First, the stack of X-ray images radiographs was rendered as planar 2-D slices in order to describe the scaffold architecture. Afterwards, the volume rendering was carried out to assess basic porosity parameters in the three-dimensional space. Figure A and B depicts a µ-CT reconstruction of two different structures respectively PHRS and PHF.

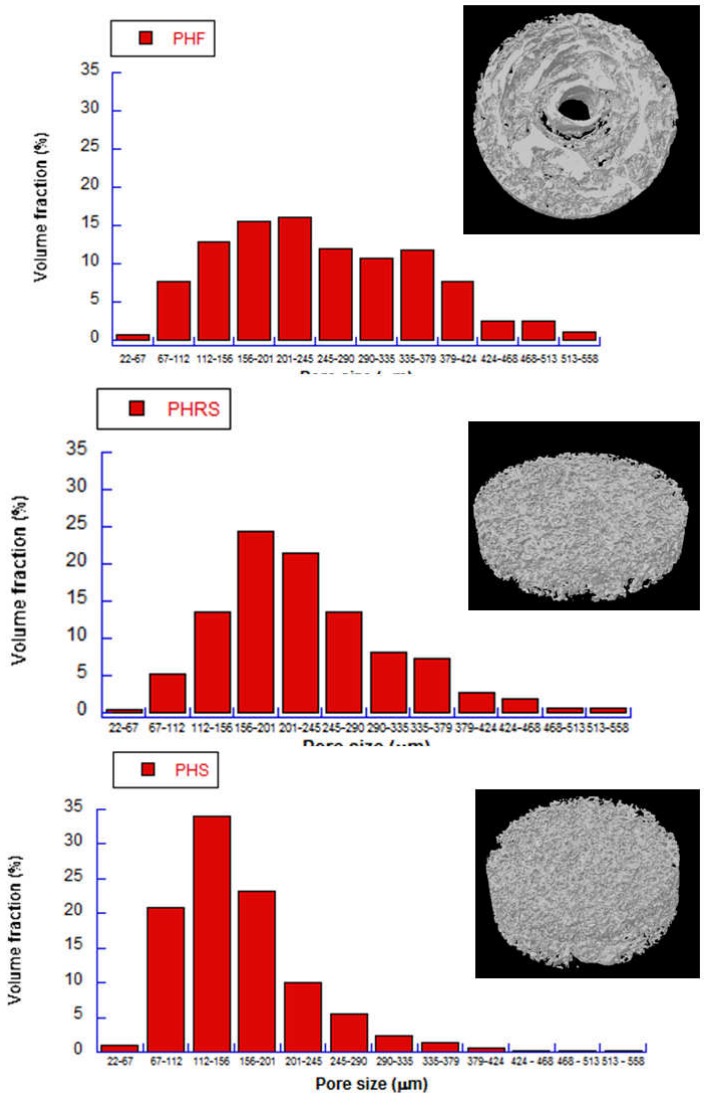

Fig. 4.10: differences in pore size distribution between reinforced PCL composite scaffolds :A) PHF, B) PHRS and C) PCL/HYAFF11 unreinforced structure.

Micro CT images confirm the preliminary indications obtained by SEM regarding pore size and spatial distribution of pores. It is apparent that the prepared scaffolds is highly porous with an irregular interconnected porosity. The µCT data can also be used to quantify relevant scaffold parameters.

	Porosity (%)	**Specific surface area** (mm^{-1})	**Average pore size (µm)**
PHS	79,4 ± 1,4	52,59 ± 1.94	132 ± 3
PHRS	78,5 ± 0,5	44.97 ± 0,72	140 ± 3
PHF	69,2 ± 0,8	29.09 ± 4.04	219 ± 3

Tab. 4.1: comparison between structural parameters of PHS, PHRS and PHF samples. All structure show high porosity degree and high value of specific surface area.

In Table 1, a summary of porosity features for the different scaffolds is reported. Porosity degrees ranged from 75.5 to 87.8%, pore sizes from 170.5 to 230.4 μm and high value of specific surface area. This result assure that scaffold provide high surface areas for cells adhesion and proliferation and fully interconnected porosity that allows vascularisation, tissue ingrowth and adequate nutrient transport.

Pore size distribution maps highlight structural differences between the PHRS and PHF samples. Fibre reinforced samples PHF show a more homogeneously distributed macroporosity with a peak around 201-245μm. Moreover in the PHF structure is possible to find also a pores with dimension around 700-800μm. This is ascribable to the different dimension of templating agent used for this typology of structures.

4.3.2 Thermal analysis

Dsc thermograms of all the scaffold typologies are shown in figure. For all materials an endothermic peak was observed, whose enthalpy change was found to depend on PCL content and attributed to the melting of PCL. The melting temperature decreased to a small extent for the composite scaffolds, from 66.66 ºC for pure PCL to 63.70 ºC for the composite. PLLA composite scaffold shows two endhtoermic peak: the first one due to the melting of PCL and a smaller second one due to the melting of the PLLA fibres at 160 °C.

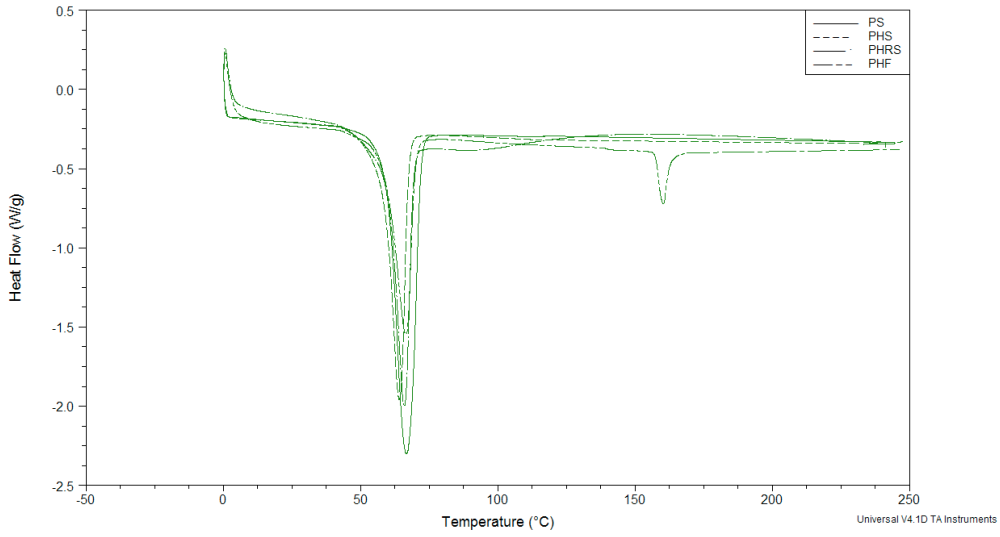

Fig. 4.12: DSC thermograms of PCL composites scaffolds

The value of melting temperatures as well as enthalpies are summarized in table

Sample	ΔH_f (PCL) (J/g)	ΔH_f (PLLA) (J/g)	T_f (PLLA)	T_f (PLLA)
PS	105.50	-	66.66	-
PHS	80.52	-	64.04	-
PHRS	70.78	-	64.41	-
PHF	60.39	7.91	63.70	160.26

Tab. 4.2:DSC results for all the four typologies of scaffolds

Thermogravimetric curves (TGA) of PCL and PCL composite are given in Figure . Thermal decomposition of each sample takes place in a programmed temperature range of 30-700ºC. In the case of PCL we have only one weight loss between 350 and 425 ºC due to the polymer degradation. For the PHS material we have a first weight loss between 60 and 100 ºC due to the heat of vaporization of water retained by the Hydrogel. The second weight loss between 200 and 300 ºC corresponds to the degradation of the Hyaff 11, finally the third weight loss between 350 and 400 ºC due to the PCL degradation. The same situation was also observed for the PHF scaffolds with the only difference that a further weight loss was registered between 250 and 300 °C due to the PLLA fibres degradation. For the calcium phosphate composite it is possible to recognize a certain percentage of material that doesn't degrades over 700 ºC. This mass retain over 700 ºC is due to the presence of R-Cem that is the mineral phase and doesn't degrade until 1000 ºC.

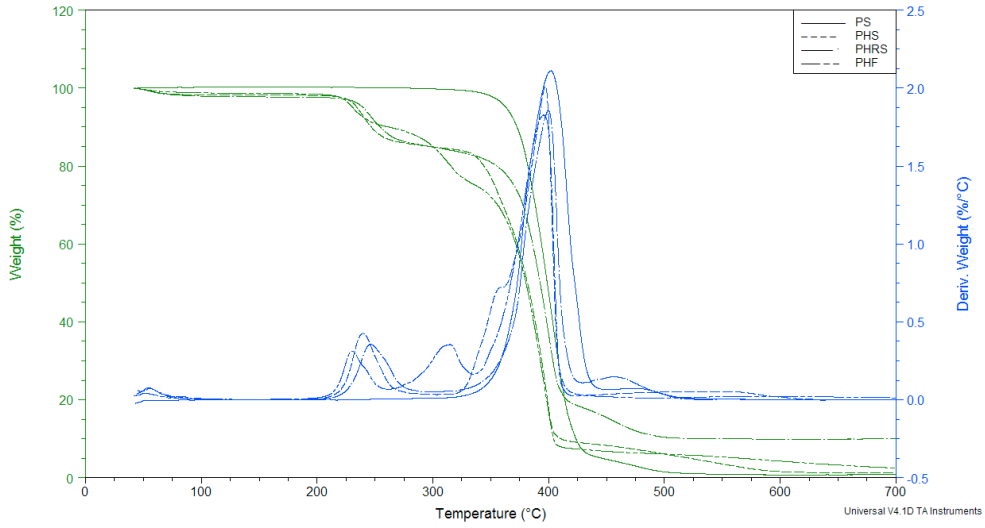

Fig. 4.11: Thermogravimetric curves of PCL composite scaffolds with relatives differences in derivates signal.

Below it is reported the percentage weight loss of pure PCL and composite PCL scaffold at different temperature.

Temperature range (°C)	PS (%)	PHS (%)	PHRS (%)	PHF (%)
30-100	0	1.7	2.5	1.2
200-250	0	13.1	12.9	8,6
250-330	0	0	0	14,7
330-450	98.9	83.3	73.5	60
Residue over 700	0.7	1	10	2,6

Tab. 4.3: Weight losses and decomposition temperatures in a programmed temperature range between 30 and 700°C

Looking at the value in the table a possible correlation between the weight loss and the initial composition of the structures can be drawn.

4.3.3 Mechanical properties

In order to observe the mechanical properties of the scaffolds, a compressive load was applied to each sample of dimensions 10mm height and 5 mm diameter. . Constant speed of 1mm/min were exerted until the final failure or densification occurred. Pure PCL scaffold was also tested for the purpose of comparison.

The static compression tests enabled to obtain the stress/strain curve of composite scaffolds. Firstly, it describes the mechanical behaviour of porous systems under static conditions: it shows a linear elasticity at low stresses followed by a long collapse plateau truncated by a regime of densification in which the stress rises steeply.

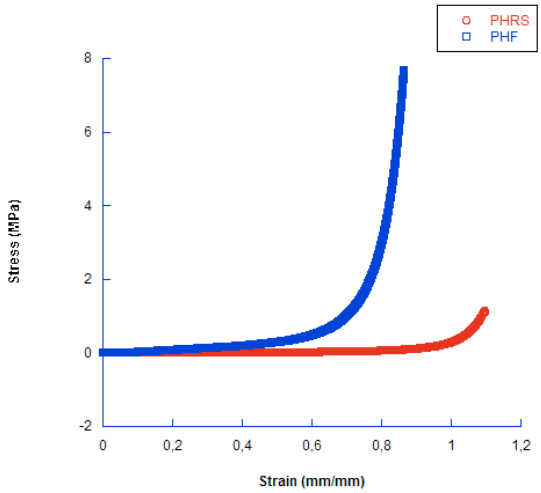

Fig. 4.12: stress strain curve of PHF and PHRS composite structure. PHF samples show better mechanical properties if compared with the calcium phosphate composite structure.

Unreinforced PS sample shows the lowest mechanical properties in the case of the elastic modulus is equal to 0.07 MPa. The addition of 13% vol hydroxyapatite particles to PCL matrix causes a small increase of elastic modulus (from 0.13 to 0.17 Mpa). Despite the addition of the R-Cem elastic modulus of the two samples remain comparable due to the high degree of porosity. For the fibre reinforced sample the elastic modulus rise up to one order reaching a value of 2.41 MPa. This increase is due either to the fibre reinforcement than to the lower porosity degree related to a more compact structure.

Tipo	PCL / NaCl	Modulo elastico (Mpa)
PHRS2	5 / 95	0.170 ± 0.025
PHS2	5 / 95	0.076 ± 0.027
PHF2	2/ 8	2.41 ± 0.55

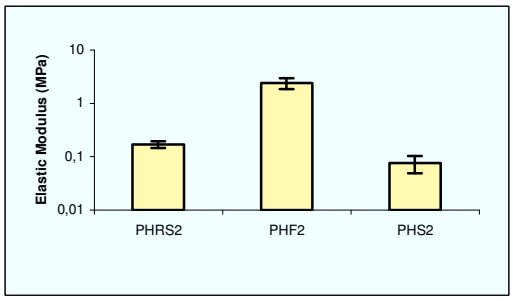

Fig. 4.13: evaluation of the elastic modulus as function of the type of reinforcement.

The evaluation of static curve is preparatory to the dynamic mechanical analyses. Indeed, the definition of the elastic range allowed to establish the average load and amplitude to apply for the cyclic stimulation.

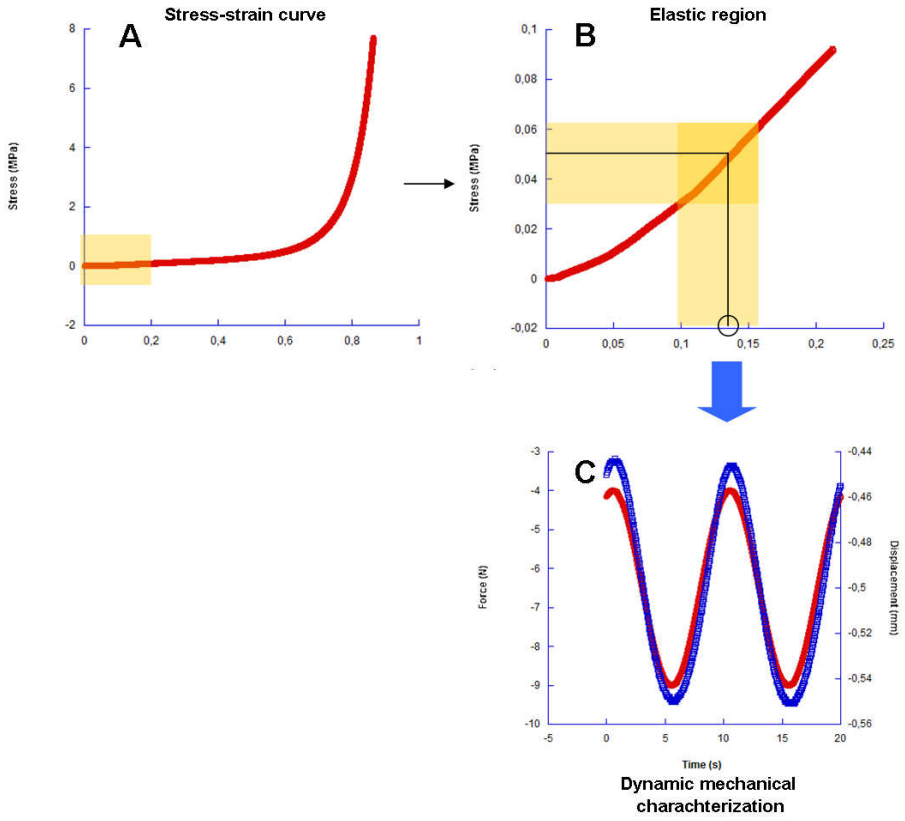

Fig. 4.14: scheme of different steps to analyze Dynamic mechanical properties: A) evaluation of linear region, B) detection of mean load value related to the elastic deformation of the sample, C) Load history imposed to the composite structure.

Dynamic tests confirm the result obtained by static compressive test. Fibres reinforced samples is much stiffer with a young modulus of 2.41 MPa, than PHRS as measured by static compressive test. The dynamic behaviour was described by the following viscoelastic moduli:

- The storage modulus: $E' = (\sigma_0/\varepsilon_0)\cos\delta$
- The loss modulus: $E'' = (\sigma_0/\varepsilon_0)\sin\delta$

In the proposed tests, the cyclic stimulation was originated by a sinusoidal stress with dynamic amplitude that has been evaluated from the elastic region of the stress-strain curve. All tests have been performed in water at body temperature in order to simulate the native microenvironment of bone tissue.

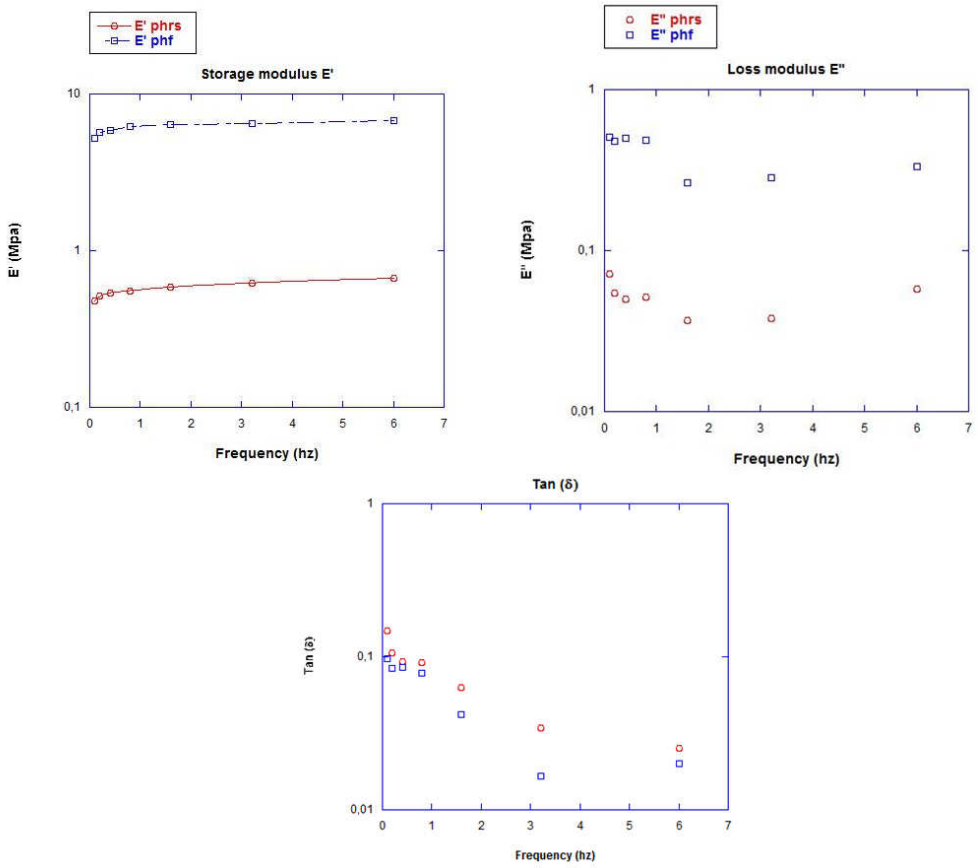

Fig. 4.15: Storage modulus, loss factor and damping of composite PCL based scaffolds in function of frequency.

Moreover the test highlights the viscoelastic behaviour of the samples showing that E' increases with frequency. Otherwise loss modulus E'' is not significantly affected as frequency varies. The evolution of elastic moduli was evaluated varying the frequency from 0.1 to 10 Hz. This enabled to estimate a comparative analysis of the storage modulus "E'" (elastic component) equivalent to the energy stored through deformation and the loss modulus "E''" equivalent to the energy dissipated through the cycled stimulation. Finally, the estimation of E'/E'' ratio (tanδ) allowed to directly visualize the relative contribution of elastic and viscous component at different frequencies, which participate to the viscoelastic behaviour of the scaffold. This study is a preliminary way to evaluate the material capability of stress transfer to cells in order to investigate the effect of mechanical stimulation on cell activities. Moreover from the dynamic characterisation it's possible to have indication about the mechanical behaviour of the sample for the *in vivo* test.

4.3.4 *In vivo* test

After 12 weeks implants were removed and prepared for the histological evaluation. Evaluation of the osseous implantation by light microscopy showed the biocompatible behaviour of all the three types of implants that did not evoke tissue inflammation or foreign body reaction in the surrounding bony tissue at the examined experimental times. As expected, the formation of new bone in the scaffold alone remained restricted to the edge of the defects and the largest part of the centre of the defect remained free of bone up to 12 weeks.

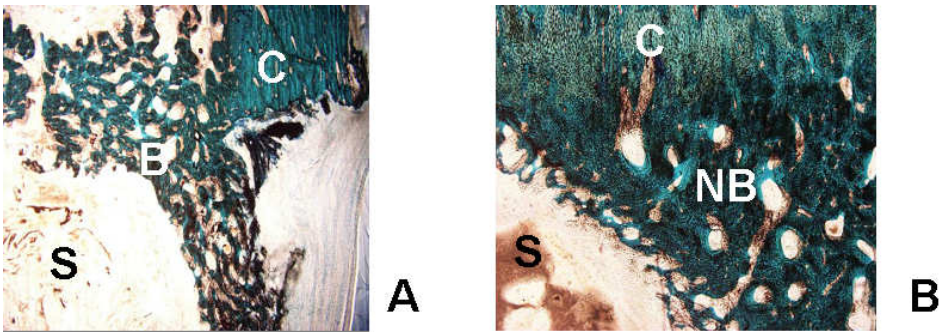

Fig. 4.16: Histological evaluation of PHF structure alone through Acid Fuchsin and Fast Green staining. (S: scaffold; C: cortical bone; NB: newly formed bone) .

The scaffold was still present into the bone gap after 12 weeks and there was totally absence of fibrous tissue all around it. Newly formed trabecular bone is present all around the impants. PHF scaffold with BMSCs treated with platelet rich plasma (PRP) showed a better response with more newly formed trabecular bone observed at the bone-scaffold interface and on the external surface of bone and scaffold.

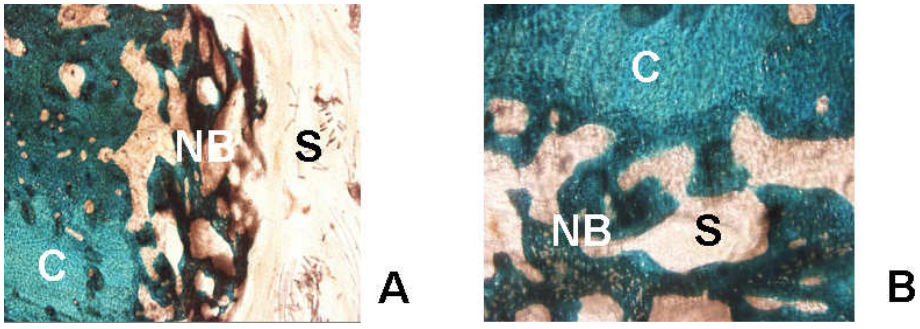

Fig. 4.17: Histological evaluation of PHF + BMSCs + PRP structure through Acid Fuchsin and Fast Green staining at different magnification: a)1.25X, b) 4X . (S: scaffold; C: cortical bone; NB: newly formed bone)

Higher amount of newly formed bone trabeculae is evident in the case of BMP7 loaded cell free PHF scaffold as is possible to see from its histology

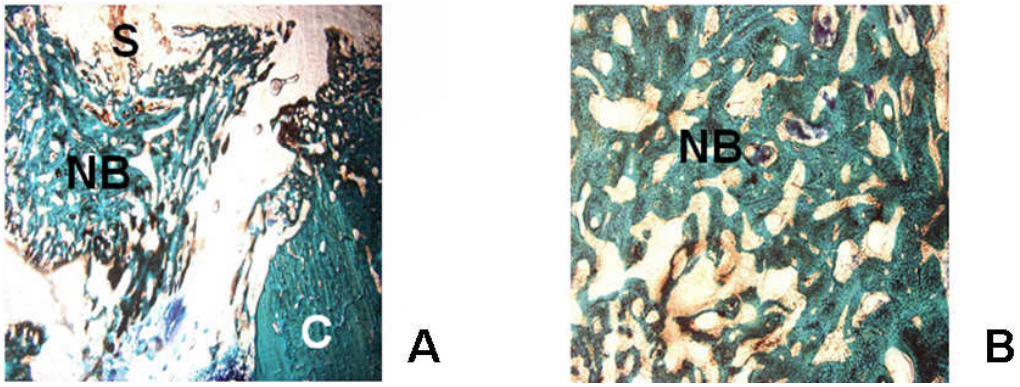

Fig. 4.18: Histological evaluation of PHF + BMP7 structure through Acid Fuchsin and Fast Green staining at different magnification : a) 1.25X, b) 4X (S: scaffold; C: cortical bone; NB: newly formed bone)

The regrown bone of this type of scaffold appear to be more similar to normal bone than that of the other two typologies of structure.

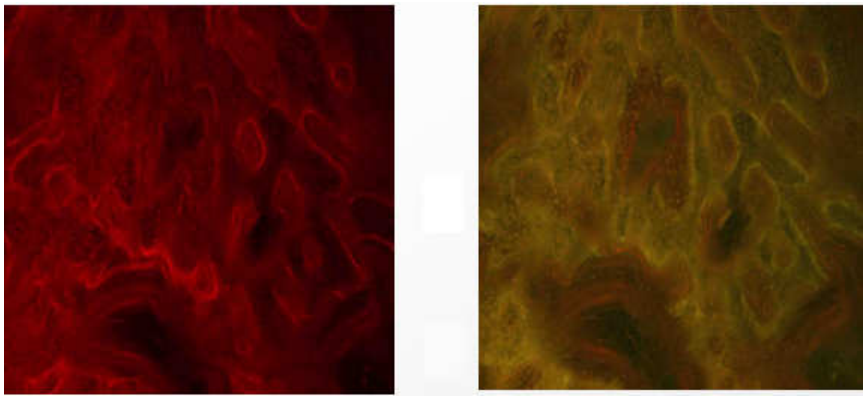

Fig. 4.19: fluorescence microscopy of a PHF/BMP7 section coloured with : a) Alizarin Red and b) Xylenol Orange

Moreover PHF/BMP7 scaffolds showed a high xylenol orange and alizarin red activity indicating an intense bone formation after 12 weeks confirming the osteogenic activity.

4.4 Conclusions

The current challenge in scaffold design is to fabricate reproducible bioactive and bioresorbable 3D scaffolds with tailored porosity and pore morphology, capable of maintaining structure integrity for a predictable period, even under load-bearing conditions. Here, three different typologies of composite scaffolds have been proposed by the integration into the PCL matrix of different material phases: HYAFF11, as a hydrophilic cue; R-cem (particles) as reinforcement systems by using conventional phase inversion/salt leaching technique (i.e., PHRS); or incorporation of PLA long fibers by filament winding technique (i.e., PHF). The morphological features, the degradation and mechanical properties and the cellular response of the three different typologies were investigated. All scaffold prototypes showed a bimodal porosity, characterized by macropores arising from salt crystal dissolution, and micropores formed by the controlled removal of solvent via non-solvent exchange. The investigation of morphology by Xray micro-computed tomography (micro-CT,), allowed a quantitative assessment of scaffold porosity features (pore size, structural porosity and degree of anisotropy) as summarized in Table 1. Porosity and pore sizes of PHS scaffolds are firstly affected by the response of the HYAFF11 phases to the water retention, leading to a slight underestimation of pore sizes (around 170 μm) due to swelling of the hydrogel through absorption of environmental moisture.

In the case of PHF scaffolds incorporating PLA fibres, a drastic decay of the porosity degree, from 81.7% to 63.1%, was observed, cause a smaller weight amount of sodium chloride crystals was used in order to reduce the solution viscosity, and thus optimize the fiber/matrix adhesion, during the winding process. Pores ranges in size from 60 to 400 μm, with an average pore size of about 200 μm, the specific surface area varies between 32 mm^2/mm^3 for the PHF scaffolds to the 63 mm^2/mm^3 of the PHRS. TGA analysis evaluate the effective weight percentage of every single components in the composite scaffold. For pure PCL samples, the TGA curve is characterized by a drastic lost mass between 330 and 450 °C. For the composite sample PHRS and PHS it is interesting to notice a first weight loss between 30 and 100 °C probably due to evaporation of the water retained in the HYAFF phase. Moreover PHRS sample show a residue over 700 °C that confirm the presence of the ceramic phase (R-Cem) inside the matrix. The incorporating of Calcium phosphate crystals into the PCL polymer matrix

slightly improve the mechanical leaving unaltered the pore morphology. Fibres reinforced samples shows the best mechanical properties with an increase of one order of magnitude in elastic modulus if compared with non reinforced PCL scaffolds. Dynamic analysis confirm the results obtained from the static characterization with the PHF sample that shows the highest elastic modulus and highlights the viscoelastic behaviour of the samples showing that E' increase with the frequency while E'' seems to be not really affected as frequencies varies. Finally an *in vivo study* has been performed in collaboration with the orthopaedic institute Rizzoli in Boulogne. The test has been performed on the fibre reinforced scaffold in three different configuration: PHF alone, PHF with BMSCs and Platelet rich plasma (PRP), PHF with BMP7. After 12 weeks all the three typologies of scaffold did not evoke tissue inflammation or foreign body reaction in the surrounding bony tissue. Histologies show that PHF scaffolds, treated with BMP7, has the highest newly formed bone trabeculae.

Acknowledgements

We would like to acknowledge the European Commission for funding (STEPS project, FP6-500465).

REFERENCES

[1]. J.M. Anderson, J.J Langone, , *J. Controlled Release*, **1999**, 57, 2, 107

[2]. J.E. Babensee, J.M. Anderson, L.V. McIntire, A.G. Mikos, *Adv. Drug Delivery Rev*., **1998**, 33, (1-2), 111.

[3]. O.M. Bostman*, J Bone Jt Surg*, **1991**, 148

[4]. D. Hutmacher ,M.B. Hurzeler ,H. Schliephake **,** *Int J Oral Maxillofac Implants*, **1996**, 11(5), 66.

[5]. L.E. Freed ,G. Vunjak-Novakovic ,R.J. Biron ,D.B. Eagles ,D.C. Lesnoy, *Bio/Technol* **1994**, 12, 689.

[6]. V. Guarino, M. Lewandoska, M. Bil, B. Polak, L. Ambrosio, *Composite Science and technology,* **2010,** 70, 1826.

[7]. H. J. Sung, C. Meredith, C. Johnson, G. Zorina, *Bioamterials*, **2004**, 25, 5735.

[8]. A. Pathiraja, G Unatillake, R. Adhikari, *European cells and Materials,* **2003**, 5, 1.

[9]. S.W. Shalaby, *US Patent* 5, 612, 052.

[10]. N. Ashammakhi, E.A. Mäkelä, P. Törmälä, T. Waris, P. Rokkanen, *Eur J Plast Surg* **2000,** 23, 423.

[11]. Freed LE, Vunjak-Novakovic G, Biron RJ, Eagles DB, Lesnoy DC, Barlow SK, et al, *Biomaterials***, 2008,** 29, 3662.

[12]. V. Guarino , F. Causa , P. Taddei , M. di Foggia , G. Ciapetti, D. Martini , C. Fagnano , N. Baldini, L. Ambrosio, *Biomaterials*, **2008**, 29, 3662.

[13]. J.A. Hubbel, *Curr. Opin. Biotech.,* **2003,** 14, 551.

[14]. V. Guarino , L. Ambrosio, *Acta Biomaterialia,* **2008,** 4, 1778.

[15]. Q.P. Hou, D.W. Grijpma, J. Feijen, *Biomaterials*, **2003**, 24, 1937.

[16]. M.C. Azevedo, R.L. Reis, M.B. Claase, D.W. Grijpma ,J. Feijen, *J Mater Sci Mat Med*, **2003,** 14, 103.

[17]. D. Campoccia, P. Doherty, M. Radice, P. Brun, G. Abatangelo, D. F. Williams, *Biomaterials*, **1998**, 19, 2101.

[18]. P.B. Van Wachem , M.J.A. Van Luyn, P. Nieuwenhuis , H.K. Koerten, L. Olde Damink, H. T. Hoopen, J. Feijen. *Biomaterials*, **1991**, 12, 215.

[19]. A. Rastrelli ,M. Beccaro , F. Biviano ,G. Calderini , A. Pastorello, *Clin.*

Implant Mat., **1990**, 9, 199

[20]. N.J. Turner, C.M. Kielty, M.G. Walker, A.E. Canfield, *Biomaterials*, **2004**, 25, 5955

[21]. B. Grigolo, L. Roseti, M. Fiorini, M. Fini, G. Giavaresi. N.N. Aldini et al, *Bioamterials,* **2001**, 22, 2417.

[22]. V. Guarino, F. Causa, L. Ambrosio, *J Appl Biomater Biomech,* **2007**, 5, 149.

[23]. L.G. Griffith, *Acta mater*, **2000**, 48, 263.

[24]. J.F. Nelson, H.G. Stanford, D, E. Cutright, *oral surgery, Oral medicine, oral pathology,* **1977**, 43, 6, 836.

[25]. J.O. Hollinger, *Journal of Biomedical research,* **1983**, 17, 1, 71

[26]. R.L. Kronenthal, *Polymer science technology,* **1975**, 8, 119.

[27]. J. C. Middleton, A. J. Tipton, *Biomaterials*, **2000**, 21, 23, 2335.

[28]. E. Bell, *Tissue Engineering*, **1995**, 1, 2, 163.

[29]. J.A. Hunt ,V.J. Stella ,E.M. Topp, *Biomedical and Biotechnological advances*, **1988**, 55

[30]. E. Milella, E. Brescia, C. Massaro, P.A. Ramires, M.R. Miglietta, V. Fiori, P. Aversa, *Biomaterials*, **2002**, 23, 1053.

[31]. R. Barbucci , A. Magnani,A. Baszkin, M.L. Da Costa,H. Bauser, G. Hellwig,E. Martuscelli, S. Cimmino, *J Biomater Sci Polym Edn* **1993**, 4(3), 245.

[32]. R. Muller, S. Matter, P. Neuenschwander, *Morphological control in multiphase polymer mixturesI,* **1997**

CHAPTER 5

Design of porous three dimensional PDLLA scaffolds using stereolithography

5.1 Introduction

Scaffold design parameters including porosity, pore size, interconnectivity, and mechanical properties have a significant influence on cell seeding and differentiationv[1][2]. This chapter evaluates the ability of Stereolithography (SLA) to be used to tailor scaffolds design to optimize these parameters.

Tissue engineering scaffold prepared by rapid prototyping techniques have several advantages when compared to those fabricated by conventional techniques that often result in inhomogeneous scaffolds with broad pores size distribution, poor pore interconnectivity and inferior mechanical properties[3]. Rapid prototyping allows the preparation of scaffolds with optimal properties regarding pore, structure and connectivity, geometry, mechanical properties , cell-seeding efficiency, and transport of nutrients and metabolites [4]. Laser micro-stereolithography (μSL) has become an accepted rapid prototyping technique that allows 3D microfabrication of solid models from images created by computer-aided design (CAD) programs [5]. Its working principle is based on spatially controlled solidification of a liquid photo-polymerisable resin[6]. The limited number of resin that are commercially available for processing by stereolithography has often been considered the main limitation of the technique. The resin should be a liquid that rapidly solidifies upon illumination with light. Most of the available resin are based on low-molecular weight, multi functional monomers, and highly crosslinked network are formed[7]. These materials are predominantly glassy, rigid and brittle. Only few resin have been described that allow the preparation of elastomeric objects by stereolithography[8]. These resin formulations include macromers with low glass transition temperatures and relatively high molecular weight often in combination with diluents such as N-methylpyrollidone (NMP) or water to reduce the viscosity of the resin[9]. Most materials used for stereolithography are conventional epoxy resins, thermoplastic elastomers, and poly(ethylene-glycol) (PEG)-

based hydrogels. They have limited application in bone tissue engineering because of the lack of biodegradability or sufficient mechanical strength [10]. The only biodegradable macromers that have been applied are based on trimethylene carbonate and ε-caprolactone oligomers, or on poly(propylene-fumarate) [11][12]. The latter requires a reactive diluent such as diethyl fumarate to obtain an appropriate reaction rate and viscosity of the resin [13].

For tissue engineering of hard tissue such as bone, strong and rigid biodegradable materials are required. Polylactide is such a material , and it has a long track record of successful application in the clinic and for the preparation of tissue engineering scaffolds. It is strong and stiff and degrades to yield lactic acid. The polymer has been extensively applied in porous scaffolds suitable for bone tissue engineering [14]. A degradable photo-polymerisable system can be obtained by chain-crosslinking hydrolysable oligomers with reactive end groups [15]. Poly(D,L-lactide) (PDLLA) functionalised with methacrylate groups can be crosslinked to form rigid polymer networks [16]. They have been applied in resorbable bone fixation devices clinically and for use in bone tissue engineering. Beside the properties of the material also the pore architecture of a scaffold is of great influence on its functionality. The architecture influences mechanical properties, cell adhesion and proliferation, transport phenomena and degradation behaviour. Using stereolithography techniques structural parameters such as porosity and pore size, and even gradients thereof, can be freely varied. In this chapter, we will show how to design biodegradable porous structure with refined architectures and prepare these by stereolithography at high resolution.

5.2 Materials and Methods

5.2.1 Materials

D,L-Lactide was obtained fromPurac Biochem, The Netherlands. Hexanediol, stannous octoate, methacrylic anhydride (MAAH), tocopherol, dibenzopyrazine were purchased from Sigma–Aldrich, USA and used without further purification. Triethyl amine (TEA) (Fluka, Switzerland), ethyl lactate (Merck, Germany), and technical grade isopropanol and acetone (Biosolve, The Netherlands) were used as received. Orasol Orange G was gift from Ciba Specialty Chemicals, Switzerland. Lucirin TPO-L (ethyl-2,4,6-trimethylbenzoylphenylphosphinate) was a gift from BASF, Germany. Analytical grade dichloromethane (Biosolve, The Netherlands) was distilled from Calcium Hydride (Acros Organics, Belgium).

5.2.2 Macromers synthesis

Oligomers are obtained by a ring-opening polymerization of the D,L-Lactide for 40h at 130ºC under an argon atmosphere, using Stannous Octoate $Sn(Oct)_2$ as catalyst. 1,6 Hexanediol is used as initiator to prepare 2-armed oligomers.

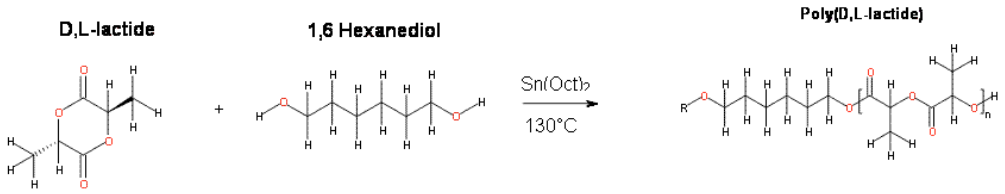

Fig. 5.1:Ring-opening polymerization reaction of (D,L-lactide) using difunctional alcohol ad initiator and $Sn(Oct)_2$ as catalyst

The molecular weight and arm lengths are varied adjusting the monomer to initiator ratio. Proton-nuclear magnetic resonance spectroscopy (^1H NMR , $CdCl_3$, Varian 300 MHz) are used to determine lactide monomer conversion and oligomers molecular weight.

Oligomers are functionalized by reacting the hydroxyl groups with Methacrylic anhydride (MAAH) under argon atmosphere. The formed methacrylic acid is scavenged with Trietilammine (TEA). An excess of MAAH and TEA per hydroxyl group is used.

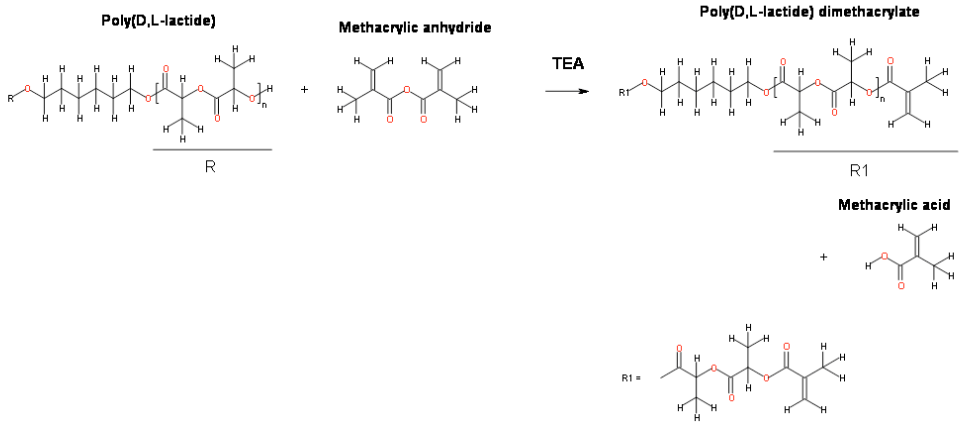

Fig. 5.2: functionalization of poly(D,L-Lactide) with Methacrylic anhydride in presence of tryethilamine

Macromer solution is filtered and precipitated into cold isopropanol, the isolated macromers are then washed with water and freeze dried. ^{1}H NMR is used to determine degree of functionalization of the macromers.

5.2.3 PDLLA resin for stereolithography

To be able to apply PDLLA macromers in stereolithography, the macromer must be in the liquid state [17]. Reactive diluents such as methyl methacrylate, butane-dimethacrylate and N-vinyl-2-pyrollidone have been used in regular photo-polymerisation reactions **[10]**[18] and in stereolithography [19][20].

To formulate liquid polymerisable poly(D,L)lactide resin, three different solvent were tested in different amount: (a) Ethyl Lactate, (b) Propylene carbonate, N-methyl-2-pyrollydone. Macromers were diluted with varying amount of solvent, and their viscosities have been determined at 25°C using a Brookfield DV-E rotating spindle viscometer, equipped with a small sample adapter. The shear rate was varied between 0.3 and 6.0 r.p.m. to prevent crosslinking 0.2 wt% of hydroquinone was added to the liquid. To obtain networks the resin containing 2.0 wt% of Lucirin TPO as a biocompatible UV photo-initiator, were irradiated with 365 nm UV-light for 15 min (Ultralum rosslinkng cabinet, intensity 3-4mW/cm^2). Teflon mould, covered with fluorinate ethylene-propylene (FEP) films to avoid oxygen inhibition, were employed to prepare film measuring 20x20x1.5 mm^3.

5.2.4 Stereolithography

To fabricate PDLLA structure with stereolitoghraphy poly(D,L-lactide) dimethilmethacrylate macromers have been solved in N-methyl-2-pyrrolidone (NMP) 45%wt. To prevent premature crosslinking 0,2% Tocopherol (Vitamine E) will be added to the solution. To obtain the network the resin contain 4,0% wt of Lucirin as a biocompatible UV photo initiator. The final resin composition will be 68% macromer, 31% Propylene carbonate (or NMP), 2.7% Lucirin photo initiator, 0,13% Tocopherol as antioxidant agent and 0,1% of Orange orasol dye. This resin will be used to prepare designed porous structures with a commercial stereolithography setup (Envisiontec Perfactory). Tensile test specimen (ISO 37-2), film measuring 20x20x1.5 mm^3 and scaffold with various 3D architecture were designed using Rhioceros 3D (McNeel Europe) and K3dSurf v 0.6.2(obtained from http://k3dsurf.sourceforge.net) computer software After building, the scaffold have been extracted with a mixture of isopropanol/acetone (3/1) and dried at 90°C for 2d.

5.2.5 Design of porous structures

To build porous tissue engineering scaffolds in a stereolithography setup a mixture of 3.0 kDa PDLLA dymethacrilate, 45 wt% (relative to the amount of macromers) NMP, 4 wt% of Lucirin photo-initiator, 0.2wt% of Tocopherol as antioxidant, 0.15wt% of Orange Orasol dye. The size of the smallest features that can be built are determinated by the size of the pixels (32x32 μm^2 in the x and y direction), the layer thickness (25µm). K3DSurf v0.6.2 software was used to generate CAD-files that describes the surfaces of Schwartz (S), Diamand (D) Gyroid (G) and Double Gyroid (DG) architectures. Their surfaces are defined by trigonometric implicit functions, where the spatial variables are symmetrically ordered within the trigonometric terms. The functions are triply periodic and are uniquely defined by its unit cell. They closely approximate the minimale surface of Schwarz and Schoen [21]. The following trigonometric functions were used with boundary condition x,y=[-10,10] and z=[-20,20]:

- **S:** $\cos(x) + \cos(y) + \cos(z) = 0.6$
- **D:** $\sin(x) * \sin(y) * \sin(z) + \sin(x) * \cos(y) * \cos(z) + \cos(x) * \sin(y) * \cos(z) + \cos(x) * \cos(y) * \sin(z) = 0.4$

- **G:** cos(x) * sin(y) + cos(y) * sin(z) + cos(z)* sin(x) = 0.6

To obtain porous structure with porosities of approximately 70% offset values of -0.6 for the Scwartz, -0.4 for the diamond and -0.6 for the gyroid are required. Rhinoceros software was used to scale the CAD files of all three architectures to the desire dimension. Envisontec Perfactory RP 2.0 software was used to slice the 3D CAD-files. The stack of bitmaps generated, is the input for the layer-by-layer building process.

5.2.6 Analysis of built structures

Structural analysis was performed by micro-computed tomography (µCT) using a Sky Scan 1072 at 10 µm resolution. Scanning was done at an X-ray tube voltage of 52 kV, a current of 152 µA with a rotation angle of 180 °C and an exposure time of 1900 ms. Scanning electron microscopy (SEM)(Philips XL30 operated at 10 (kV)was used to visualize the built structures.

5.2.7 hMSCs culturing

Bone marrow-derived hMSCs (Clonetics, Italy), at passage 5, were cultured in a-modified Eagle's medium (a-MEM) (BioWittaker, Belgium) containing 10 vol.% foetal bovine serum (FBS), 100 U/ml penicillin and 0.1 mg/ml streptomycin (HyClone, UK), in a humidified atmosphere containing 5% CO2 at 37 °C.

5.2.8 Scaffold cell seeding

Scaffolds for cell culture experiments, with a Double Gyroid architecture , were prepared for cell seeding by first soaking in 70% ethanol (1 h) and then 1% antibiotic/antimycotic in phosphate-buffered saline (PBS) (2 h), and pre-wetting in medium (2 h). 4 x 10^5 cells, resuspended in 50 µl of medium, were statically seeded onto the scaffold. After seeding the scaffolds were placed in 24-well culture plates (1 scaffold per well) and, incubated for 2 h in a humidified atmosphere (37 °C, 5% CO2).

5.2.9 Alamar blue assay

Cell viability and proliferation were evaluated using the Alamar blue assay. This is based on a redox reaction that occurs in the mitochondria of the cells. The coloured product is transported out of the cell and can be measured spectrophotometrically. The cell–scaffold constructs were removed from the culture plates on days 1, 7, 14, 21 and 28, rinsed with PBS (Sigma–Aldrich, Italy) and placed in 24-well culture plates. For each construct 1 ml of Dulbecco's modified Eagle's medium (DMEM) without Phenol red (HyClone, UK) containing 10 vol.% Alamar blue (AbD Serotec Ltd., UK) was added, followed by incubation in a 5% CO2 atmosphere for 4 h at 37°C. An aliquot of 200 µl of the solution was subsequently removed from the wells and transferred to a 96-well plate. The optical density was immediately measured with a Sunrise spectrophotometer (Tecan, Männedorf, Switzerland) at wavelengths of 540 and 600 nm. The number of viable cells correlates with the level of dye reduction and is expressed as percentage of Alamar blue reduction (%AB reduction), according to the manufacturer's protocol. Moreover, the number of viable cells on the scaffolds was determined by comparing the absorbance at different culture times with a calibration curve obtained by correlating known cell numbers in the 24-well culture plates with the corresponding absorbance values. Each experiment was performed three times in triplicate.

5.2.10 SEM analysis

SEM analysis was performed to evaluate cell morphology and colonization 4 weeks after seeding. The cell–scaffold constructs were extracted from the wells, the medium was removed and the specimens were fixed in 2.5% glutaraldehyde in 0.1 M sodium cacodylate buffer, pH 7.4 for 1 h at room temperature. This was followed by rinsing twice with PBS and dehydration in a graded series of ethanol (50, 60, 70, 80, 90 and 100 vol.%) for 5 min each. Finally, the specimens were air dried and sputter coated with gold. The cell morphology on the scaffold was observed with a Leica Cambridge (Stereoscan S440) scanning electron microscope**.**

5.2.11 CLSM

For the CLSM analysis the construct were extracted at 21 days after seeding, fixed with 4% parapholmadeyde for 20 min at RT, rinsed twice with PBS buffer and incubated with PBS-BSA 0,5% to block nonspecific binding. Actin microfilament were stained with phaloidin tetramethylrhodamine B isothiocyanate (Sigma-Aldrich, Italy). Phalloidin was diluted in PBS-BSA 0,5% and incubated for 30 min at RT. Samples were then observed by an inverted fluorescence microscope (IX50, Olympus, Italy), using 4X, 10X and 20X objectives.

5.3 Results and Discussions

5.3.1 Macromer synthesis

The monomer conversion and the arm length of the synthesised lactide oligomers was derived from ^{1}H-NMR spectra. The lactide conversion was determined from the ratio of the peak areas corresponding to the monomer -C**H**COO- protons (5.05 ppm) [a'] and the oligomer -C**H**COO- protons (5.15 ppm) [a]. Conversion reached were above 90%.

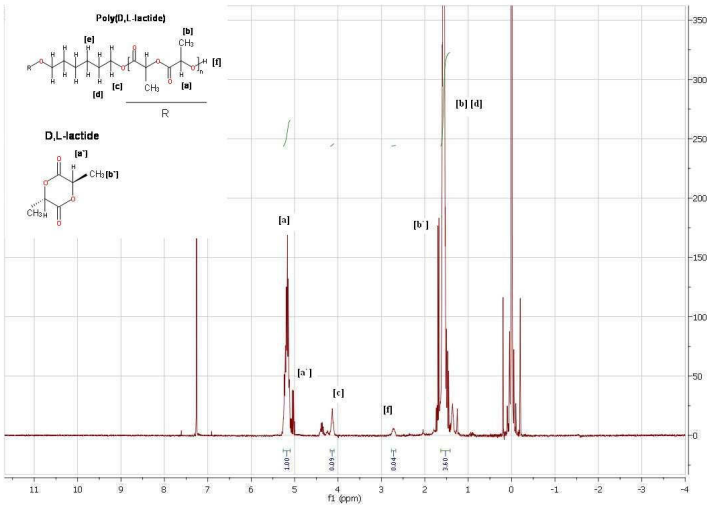

Fig. 5.3: ^{1}H NMR Spectra of lactide oligomer

Looking at the peak of the spectra and matching the oligomer -C**H**COO- proton (5.15 ppm) [a] with the hexandiol -C**H$_2$**O**-** proton (4.1 ppm) [c] , it is possible to estimate molecular weight of oligomers in this way:

$$\frac{\frac{Area[c]}{4}}{\frac{Area[a]}{2}} = \frac{1}{x_n}$$

Where Area[c] = 0.09;

Area[a] = 1; Xn = 22 Where x_n is number of monomer for chains.

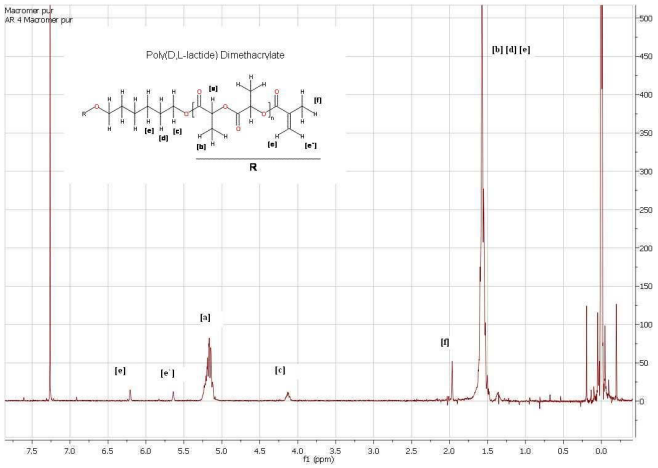

Fig. 5.4: ^{1}H NMR Spectra of functionalized macromers

The degree of functionalization was determined from the peak areas corresponding to the methacrylate protons (5.65 and 6.1 ppm) [e] and [e'] and the hexanediol - C**H$_2$**O- protons (4.1 ppm) [c]. degree of functionalization of 100% was a guaranteed from the absence of end groups peak at 2.75 ppm.

5.3.2 Viscosity test

Macromers were dissolved in three different unreactive solvent: Propylene carbonate (PC), ethyl lactate (EL) and N-methyl-2-pyrollidone (NMP) and their viscosity were determined at 25 °C. The viscosity of all formulation were strongly dependent on the amount and the type of solvent used. Our goal was to reach the lower viscosity with the lowest amount of solvent. As is possible to notice in Figure 11 the best solvent to use was NMP.

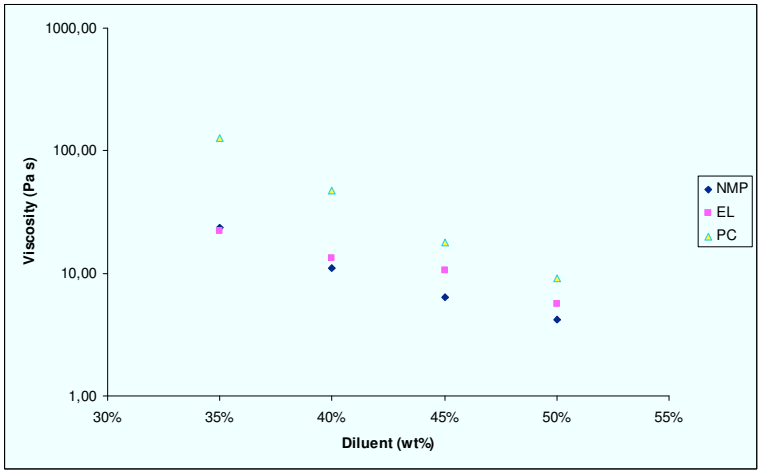

Fig. 5.5: the resin viscosity of PDLLA macromers dilueted with different amount of solvent.

	Viscosity (Pa·s)		
Amount of solvent (wt%)	Propylene carbonate	Ethyl lactate	N-Methyl-2-Pyrollidone
35	127,5	21,89	23,48
40	47,05	13,22	11,14
45	18,05	10,54	6,36
50	9,12	5,65	4,22

Tab. 5.1: PDLLA resin viscosity strongly depend from the amount and type of solvent used to diluite the macromers.

Once that it was found the best solvent it is necessary to find the right amount to use for stereolithography application. So PDLLA macromers were dissolved in different amount of NMP and their viscosity were determined at 25°C varying the shear rates between 0.3 and 6.0 r.p.m. To obtain resin with a viscosity comprised between 5 and 10 Pa·s an amount of 45 wt% of NMP was required.

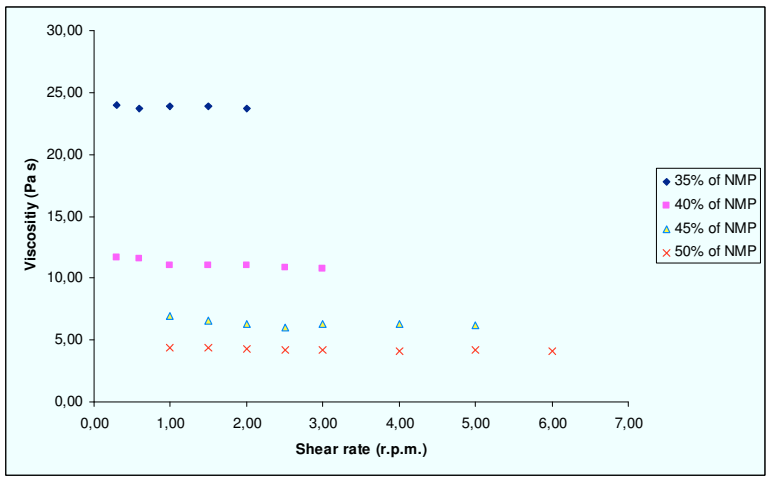

Fig. 5.6: The resin viscosity of PDLLA macromer as a function of the solvent diluent concentration.

5.3.3 Stereolithography

Similar to a conventional stereolithography process, the DMD (Digital micro Device)SL created 3D microstructures in a layer-by-layer fashion. The shapes of the constructed layers were determined by slicing the desired 3D scaffold design into a series of evenly spaced planes. Patterns of each layer were drawn in a series of

PowerPoint slides, which were then executed on the DMD chip to generate a dynamic mask . The illuminated area was solidified simultaneously under one exposure, while the dark regions remained in the liquid phase. After one layer was patterned, the substrate was lowered and the as-patterned layer was then covered by fresh macromer solution. Microstructures with complex geometries were created by sequentially polymerizing the layers [5]. The thickness of a solidified layer (cure depth, C_d in µm) is controlled by the light irradiation dose E(mJ/cm^2). A plot of the cure depth versus the irradiation dose is termed *Working curve* and can be described by:

$$C_d = D_p \ln\left(\frac{E}{E_c}\right)$$

This equation is an adapted form of the Beer-Lambert equation, which describer the exponential decay of intensity of light as it passes through a medium in which it is absorbed. The depth at which the resin is cured to the gel point (C_d) increases logarithmically with time, and thus with the applied irradiation dose (E). for a specific stereolithography setup, a resin can be characterized by a critical energy E_c(mJ/cm^2) and a penetration depth D_p. As the applied irradiation dose (E) exceeds the critical energy E_c, a solidified layer forms from the resin surface. The penetration of light into the resin is directly related to the extinction coefficient in the Beer-Lambert equation, and is characterized by D_p. to achieve good attachment between layers, the conversion of the macromer at the interface of the layers should be slightly higher than the gel point. In our experiments, a light irradiation dose that is between 30 to 35% higher than that required to realize the step height of the building platform, was found to be well suited. This overcure will affect inevitably pore size and geometry when building porous structures. A high value of the extinction coefficient of the resin correspond to a small D_p, and will allow minimal overcure and most accurate control of the building process.

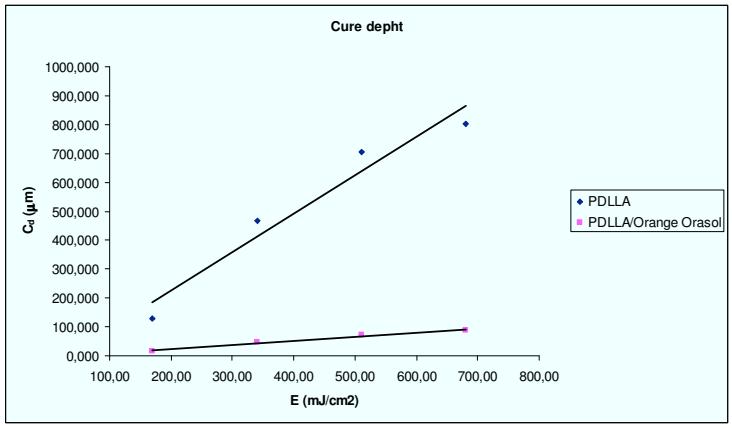

Fig 5.7. Stereolihography working curves of 1.5 kDa PDLLA macromer-based resins containing 0,2 wt% of Orange Orasol (Purple dot) and containing no dye (blue dot)

Figure 6 shows working curves for resin prepared from 1.5 kDa PDLLA macromer, which further contain 31% of NMP and 2,7% of Lucirin photo-initiator. From the slope of the working curve , it can be seen that the penetration depth of the resin decrease from 800µm to 100 µm upon the addition of 0.2 % of Orasol Orange G dye.

5.3.4 Design of porous structure

Scaffold design parameters such as porosity, pore size , interconnectivity and mechanical stiffness, have been shown to influence the cell attachment and differentiation on scaffold both in vitro and in vivo [22][23].

The demonstrated importance of these scaffold parameters dictates that an optimal bone tissue engineering scaffold must be achieved for the stimulation of desired signal expression and the induction of osteogenic differentiation of the recruited cell population. Along with the combination of other chemical and biological factors such as the administration of growth factor proteins, the repeated construction of precisely controlled architectures with the optimal design parameters is necessary to achieve an optimal bone tissue engineering scaffold. SLA technique enables scaffolds to be reproduced with controlled porosity, pore size, interconnectivity, and mechanical properties, all of which greatly influence cell attachment and differentiation. Using the SLA, three different sophisticated structure were built: a Scwartz, a Diamond and Double Gyroid architecture.

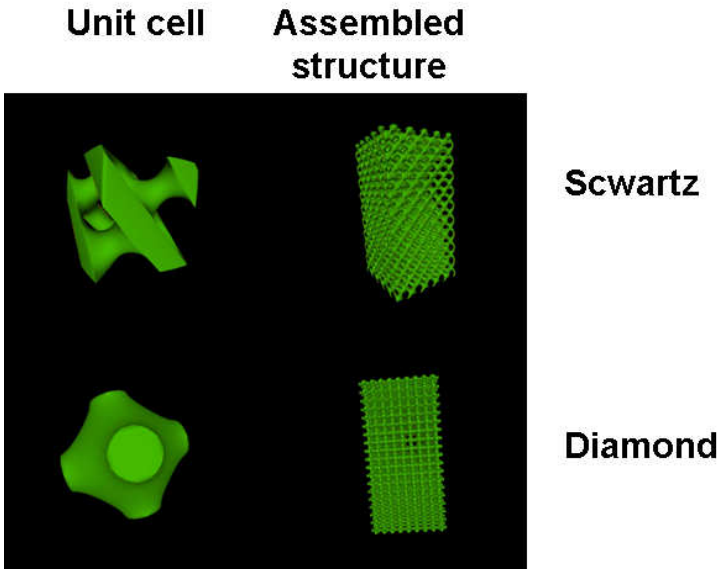

Fig. 5.8: Visualization of different porous architectures. Columns: (1) CAD- design of the repeating unit cells, (2) CAD-design of final structure.

Computer models can be generated repeating the respective unit cells in the space. Structure measuring 5x5x10 mm^3 were then built by stereolithography using a resin based on PDLLA macromers and a non-reactive diluents using Lucirin TPO as photo initiator ad hydroquinone to prevent crosslinking. Upon removal of solvent the structure shrink by 45%. This shrinkage is homogeneous and reproducible, and could be compensated by adjusting the dimension of the design.

5.3.5 Double Gyroid architectures

Starting from the Gyroid architectures [9] it has been developed a new architecture that we have called Double Gyroid. The idea has been to consider the absolute value of the Gyroid equation, in this way it has been realized an architecture in which we had two interpenetrated Gyroid structures.

- $abs(\cos(x)\cdot\sin(y)+\cos(y)\cdot\sin(z)+\cos(z)\cdot\sin(x))-1.15$

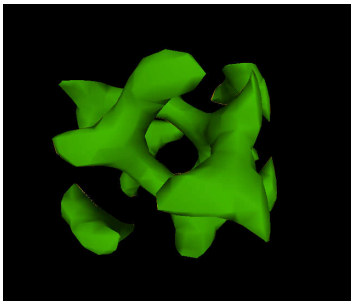

Unit cell

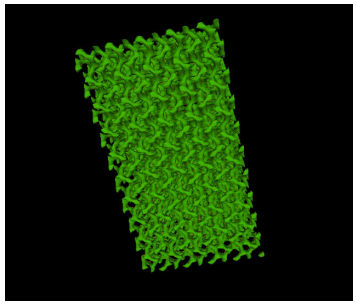

Final structure

Fig. 5.9: Visualization of the unit cell and final structure of the Double Gyroid architecture

Using the following boundary conditions:

- $\left(x^2 + y^2\right) \leq (5\pi)^2$ & $|z| \leq 5\pi$

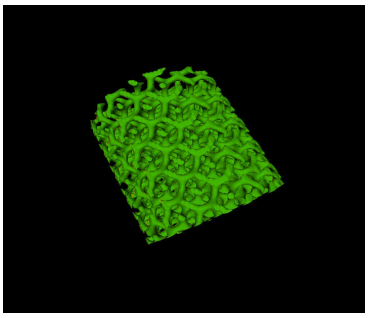

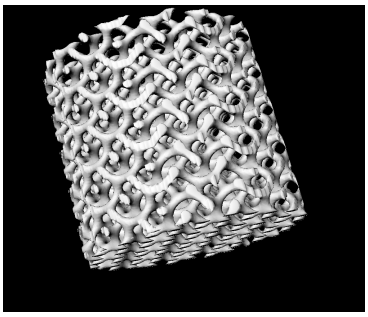

Fig. 5.10: CAD- visualization of the Double Gyroid architecture after the application of boundary conditions.

Structure built according with to this mathematically defined architecture for tissue engineering, have a large specific surface and high pore interconnectivity. These characteristics make it an excellent architecture for tissue engineering, as it enables cells-seeding at high density, and allows homogeneus distribution of cells ad flow of nutrient throughout the scaffold. To obtain porosity of approximately 78%, offset value of 1.15 is required. Rhinoceros software was used to scale the CAD-files to the desired dimensions. Envisiontec Perfactory RP 2.0 software was used to slice the 3D CAD-files.

5.3.6 Analysis of porous structure

To asses the accuracy of the stereolithography technique Scanning electron microscopy and µCT analysis was performed over the three different architecture. The graphical data obtained with µCT scanning was compared with the CAD data enabling quantifiable comparison. Under the applied experimental condition,

building times were approximately 8 h. Figure 17 shows SEM images respectively of the : (A) Schwartz architecture, (B) Diamond architecture and (C) Double Gyroid architecture.

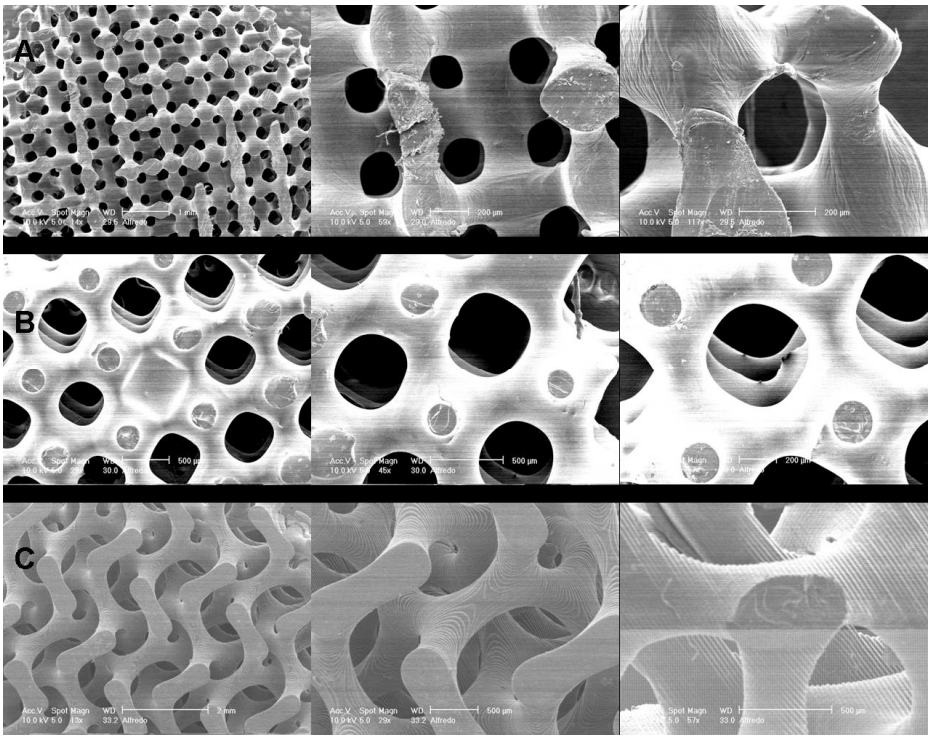

Fig. 5.11: SEM images of porous structures with different architectures built by stereolithography: (A) Schwartz architecture, (B) Diamond architectures, (C) Double Gyroid architectures.

The ability of a scaffold to enhance specific signal expression and support tissue formation is largely dependent on the pore size and porosity of the structure. Porosity refers to the overall percentage of void space within a solid, whereas pore size reflect the diameter of individual voids of the scaffold [24]. Porosity and pore size have significant ramification on the ability of tissue engineering scaffolds to support tissue regeneration for several reason. First, porosity and pore size have been show to affect cell differentiation through changes in signalling distances [25]. Pore size has been observed to influence also the vascularization , which is crucial to successful tissue formation. Rapid vascularisation is important for tissue growth in an implanted scaffold as cells on the interior portion of the scaffolds will not survive without a blood nutrient supply. Interconnectivity between the pores is another important requirement of scaffold architecture. Scaffolds that feature a

highly interconnected architecture allow communication between cells different areas within a scaffold and promote tissue ingrowth. The built scaffold closely resembled the design and it can be seen that the pore network is homogeneous in size and fully interconnected. At higher magnification, the layer-by-layer nature of the construct is clearly visible (Fig. 18).

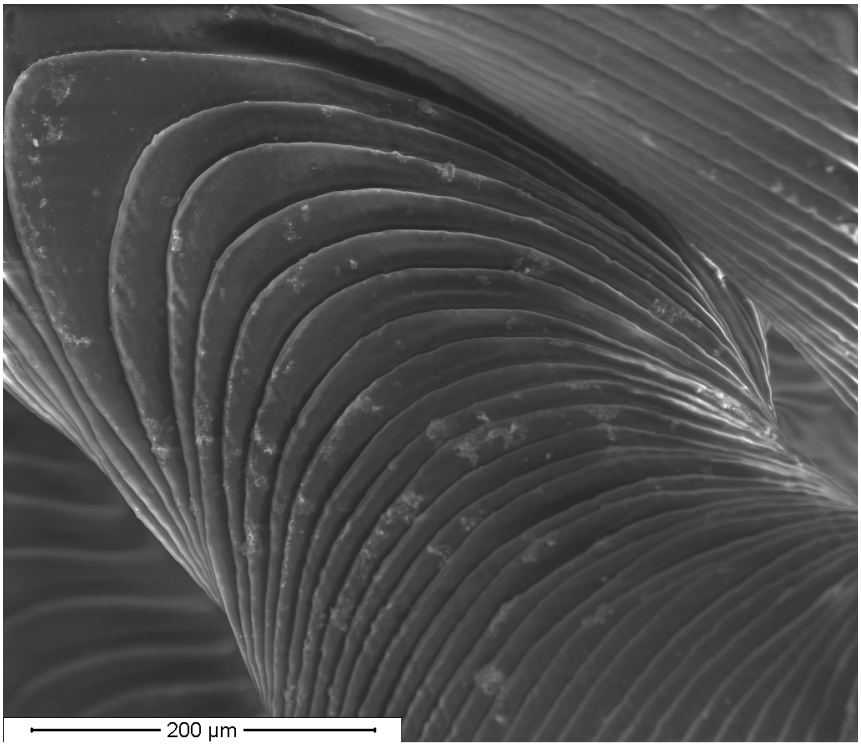

Fig. 5.12: layer by layer structure of double gyrois architecture.

It follows that the use of PDLLA dimethactrilate/NMP enables the preparation of biodegradable scaffolds with highly controlled architectures and suitable characteristics for cells culturing. Because the complexity of the network inside a scaffold pore inteconnectivity can be difficult to assess, but the use of micro-computed tomography (µCT) allows for a more precise definition and better assessment of scaffold characteristic.

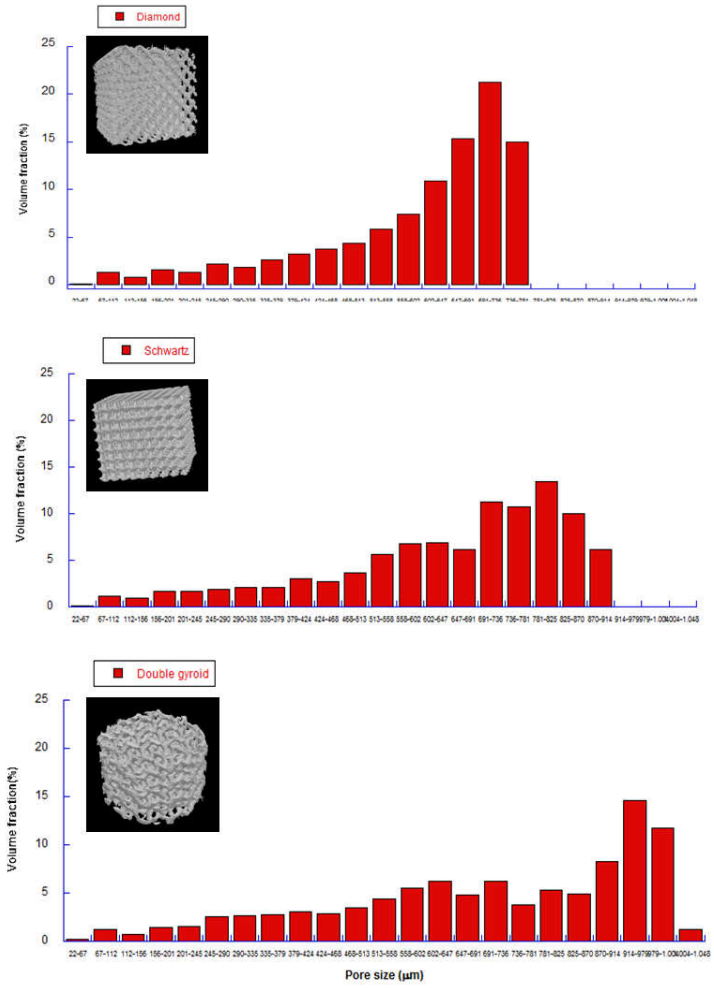

Fig. 5.13: visualization of µCT-scanning of the Double Gyroid structures.

From the µCT data, the structural parameters of the built scaffold after removal of the diluent were determinated. The designed architectures is preserved and porosity is almost unaffected. Table 1 summarizes porosity and specific surface parameters evaluated from the µ-CT.

	Porosity (%)		**Specific surface area** (mm^{-1})		**Average pore size (mm)**
Architecture	CAD	Built	CAD	Built	Built
Schwartz	63.68	66.97±1,44	6.18	11.41±1,56	0,615±0,04
Diamond	72.51	79.25±1.44	7.09	19,62±1,56	0,559±0,04
Double Gyroid	78,47	78,16±1,54	10.02	13,89±0,68	0,745±0,02

Tab. 5.2: Comparison of structural parameters of the designed structures and built porous structures as determined by µCT

High specific surface value and a porosity fully interconnected allow to think that Double gyroid is a good architecture for cell culturing.

5.3.7 Biological characterization of seeded scaffold

To demonstrate the suitability of these material for use in medical application such ad bone tissue engineering, hMSCs were seeded and cultured for 21 days on PDLLA Double Gyroid structure. Ferry et all. have already demonstrated that PDLLA network film obtained by stereolithography are excellent substrates for the culturing of cells [14]. Now it will be showed that Double Gyroid architecture is a suitable structure for cell seeding and and growing. The very open structure facilitates the penetration of water into our PDLLA scaffolds prepared by stereolithography. This allowed for intrusion of the cell suspension deep into the scaffolds and cells were distributed all throughout. So the cells seeding could be performed effortlessly by simply pipetting the cell suspension onto the scaffold.

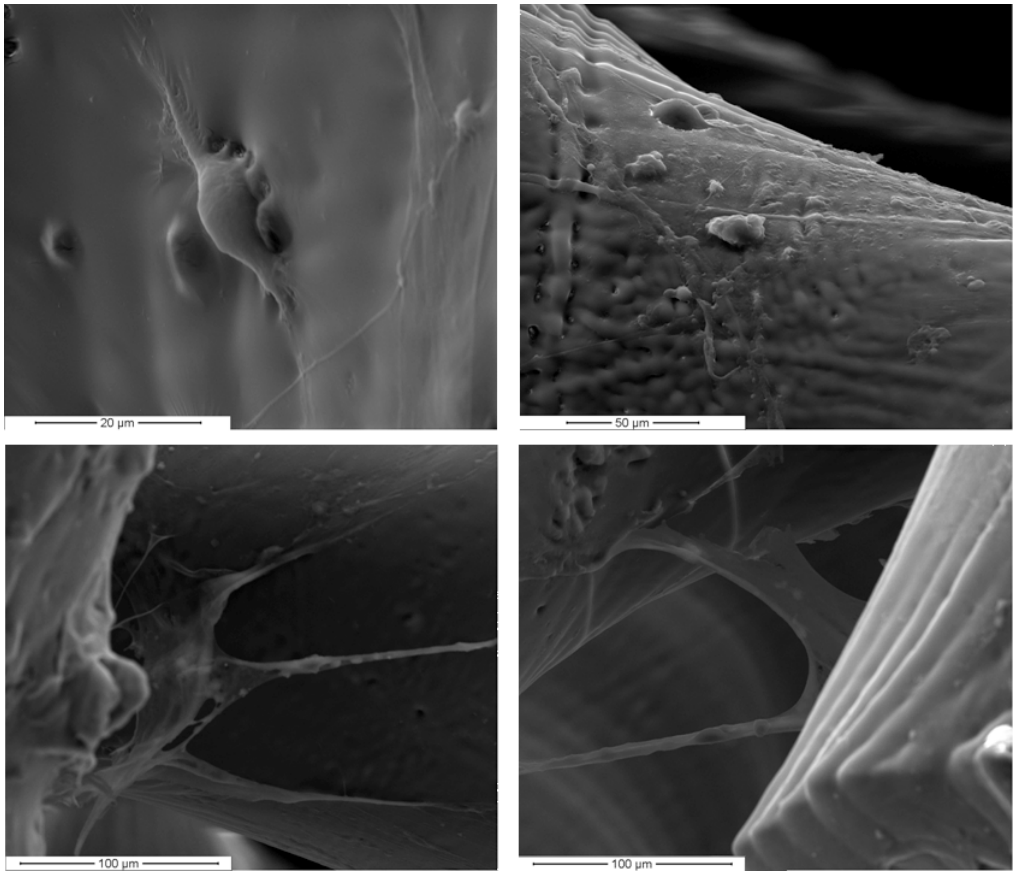

Fig. 5.14: Sem images of PDLLA Double Gyroid scaffold seeded with hMSCs after 21 days of culture.

The results demonstrate that the open architecture of the DB scaffold facilitates the infiltration of a cell suspension into the scaffold, despite its hydrophobic nature. In the static seeding there is a clear effect of scaffold permeability on final cell distribution. Cause the DG architecture is a very open structure, large cell cluster were found on the bottom of the scaffold. However due to the surface roughness many cell are retained inside the structure allowing their seeding and proliferation. Representative fluorescence and histological images of the cell-scaffold construct at day 21 after seeding are reported in figure 21.

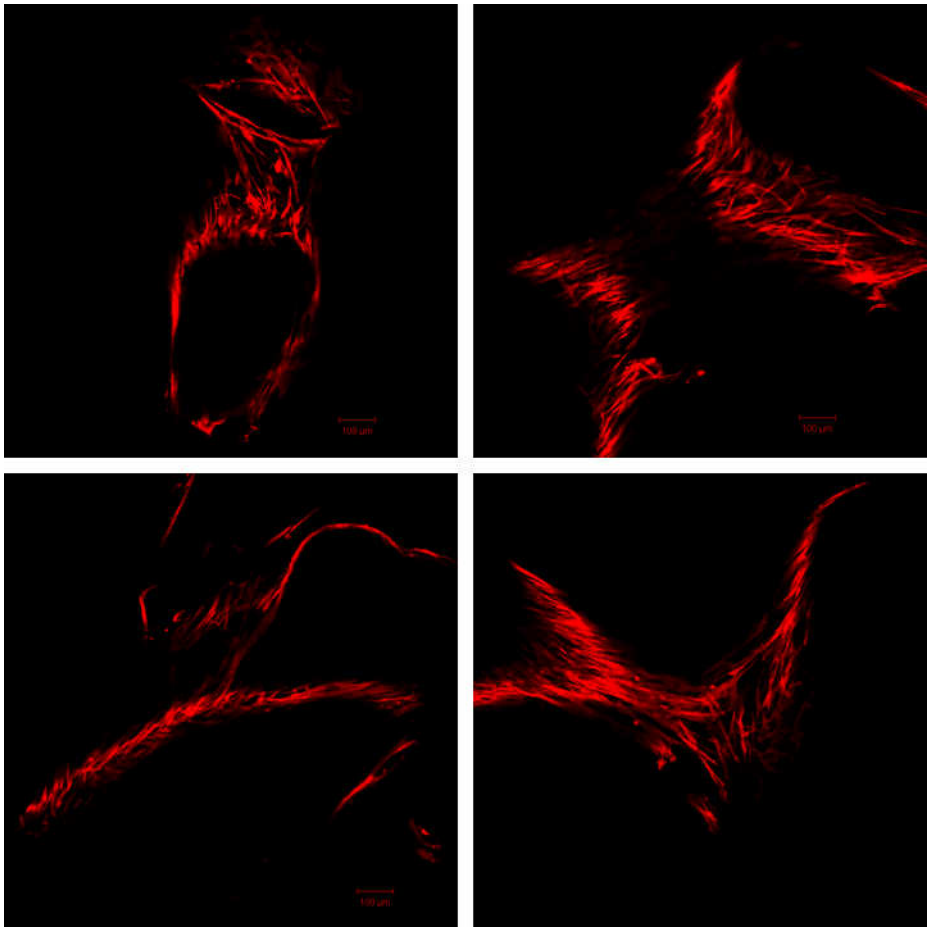

Fig. 5.15: Fluorescence microscope images of the cross sections of the cell-scaffold construct (objective 10X)

It was possible to observe as that large cell cluster are present on the bottom and upper surface of the scaffold, as well as the progressive reduction of hMSCs colonization in the inner region of the porous structure, probably due to the high dimension of pore size.

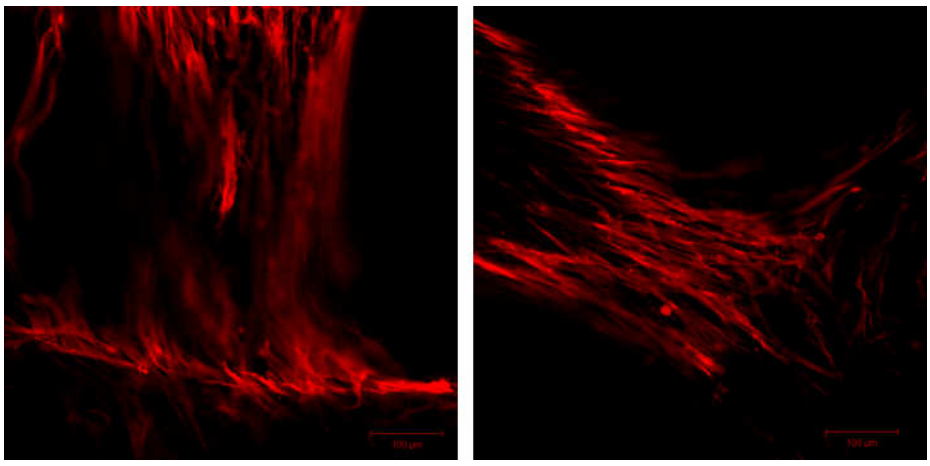

Fig. 5.16: fluorescence microscope images at higher magnification (objective 20X)

The values for Alamar blue assay provided a quantitative evaluation of the proliferation and the number of viable cells in the scaffold. As shown in Fig. 19 the proliferation of hMSCs reached a plateau at 2 weeks and at the 3 weeks it starts to decrease.

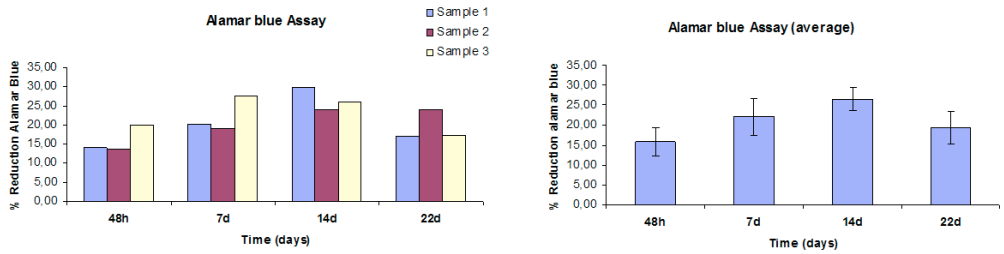

Fig. 5.17: Alamar blue assay for proliferation of hMSCs cultured on PDLLA Double gyroid scaffold at 48h, 7 days, 14 days and 21days.

5.4 Conclusions

In bone tissue engineering, a series of structural cues including pore size, porosity, interconnectivity, and stiffness have been found to be critical factors in activating osteogenic signal expression. Successful manipulation and fabrication of controlled architecture with optimal conditions of construction parameters may stimulate osteogenic signal expression as well as subsequent osteogenic differentiation. To this end, SLA is a promising and feasible strategy for fabrication of a designed architecture, which may show the best performance in vitro and in vivo. A resin based on poly(D,L-lactide) macromers and non-reactive diluent was developed and applied in stereolithography. Designed solid structures and porous scaffolds were prepared and

characterised from a morphologic, mechanical and biological point of view. Stereolithography fabrication methods can be used to accurately prepare tissue engineering scaffolds with design that can be modelled, allowing optimisation of the properties of the structures. Therefore, controlling the structural parameters may promise successful integration of the implants into the surgical sites and enhancement of boneregeneration. Mathematically defined porous structures with different architectures (Diamond, Schwartz, Double gyroid), were prepared using a liquid resin based on 2-armed PDLLA macromers and N-methyl-2-pyrollidone. The characterized PDLLA structures show good mechanical properties with a open pore architecture fully interconnected. It was shown that the open, accessible architecture has improved cell seedability in fact hMSc readily adhered and proliferated well on this network.

Acknowledgments

We would like to acknowledge Prof. Dirk Grijpma and all the staff of the department of Polymer Chemistry and Biomaterials of the University of Twente for supporting the experimental research during the exchange project. Special thanks also to Dott. S. Zeppetelli for the in vitro biological characterization.

References

[1]. K. Kim, A. Yeatts, D. Dean, and J. P. Fisher, *Tissue Engineering: part B,* **2010**, 0, 0.

[2]. K. Kyriakidou, G. Lucarini, A. Zizzi, E. Salvolini, M. Mattioli Belmonte, F. Mollica, A. Gloria and L. Ambrosio, *Journal of Bioactive and Compatible Polymers,* **2008,** 23, 227.

[3]. A. Gloria, T. Russo, R. De Santis, L. Ambrosio, *journal of Apllied Biomaterials & Bioceramics*, **2009**, 3,7, 141

[4]. S.J. Hollister, *Nature materials* **2005,** 4, 518.

[5]. Yi Lu, G. Mapili, G. Suhali, S. Chen, K. Roy, *Journal of Biomedical Material Research* **2006,** 77A, 2, 396.

[6]. H.W. Kang, Y.J. Seol, D.W. Cho, *J. Micromech. Microeng*, **2009**, 19

[7]. D.T. Pham, R.S. Gault, *International Journal of Machine Tools & Manufacture,* **1998,** 38, 1257.

[8]. I. H. Lee, D.W. Cho, *Microsystem Technologies,* **2004,** 10, 592.

[9]. F.P.W Melchels, K. Bertoldi, R. Gabbrieli, A. H. Velders, J. Feijen, D.W. Grijpma

[10]. Kee-Won Lee, Shanfeng Wang, Bradley C. Fox, Erik L. Ritman, *Biomacromolecules* **2007,** 8, 1077.

[11]. Lee SJ, Kang HW, Park JK, Rhie JW, Hahn SK, Cho DW, *Biomedical Microdevices* **2008**, 10, 233

[12]. Matsuda T, Mizutani M, *Journal of biomedical material reserach,* **2002,** 62, 395

[13]. Lee KW, Wang SF, Fox BC, Ritman EL, Yaszemski MJ, Lu LC, *Biomacromolecules,* **2007**, 8, 1077

[14]. F.P.W. Melchels, J. Feijen, D.W. Grijpma, *Journal of control release*, **2008,** 132, 3, e71.

[15]. A.S. Sawhney, C.P. Pathak, J.A. Hubbell, *Macromolecules,* **1993,** 26, 581.

[16]. R.F. Storey, S.C. Warren, C.J. Allison, J.S. Wiggins, A.D. Puckett, *Polymer,* **1993**, 34, 4365

[17]. F. P.W. Melchels , J. Feijen , D. W. Grijpma, *Biomaterials*, **2009**, 30, 3801.

[18]. Helminen AO, Korhonen H, Seppala JV, *Journal of Apllied Polymer Science,* **2002,** 86, 3616.

[19]. J. Jansen, F.P.W Melchels. , D.W. Grijpma, J. Feijen. *Biomacromolecules,* **2009,** 10, 214.

[20]. M.N. Cooke, J.P. Fisher, D. Dean, C. Rimnac, A.G. Mikos, *Journal of Biomedical Materials Research Part B – Applied Biomaterials,* **2003,** 64B, 65.

[21]. A.H. Schoen, Nasa technical Note, NASA-TN:D.5541, **1970**

[22]. P. Kasten, I. Beyen, P. Niemeyer, R. Luginbuhl, M. Bohner, W. Ritcher, *Acta Biomaterialia,* **2008**, 4, 1904.

[23]. C.B. Khatiwala, S.R. Peyton, A.J. Putnam, *Cell Physiology,* **2006**, 290, C1640.

[24]. V. Karageorgiou, D. Kaplan, *Biomaterials*, **2005**, 26, 5474.

[25]. K. Kim, D. Dean, A.G. Mikos, J.P. Fisher, *Biomacromolecules,* **2009**, 10, 1810.

CHAPTER 6

Scaling the stereolithography process to develop new Poly(D,L-Lactide)/Nano-Hydroxyapatite bioactive composite scaffold.

6.1 Introduction

Natural bone is a nanocomposite consisting of mineral fraction including small apatite crystals and non-stoichiometric calcium phosphate and organic fraction which together confer mechanical resistance. It is a living tissue that constantly undergoes a coupled resorption–reparative process known as bone remodeling. The incorporation of a graft into bone will inevitably involve cellular and tissue response with regard to resorption of the implant material and bone formation at the interface [1]. The reason behind the development of composite by smart combination of biodegradable polymers and bioactive ceramics or glasses for tissue engineering have been discusses extensively [2][3]. Briefly: they include : a) the possibilities of developing materials with improved mechanical properties due to the inherent higher stiffness and strength of the inorganic material, c) the possibility of altering the surface topography of the material by combination of nano-sized inorganic particles as fillers or coating [4]. As widely reported in literature synthetic hydroxyapatite [HAP, $Ca^{10}(PO^4)^6(OH)^2$] has assumed substantial interest and importance because of its chemical similarity to the natural Ca phosphate mineral present in biological hard tissue [5][6]. Its surface is highly bioactive and can bond strongly with the host bony tissue [7]. The extent of osteointegration between bone and a newly implanted material is influenced by many factors including a number of host biological and surrounding tissue responses. Properties of the biomaterial surface (such as topography and chemistry) control the type and magnitude of cellular and molecular events at the tissue-implant interface [8]. The ultimate tissue response to the implanted material may depend on the adsorbed proteins that control cell migration and adhesion. Surface properties modulate the characteristics of the protein layer adhered [9][10] and such proteins are in the nanometer scale [11]. Design of biomaterials with surface properties similar to physiological bone

(characterized by surface grain sizes in the nanometer regime) would undoubtedly aid in the formation of new bone at the tissue/biomaterial interface and, therefore, improve orthopaedic implant efficacy [12]. With the advent of nanostructured materials (materials with grain sizes less than 100 nm in at least one direction [13]) it may now be possible to synthesize materials which simulate the surface properties of physiological bone. Orthopedic research has placed considerable emphasis on developing bioactive composites of nano-scale HA (n-HA) and polymers, [14][15] because bone is composed of apatite and collagen on the nano-scale level. Well-dispersed n-HA with an ultrafine structure has the potential for improved performance, because its surfaces have minimal defects and it has a high ratio of surface area to volume [16][17]. Recently, various nano-hydroxyapatite (nHA)/polymer composites scaffolds were developed as potential support for bone substitutes due to their compositional analogy to bone [18][19].

These scaffolds should have a well interconnected porous structure to encourage cell proliferation when implanted in the body [20][21]. The manufacture of scaffolds using computer-controlled design has received special attention focused on modified rapid prototyping methods such as fused deposition modelling, selective laser sintering, 3D printing, multiphase jet solidification, and 3D plotting [22][23]. Of the rapid prototyping techniques, stereolithography is the most versatile method with the highest accuracy and precision [24]. The working principle of stereolithography is based on spatially controlled solidification of a liquid photo-polymerisable resin. Using a computer- controlled laser beam or digital light projection, and a computer-driven support platform, a 3D object can be constructed in a layer-by-layer way [25]. The availability of suitable resin is very limited, which in general leads to non-degradable polymer networks. Recently we have reported the use of stereolithography and methacrylate end-functionalised poly(D,L-lactide) (PDLLA) oligomers with non reactive diluent that allows the fabrication of tissue engineering scaffold by computer aided design(CAD) [26]. In this work a combination of nano-HA powder and PDLLA/N-methyl pyrollidone resin is proposed as the basis to realize composite bioactive scaffold by stereolithography.

6.2 Materials and Methods

6.2.1 Materials

D,L-Lactide was obtained fromPurac Biochem, The Netherlands. Hexanediol, stannous octoate, methacrylic anhydride (MAAH), tocopherol, dibenzopyrazine were purchased from Sigma–Aldrich, USA and used without further purification. Triethyl amine (TEA) (Fluka, Switzerland), ethyl lactate (Merck, Germany), and technical grade isopropanol and acetone (Biosolve, The Netherlands) were used as received. Orasol Orange G was gift from Ciba Specialty Chemicals, Switzerland. Lucirin TPO-L (ethyl-2,4,6-trimethylbenzoylphenylphosphinate) was a gift from BASF, Germany. Analytical grade dichloromethane (Biosolve, The Netherlands) was distilled from calcium hydride (Acros Organics, Belgium). Nano-sized Hydroxyapatite (particle size < 200nm) was obtained from Sigma Aldrich.

6.2.2 Polymer synthesis

Linear oligomers were synthesised on a 100gr scale by ring opening polymerization of D,L-lactide for 40h at 130°C under an argon atmosphere, using stannous octoate as a catalyst. Hexanediol were used as initiator to prepare 2-armed oligomers, the molecular weights and arm length were varied adjusting the monomer to initiator ratio. Proton-nuclear magnetic resonance spectroscopy (H-NMR, $CDCl_3$ Varian 300 Mhz) was used to determine lactide conversion and oligomer molecular weight. Oligomers were functionalised by reacting the terminal hydroxyl groups with methacrylic anhydride in dry dicloromethane under an argon atmosphere. The formed methacrylic acid was scavenged with triethyl amine (TEA). An excess of 20 mol% of MAAH and TEA per hydroxyl group was used. The macromer solution were filtered and precipitated into cold isopropanol. The isolated macromers were then washed with water and freeze-dried. The yeld was around 80 to 85%.

6.2.3 Nano-sized hydroxyapatite

Hydroxylapatite (HA) and is a calcium phosphate biomaterials with an excellent biocompatibility and bioactivity [27] which is probably due to their similarity with the hard tissues of the body. As is known, calcium phosphate materials form the main mineral part

of calcified tissues, the apatite crystals in bone are formed as thin needles, out 5-20 nm by 60 nm with a poor crystallinity in the collagen fibre matrix [28]. A nano-hydroxyapatite (particle size <200nm) purchase from Sigma-Aldrich was adopted to realize the composite resin.

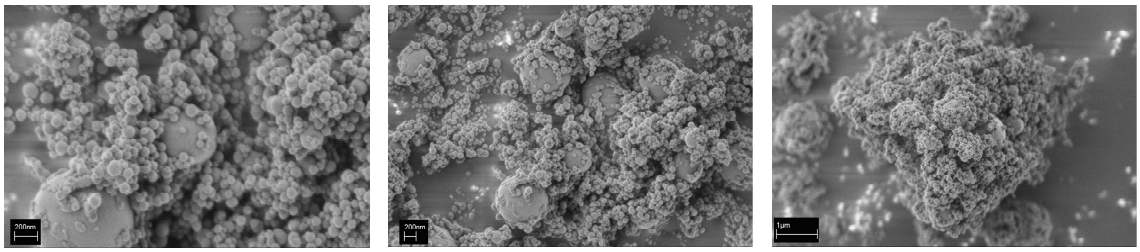

Fig. 6.1: SEM images of nano-sized Hydroxyapatite purchased from Sigma Aldrich

6.2.4 Composite resin formulation and network preparation

Nano-HAP powder was dispersed in different amount 5%-10%-20% at 60ºC in poly(D,L-Lactide) dimethacrylate macromere(molecular weight 3.0 kDa). To formulate liquid polymerisable poly(D,L-lactide)/n-HAP composite resin, macromer were diluited with N-methyl-2-pyrollidone. A viscosity of approximately 5 Pa s will be appropriate for our purposes. The resins viscosity was determinated over a range of diluent concentration at 25°C using a Brookfield DV-E rotating spindle viscometer, equipped with a small sample adapter. The shear rate was varied between 0.6 to 5.0 r.p.m.

Then a solution of of Lucirin TPO-L as biocompatible UV photo initiatior, Tocopherol as antioxidant to prevent premature crosslinking of the resins and Orasol Orange G dye in N-Methyl-2-pyrollidone (NMP) was mixed in. The final resin composition was 68% macromer, 31% NMP, 2,7 % Lucirin photo initiator, 0,13% Tocopherol, 0,1% Orange Orasol dye. Starting with this resin 4 different types of composite resins have been prepared as shown in the table below.

	PDLLA (wt%)	**NMP** (wt%)	**Lucirin** (wt%)	**Tocopherol** (wt%)	**Orange orasol** (wt%)	**n-HA** (wt%)
0% n-HAP	67	30	2,7	0,13	0,1	0
5% n-HAP	67	30	2,7	0,13	0,1	5
10% n-HAP	64,7	32,4	2,7	0,13	0,1	10
20% n-HAP	64,7	32,4	2,7	0,13	0,1	20

Tab. 6.1: The different composite resins compositionsrelated to the amount of n-HA added.

To obtain network , the resin were irradiated with 365nm UV-light for 20 min (ultralum crosslinking cabinet, intensity 3-4 mW/cm^2). Silicone rubber moulds, covered with fluorinated ethylene-propylene (FEP) film to avoid oxygen inhibition, were employed to prepare composite specimen.

6.2.5 Network characterization

After the UV curing process, PDLLA network were extracted with 3:1 mixtures of isopropanol and acetone, and dried at 90°C under nitrogen flow for 2d. The mechanical properties of the extracted and dried networks were determinated in tensile and 3-point bending tests using a Zwick Z020 universal tensile tester. For the tensile test dumbbell-shaped specimen were used according with the ISO 37-2 norm. Specimens have been cut from a film measuring 70 x 24 x 0.5 mm^3 and their dimensions are in accordance with the table below:

Dimensions	**Specimen (mm)**
A Overall length	75
B Width of ends	12,5 ± 1,0
C Length of narrow portion	25,0 ± 1,0
D Width of narrow portion	4,0 ± 0,1
E Transition radius outside	8,0 ± 0,5
F Transition radius inside	12,5 ± 1,0

Tab. 6.2: Measure of dumble-shaped specimen for thensile test according with the ISO 37-2

For the tensile test a cross-head speed of 5.00 mm/min have been used with a load-cell of 500N. The elastic modulus was defined as the initial linear modulus and at least five specimens were tested for each sample.

Flexural properties have been evaluated with 3-poin bending test in agreement with the ISO 178. Test specimens have been cut in rectangular shape with the following dimensions:

Dimension	Specimen (mm)
Tickness	0.5±0.01
Length	40±0.01
Width	25±0.01
Support span	174±0.01

Tab. 6.3: measure of rectangular bars for 3-point bending test according with the ISO178

The cross-head speed have been calculated with the following equation:

$$R = \frac{ZL^2}{6d}$$

where :

R = Rate of crosshead motion, mm/min

L = support span, mm

d = depth of specimen, mm

Z = rate of straining of the outer fiber, mm/mm/min. it was equal to 0.01 in accordance with the ISO

The equation gave us a cross-head speed of 1 mm/min.

6.2.6 Stereolithography

The composition of the resins used for stereolithography is summarized in tab.5. Depending on the amount of n-HA used (0,5,10,20%) the weight % of NMP used varies between 45 to 50%. All the 4 types of composite resin contain 2,7% of ethyl-2,4,6-trimethylbenzoylphenylphosphinate (Lucirin TPO-L photo initiator from BASF), 0,1% of Orange Orasol G dye (Ciba SC) and 0,13% of α-tocopherol inhibitor (Fluka). A commercial stereolithography apparatus (Envisiontec Perfactory Mini Multilens SLA) was employed to build designed structures. The building process involves subsequent projections of 1280x1024 pixels, each 32x32µm^2 in size. Layer with thickness of 25µm were cured by irradiating for 25-30s (depending from the resin) with blue light (intensity 17 mW/cm^2). Composite resin were sonicated for 20 min before using in stereolithography to make it more homogeneus and to avoid that nano-HA particles could settling on the bottom of the bottle. Uncured excess resin was washed out and the diluent, non-reacted macromer and photo-initiator were extracted from the structures

with a mixture isopropanol/acetone 3/1. The extracted structure were then dried at 90°C for 2d under a nitrogen flow.

6.2.7 Design of porous structures

The three dimensional design that was chosen for the scaffold architecture was a Double Gyroid. The function is triply periodic and is uniquely defined by its unit cell. The following trigonometric functions were used:

$$abs(\cos(x)\cdot\sin(y)+\cos(y)\cdot\sin(z)+\cos(z)\cdot\sin(x))-1.15$$

with boundary conditions:

$$\left(x^2+y^2\right)\le(5\pi)^2 \;\&\; |z|\le 5\pi$$

K3DSurf v0.6.2 software (http://k3dsurf.sourceforge.net) was used to generate CAD-files that describes the surfaces of Double Gyroid structure. To obtain porosity of approximately 78%, offset value of 1.15 is required. With this architecture cylindrical Double Gyroid composite structure have been built using resins with different amount of n-HA. Rhinoceros software was used to scale the CAD-files of the structure to the desire dimension. Cylinder have been scaled up compared to the desired dimension of 10x10x10mm^3 anticipating the shrinkage upon extraction of non-reactive diluent from the built structures.

6.2.8 Morphological analysis

Structures have been analyzed from a structural point of view using a micro-computed tomography (µCT), (Skyscan 1072 at 10µm resolution). Scanning was done at an X-ray tube voltage of 52 kV, a current of 179 µA and a rotation angle of 180 °C. After reconstruction using the Skyscan software thresholded isosurfaces images were obtained. The software was also used to generate pore size distribution maps of the structures. To compare the built structures with the software design, the latter were evaluated in the same manner as well.

6.2.9 Mechanical test

Static and dynamic mechanical characterization was performed on poly(D,L-lactyde) Double Gyroid structures. Concerning the static compression analysis, test have been

performed by using a dynamometric machine (Instron 5566) equipped with a load cell of 1 kN and requiring a crosshead spead of 1mm/min. Porous cylindrical specimen characterized by height of 10mm and a diameter of 10mm have been tested. At least five samples of each composition were measured and the result averaged. Young's modulus (MPa) was calculated from the stress-strain curve as the slope of the initial linear portion of the curve. The evaluation of static curve is preparatory to the dynamic mechanical analyses. Indeed, the definition of the elastic range allowed to establish the average load and amplitude to apply for the cyclic stimulation.

Dynamic mechanical analysis were performed by Bose Electroforce biodynamic system by superimposing a sinusoidal stress to the specimen and recording the relates strain.

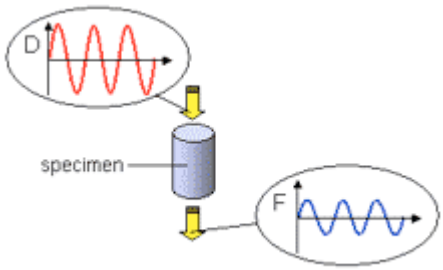

Fig. 6.2: Schematic view of a Dyanmic mechanical analysis in which superimposing a sinusoidal stress it was recorded the related strain

Specimens were tested under the stress control mode, where a pre-load of 0.5 N was initially applied followed by a dynamic load of 20N. The evolution of elastic moduli was evaluated varying the frequency from 0.1 to 9 Hz.

6.2.10 hMSCs culturing and scaffolds seeding

Bone marrow-derived hMSCs (Clonetic, Italy) were expanded and cultured in proliferation medium consisting of α-modified Eagle's medium (α-MEM)(Biowittaker, Belgium), 10% foetal bovine serum (FBS), 100U/ml penicillin and 0,1 mg/ml streptomycin (Hyclone, UK). Medium was refreshed three time per week and cells were trypsinised whenever a confluency of 70-80% was reached. in a humidified atmosphere containing 5% CO_2 at 37°C. Prior to seeding, the scaffolds were disinfected in 70% ethanol (1h) and then 1% antibiotic/antimycotic in phosphate-buffered saline (PBS) (2h), and incubated in medium (2h) to allow pre-wetting of the material and protein

adsorption on its surface. hMSCs were trypsinised and resuspended in 50µl of medium at a concentration of 4 x 10^5 cells per scaffold seeding volume. The cell suspension was pipetted on top of the scaffolds that were placed each in a well of non cell-adherent polystyrene surface and incubated for 2 h in a humidified atmosphere (37°C, 5% CO_2). Scaffold were maintained in culture for 28 days, with the cell culture medium being changed every 3-4 days.

6.2.11 Alkaline phosphatise (ALP) assay

The cell-scaffold constructs were removed from the culture plates on days 1, 7, 14, 21 and 28 and washed with PBS (Sigma–Aldrich, Italy). The cells were lysed in Cell Lysis Buffer (BD Pharmingen ™) and ALP activity was measured using a SensoLyte™ pNPP alkaline phosphatase assay kit (AnaSpec, DBA, Milano) according to the manufacturer's instructions. The ALP activity was read off a standard curve obtained with ALP concentrations of 0 - 200 ng/ml (detection limit 0.01 ng/ml). Double stranded DNA (dsDNA), as a marker for cell number, was measured using a PicoGreen® dsDNA quantification kit (Molecular Probes). First, 100 µl of 200x diluted Picogreen® dsDNA quantification reagent was added to 100 µl of cell lysate in a flat-bottomed, 96-well plate. Following 10 min incubation, the fluorescence of Picogreen® was determined at a wavelength of 520 nm after excitation at 585 nm using a plate reader (multilabel counter 1420 Victor, Perkin-Elmer, Italy). dsDNA was quantified according to a calibration curve of l-dsDNA standard in 10 mM Tris, 1 mM EDTA, pH 7.5, buffer. Each experiment was performed three times in triplicate.

6.3 Results and Discussions

6.3.1 Macromers synthesis

The monomer conversion and the arm length of the synthesised lactide oligomers could be derived from ^{1}H-NMR spectra. A typical spectrum is depicted in Figure. The degree of functionalization of the obtained oligomers was determined from the peak areas corresponding to the methacrylate protons (5,65 and 6.2 ppm) and the hexandiol -CH_2O- protons (4.1 ppm). Conversion reached was above 98%.

Macromers were diluited with varying amounts of N-methyl-2-pyrollidone (NMP), and nano-HA was added in different wt%. the viscosity of the composite resin was determined at 25°C over a range of shear rates. Behaviour of the resin was essentially Newtonian and it clearly changes with the amount of n-HA. so we modified the composition of the resin, in particular the amount of solvent, depending on the amount of Hydroxyapatite

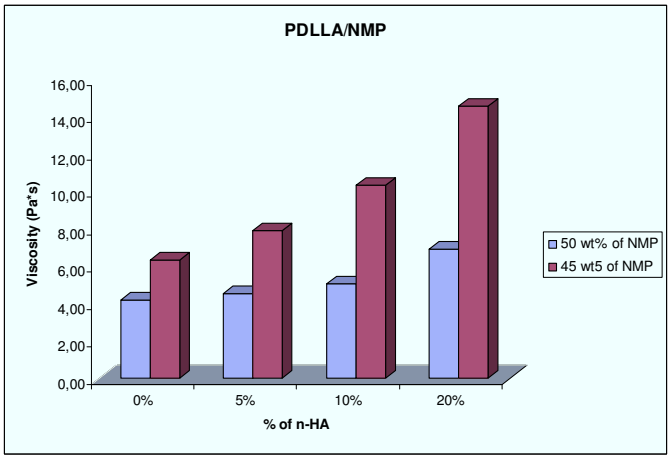

Fig. 6.3: The resin viscosity of PDLLA/nano-HA resin as a function of the amount of nano-HA.

	η (centipoises)		η (Pa s)	
	45% of NMP	**50% of NMP**	**45%of NMP**	**50% of NMP**
0% n-HA	4220,38	6357,14	4,22	6,36
5% n-HA	4530,41	7885,71	4,53	7,89
10% n-HA	5042,86	10371,43	5,04	10,37
20% n-HA	6954,29	14610,00	6,95	14,61

Tab. 6.4: Viscosity of the composite resin related to the amount of solvent and n-HA used during the preparation.

6.3.2 Network characterization

The mechanical properties of the extracted and dried composite networks were determined in tensile and 3-point bending test.; the result are shown in Figure and table. Results are shown in the graph below and it's possible to see that the elastic modulus rise with the amount of n-HA.

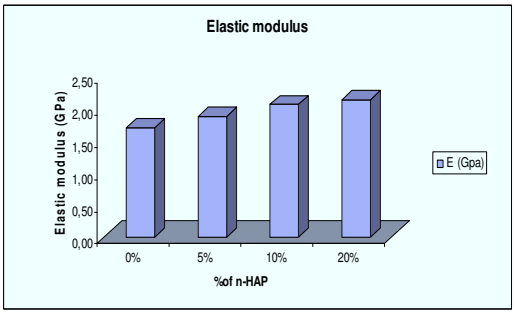

Fig. 6.5: the flexural modulus (E') as function of nano-HA amount.

n-HAP (%)	**σ_{max}** (MPa)	**E** (Gpa)	**ε_{max}** (%)
0%	20.84±3.72	1.70±0.17	1.33±0.2
5%	19.44±2.15	1.88±0.12	1.10±0.2
10%	25.88±3.33	2.06±0.06	1.46±0.3
20%	27,80±3,20	2.13±0,13	1,41±0,2

Tab.5: Tensile properties of photo crosslinked PDLLA/nano-HA networks. Determination of the Young modulus (E'), tensile strength (σ_{mx}) and strain at failure (ε_{max})

The 3-point bending test follow the trend of tensile as it's possible to see in the graph below:

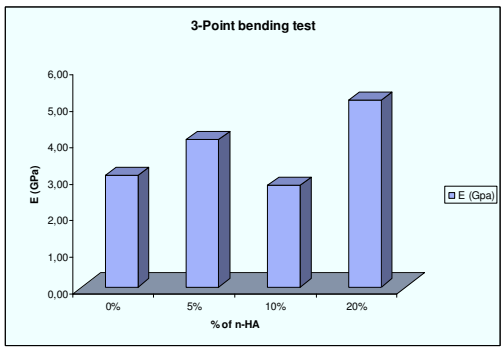

Fig.5: the flexural modulus (E') as function of nano-HA amount

n-HAP (%)	**σ_{max}** (Mpa)	**E** (Gpa)	**ε_{max}** (%)
0%	65.98±9.51	3.06±0.43	3.5±1.3
5%	45.33±9.44	4.05±0.33	1.3±0.2
10%	38.33±6.44	2.79±0.32	1.7±0.6
20%	50.62±6.48	5.13±0.61	1.2±0.2

Tab.6: The flexural properties of photo crosslinked PDLLA composite network.

The presence of the HA nanocrystals substantially increase the tensile modulus relative to the PDLLA polymer. For the nanocomposite containing 20% n- HA, the modulus calculated from the 3-point bending test even reaches to 5.13 GPa as compared to 3.06Gpa for pure PDLLA. For the tensile test the increase in mechanical properties is

not so evident as for the 3-point bending test, this is probably due to the fact that, as we will see in the SEM images, n-HA mainly tend to localize on the surface of the material after the cross-linking process.

6.3.3 Stereolithography

Stereolithography is a solid freeform technique (SFF) that was introduced in the late 1980s. Although many other techniques have been developed since then, stereolithography remains one of the most powerful and versatile of all SFF techniques [29]. Complex structures can be built by illuminating sequential layers of a polymerisable resin using digital pixel mask or arrays or mirrors. In stereolithography, control of the thickness of the layer that is cured is essential. For a given resin, the cure depth is determined by the energy of the light to which the resin is exposed. This energy can be controlled by adjusting the power of the light source, and the scanning speed (for laser systems) or the exposure time (for projection systems). Time of exposure depend from the resin and was calculated from the *Working curve,* as shown in fig. the experimental measurements of working curve are obtained by measuring the curing depth under various UV exposure times. To create polymer-ceramic composite objects [30][31], ceramic particles (e.g. allumina or hydroxyapatite) are homogeneously suspended in the stereolithography resin and photo-polymerised in the SLA. Processing of the resin is more difficult, as the viscosity of the resin can significantly increase upon addition of the powder. Maximum ceramic contents of up to 53 wt% have been reported. The curing characterization of composite resins with different amount of n-HA (0,5,10,20%) has been compared. The result indicates that for high exposure time the curing depth is in inverse proportion with the amount of n-HA, in particular resin with 20% of n-HA showed a plateau over 90µm for the D_p (light penetration depth).

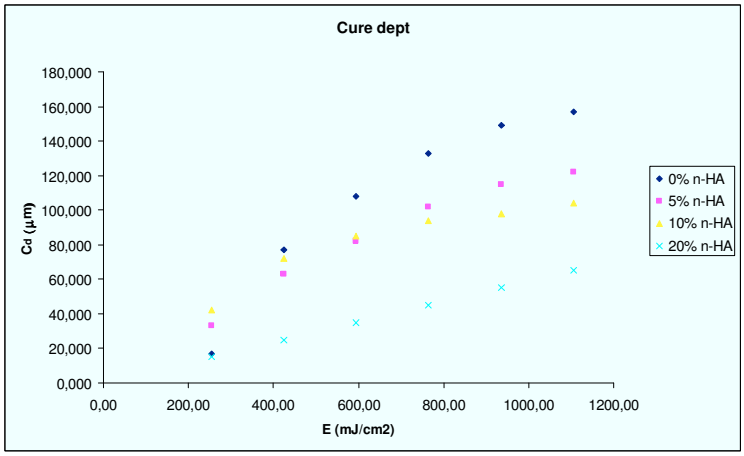

Fig. 6.6: Stereolithography working curves of PDLLA/nano-HA composite resin containing different amount of nano-HA

With this dye containing resin, stereolithography was used to build ISO37-2 non-porous dumbbell-shaped for tensile testing, ISO 178 non porous specimen for tensile test and porous Double Gyroid structure.

6.3.4 Analyses of porous structures

Porosity and pore size have significant ramifications on the ability of tissue engineering scaffolds to support bone regeneration for several reasons. First, porosity and pore size have been shown to affect cell attachment efficiency, which consequently impacts the cell seeding density, cell distribution, and cell migration [32][33]. These factors have been shown to affect osteogenic differentiation through changes in signalling distances [34]. Moreover, pore size and porosity have a significant effect on the mechanical strength of a scaffold. Sufficient scaffold strength to provide mechanical support to a defect is often required for a hard tissue engineering scaffold such as bone, especially when the bone is load bearing [35]. Further, porosity and pore size affect the ability of the scaffold to promote in vivo osteoconduction and vascularization. Integration of native tissue into a scaffold is fostered through growth into interconnected pores, and thus both optimal and minimal pore sizes have been established to support tissue ingrowth [36]. Finally, pore size and porosity affect in vivo and in vitro cell signaling, which in turn affects osteoblastic differentiation of MSCs and the production of ECM protein. The double gyroid architecture has an open accessible pore network where the number, size and location of the interconnections play an important role in cell seeding, and in nutrient transport and cell migration during cell culturing phase.

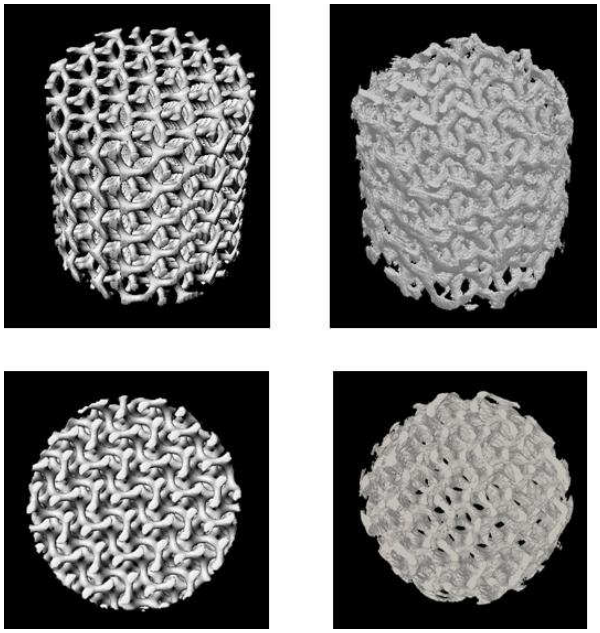

Fig. 6.7: Visualization of the Double gyroid porous architecture. Columns : (1) CAD-Design of the Double gyroid structure, (2) µCT scanning of the built structure

The presence of n-HA doesn't affect the porosity and the interconnectivity of the structure, their value and specific surface area remain the same for the composite structure. Table 8 shows the parameters related to the pore network architecture of PDLLA and PDLLA/n-HA composite scaffold.

	Porosity (vol%)	**Specific surface area** (mm^{-1})	**Average pore size** (mm)
Double gyroid HAP	77,46±0,69	13,21±0,72	0,695±0,015
Double gyroid	78,16±1,54	13,89±0,68	0,745±0,020

Tab. 6.7: comparison between structural parameters for Double Gyroid architecture obtain with PDLLA and PDLLA/nano-HA composite resin.

Scanning electron microscopy (SEM)(Philips XL30 operated at 10 (kV) was used to assess the porous architecture and the distribution of the n-HA within the structure. Figure 7 shows 3 different scaffold architecture: (A) Scwartz, (B) Diamond and (C) Double Gyroid built with PDLLA resin with 5% of n-HA. Geometry of the structures remain almost unaffected by the presence of the n-HA and is still possible to notice the layer by layer architectures that characterized the stereolitography process.

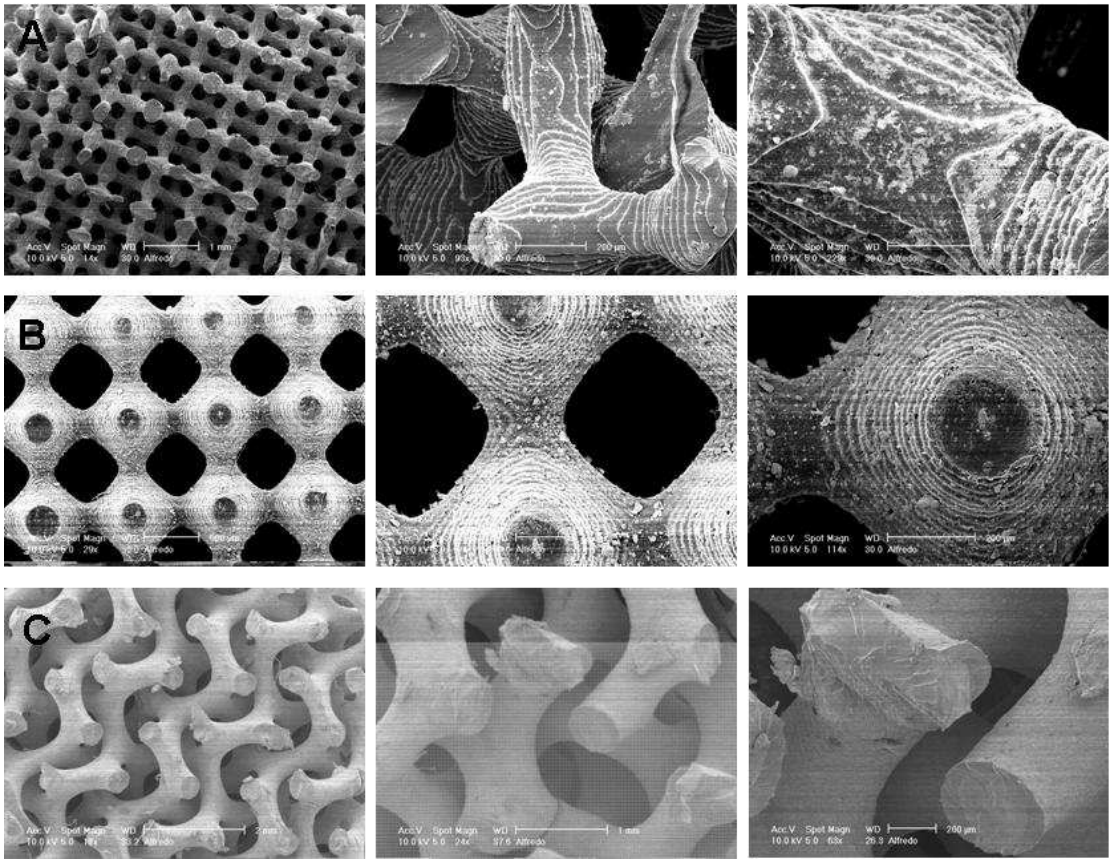

Fig. 6.8: SEM images of porous PDLLA/nano-HA composite structure with different architecture built by stereolithography: (A) Diamond architecture, (B) Schwartz architecture, (C) Double Gyroid architecture.

Figure 8 shows the comparison between structures with different amount of n-HAP (0%, 5%, 10%, 20%) and it is possible to notice how the n-HAP is well dispersed inside the scaffold. It was expected to find the n-HAP inside the trabecule of the structure but the sem reveal that the n-HA is mainly localized on the surface of the scaffold. This is probably due to a phase separation between the hydrophobic PDLLA and the hydrophilic n–HAP, during the cross-linking process.

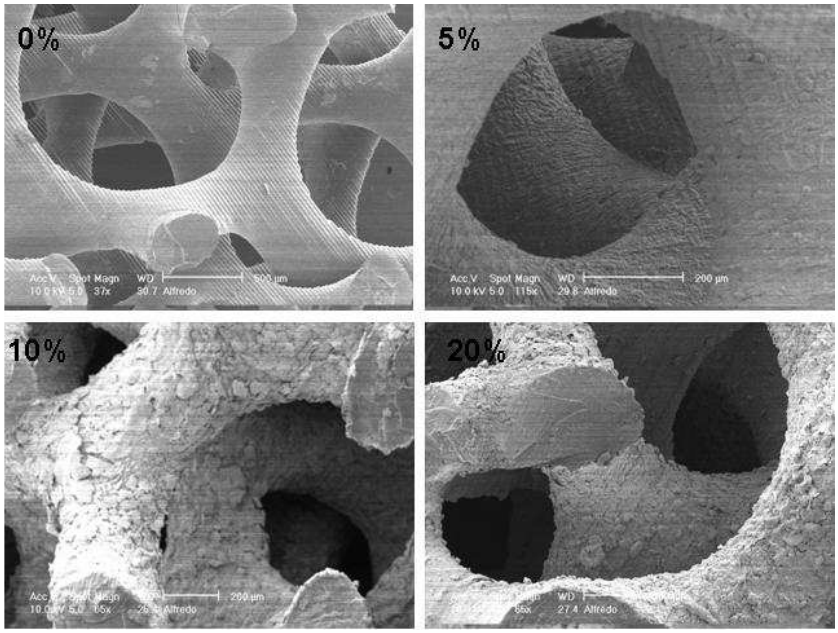

Fig. 6.9: comparison between Double gyroid structures with different amount of n-HA, respectively 0%, 5%, 10% 20%.

Using high resolution SEM is possible to find small cluster of n-HA inside the matrix of PDLLA. This clusters could affect in a bad way the mechanical properties of the structure reducing its mechanical strength.

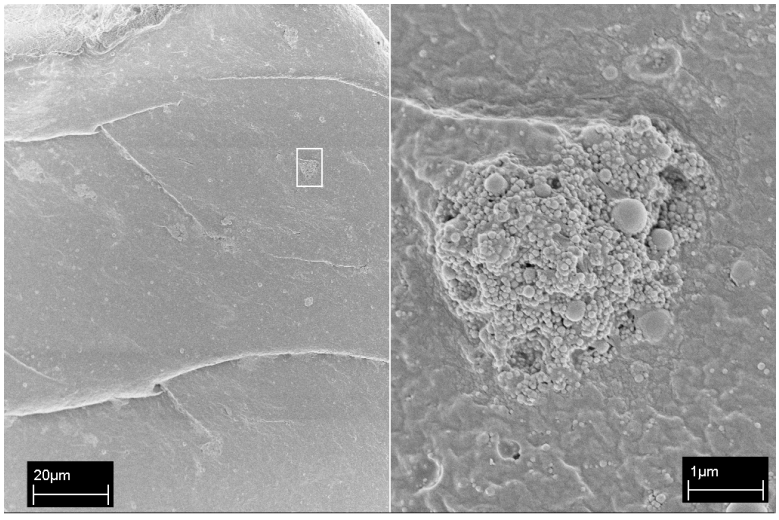

Fig. 6.10: High resolution SEM of composite structure. It evaluates the presence of n-HA cluster inside the PLLA matrix.

6.3.5 Mechanical characterization

The influence of the nano-HAP on the mechanical properties of the structures was analysed as well through static and dynamic compression test.. The Young's modulus varies from 13 MPa for PDLLA Double Gyroid structures till over 30 MPa for the Composite PDLLA/nano-HAP structures with 20% amount of hydroxyapatite. The plot shows the two stress-strain curves for PDLLA (red plot) and PDLLA/n-HAP 20 wt% (blue plot) in . The curve describes the mechanical behaviour of porous systems under static compression test: it shows a linear elasticity till failure describing a typical brittle behaviour.

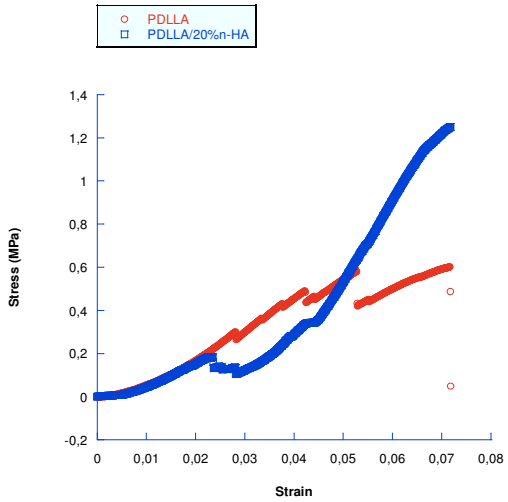

Fig. 6.11: Stress-Strain diagram of PDLLA and PDLLA/n-HA composite structures at similar porosity.

n-HAP (%)	σ_{max} (Mpa)	E (Gpa)	ε_{max} (%)
0%	0.61±0.20	12.27±2.6	0.07±0.01
10%	0.68±0.20	23.14±4.9	0.07±0.02
20%	1.23±0.20	30.76±6.9	0.09±0.01

Tab. 6.8: Mechanical properties of Double Gyroid structures as function of the amount of n-HA.

Observing the plot it is possible to see some discontinuity point due to the particular architecture of the scaffold. Double Gyroid is characterized by two interpenetrating non communicating Gyroid structure so the discontinuity point could be due to the collapse of one of the Gyroid structure before the other. Dynamic mechanical analysis (DMA)

measure the response of a material to a sinusoidal stress over a range of frequencies and is sensitive to chemical and physical structure of polymers and their composites.[37] DMA was carried out on cylindrical specimen (measuring 10x10mm) characterized by Double Gyroid architecture. See supporting information for details on the calculation of the various dynamic properties. The main variables obtained from DMA are the storage modulus (E'),which represent the elastic component of a system and is equivalent to the energy stored through deformation, the loss modulus (E'') which represents the viscous component and is equivalent to the energy dissipated through deformation, and tan(δ), which is the ratio E'/E'' and provides a measurement of the damping of the material. Specimens were tested over a range of frequency (from 0.1 to 9 hz), this enabled to estimate a comparative analysis of the storage modulus "E'" (elastic component) equivalent to the energy stored through deformation and the loss modulus "E''" equivalent to the energy dissipated through the cycled stimulation.

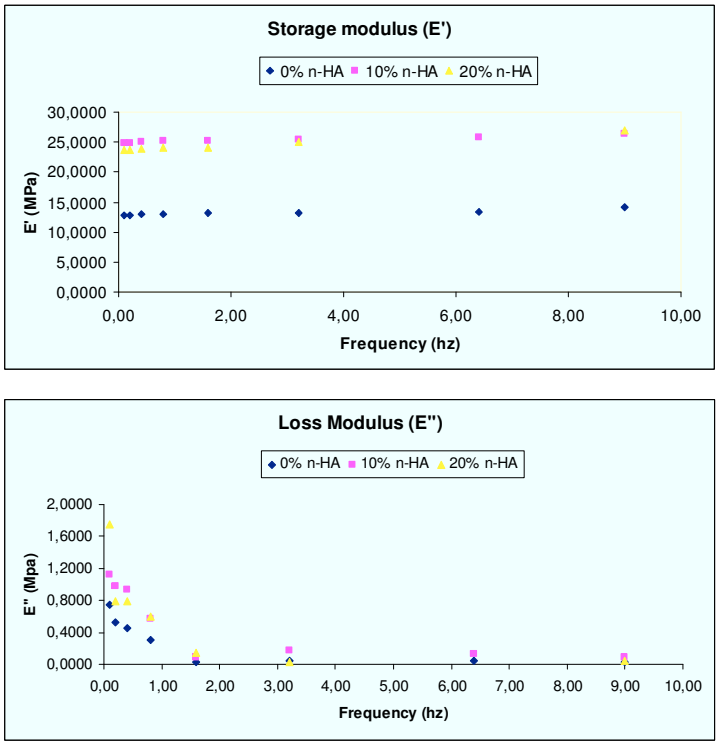

Fig. 6.12: the principal dynamic properties are : (a) the storage or elastic modulus (E'), that is a measure of how elastic the material is and ideally is equivalent to the Young's modulus. (b) the loss modulus (E''), also called the viscous or imaginary modulus that represent the energy lost to friction and internal motion.

Moreover the test highlights the viscoelastic behaviour of the samples showing that E' increases with frequency. Otherwise loss modulus E'' is not significantly affected as frequency varies.

6.3.6 ALP and DNA assays.

In order to evaluate the biocompatibility and osteogenic properties of the PDLLA/nano-HAP composite scaffold hMSCs were seeded and cultivated for 21 days in basic medium. The proliferation of hMSCs in direct contact with the scaffold was quantitatively measured by DNA Picogreen assay. According to our results the nano-HAP had a positive effect on cell adhesion and proliferation. The presence of nano-HAP is a bioactive signal for cells and it encourages proliferation on the structure. In fact the proliferation peak is reached at 14 days for the PDLLA/nano HAP composite scaffold with 10 wt% of HAP. Meanwhile samples with 20 wt% of nano-HAP have a different behaviour and at 21 days proliferation is still growing probably due to the greater presence of HAP on the surface that generates a tortuous walk for the cells. It follows that cells have great difficult to see each other and reach confluence.

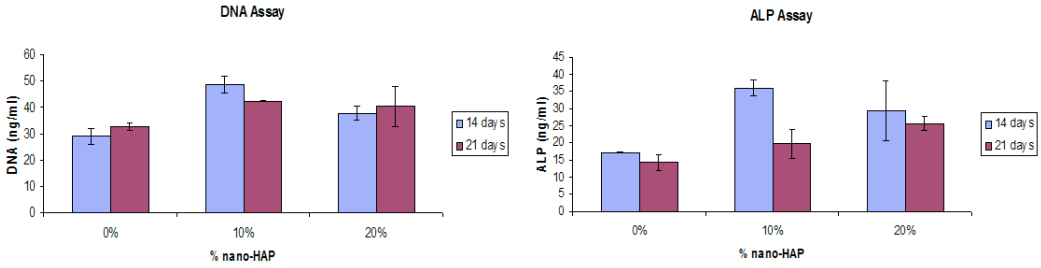

Fig. 6.13: DNA and ALP assays for composite PDLLA scaffold with different amount of nano-HAP

A preliminary study of the differentiation of hMSCs towards the osteoblastic phenotype was quantitatively determined by carrying out a destructive assay for ALP activity using the p-nitophenyl phosphate method. ALP is an enzyme produced by differentiating osteoblasts and can be responsible for the construction of bone matrix. An increase in ALP activity was observed for composite scaffold if compared with the pure PDLLA ones. This is a confirmation that nano-HAP have a central role in cell differentiation towards the osteoblastic phenotype. Moreover, ALP activity shows a peak at 14 days

both for pure PDLLA scaffold than for composite ones. However, the ALP data offer only a preliminary indication and further investigation of mineralization should be performed in order to evaluate the formation of mineral deposits and gene espressions, required to reproduce the bone ECM matrix.

6.4 Conclusions

Scaffolds for osteogenesis should mimic bone morphology, structure and function to optimize integration into surrounding tissue. It is well-known that bone is a structure composed of hydroxyapatite ($Ca_{10}(PO_4)_6(OH)_2$) crystals deposited within an organic matrix (95% is type I collagen) [38]. Nanometric-scale Hydroxyapatite seems more similar to bone apatite, and it has the ability to promote the attachment of cultured osteoblasts and to improve their metabolic activity. The major objective of this study was to create biocompatible and bioactive PDLLA/nano-HAP composite scaffolds for bone tissue engineering. Many studies have suggested methods for fabricating 3D scaffolds. However, the limitation of conventional methods is that they cannot perfectly control the pore structure. This means that cells and/or tissues cannot easily penetrate into the scaffold. The saturated cell density on the scaffold surface eventually prohibits cell and/or tissue proliferation, regeneration, and other biological activities in the long run. To overcome these problems, new techniques are required. For this, we suggested the stereolithography for easily creating 3D scaffolds with controlled macropores using composite materials. This produces scaffolds whose properties are controlled and reproducible. The scaffold used for bone regeneration must be biocompatible and bioactive. Given that bone is a typical example of a nano-composite, n-HAP could have an important role in various areas of bone tissue engineering, including the formation and maintenance of the tissue-biomaterial interface. This has focused recent attention on n-HAP as a bone tissue engineering material. PDLLA/nano-HAP scaffolds with well interconnected pores and good reproducibility were successfully fabricated using stereolithography technique, and the biological properties of the biocomposites were investigated for the first time. The stereolithography resin was a homogeneous dispersion that showed no settling of nano-HAP particles. Different composite structure were prepared from this resin by stereolithography (Diamond, Schwartz, Double

Gyroid). SEM images show that the ceramic particles are exposed to the surface, allowing interaction of cells with the nano-HAP. Mechanical tests indicated that the composite scaffold had higher compressive modulus than the PDLLA one. In addition, the ALP activity of hMSCs in direct contact with PDLLA/nano-HAP scaffolds were significantly higher than the pure PDLLA after 14 days of culture, indicating that the nano-HAP improved biological properties of the materials.

Acknowledgments

We would like to acknowledge Prof. Dirk Grijpma and all the staff of the department of Polymer Chemistry and Biomaterials of the University of Twente for supporting the experimental research during the exchange project. Special thanks also to Dott. S. Zeppetelli for the in vitro biological characterization.

References

[1]. C. Du,1 F. Z. Cui, Q. L. Feng, X. D. Zhu, K. de Groot, *J. Biomed Mater Res*, **1998**, 42, 540.

[2]. V. Guarino, F.Causa, L.Ambrosio, *Expert Rev. Med. Dev.* **2007**, 4, 405.

[3]. D.W. Hutmacher, J.T. Schantz, C.X.F. Lam, K.C. Tan, T.C. Lim, *J. Tissue Eng. Regen. Med,* **2007**, 1, 245

[4]. T.J. Webster, E.S. Ahn, *Adv. Biochem. Eng/Biotechnol,* **2007,** 103, 275.

[5]. J. Currey, *Nature*, **2001**, 414, 699.

[6]. J.B. Thompson, J.H. Kindt, B. Drake, H.G. Hansma, D.E. Morse, P.K. Hansma, *Nature*, **2001**, 414, 773.

[7]. J. J. A. Barry, A. V. Evseev, M. A. Markov, C. E. Upton, C. A. Scotchford, V. K.Popov, S. M. Howde, *Acta biomaterialia,* **2008**, 4, 1603

[8]. T. J. Webster, R. W. Siegel, R. Bizios, *Biomaterials* **1999G,** 20 , 1221.

[9]. B. Walivaara ,B.O. Aronsson ,M. Rodahl, J. Lausma, P. Tengvall. *Biomaterials* **1994**, 15, 827.

[10]. J.E. Ellingsen, *Biomaterials* **1991**, 12, 593.

[11]. E.D. Hay , *New York Plenum*, **1991.**

[12]. F.S. Kaplan ,W.C. Hayes, T.M. Keaven , A. Boskey , T.A. Einhorn, J.P.Iannotti, *American Academy of Orthopaedic Surgeons*, **1994**, 127.

[13]. R.W. Siegel, *Scientific American*, **1996**, 275, 42.

[14]. D. Nebahat ,M.K. Dilhan ,B. Elvan, *Colloid surface,* **2006,** 48, 42.

[15]. W. Patcharaporn ,S. Neeracha , et al. *Macromolecule Biosc.*, **2005**, 6, 70.

[16]. C. Du ,F.Z. Cui ,X.D. Zhu ,K. de Groot, *J.Biomed.Mat.Res,* **1999**,44, 407.

[17]. P.X. Ma ,R. Zhang, *J.Biomed.Mat.Res,* **1999**,46, 60.

[18]. K. I. Clarke, S. E. Graves, A. T.-C. Wong, J. T. Triffitt, M. J. O. Francis, and J. T. Czernuszka, *J. Mater. Sci. Mater. Med,* **1993,** 4, 107

[19]. K. S. Tenhuisen and P. W. Brown, *J. Biomed. Mater. Res,* **1994**, 28, 27.

[20]. K.F. Leong, *Biomaterials,* **2003**, 24, 2363.

[21]. K. Rezwan ,Q. Chen ,J. Blaker , et al, *Biomaterials,* **2006** 27, 3413.

[22]. K.H. Tan ,C.K. Chua ,K.F. Leong, *Biomaterials,* **2003**, 24, 3115.

[23]. W.H. Dietmar ,S. Thorsten ,Z. Iwan, *J Biomed Mater Res*, **2001**, 55, 203.

[24]. F. P.W. Melchels, J. Feijen, D. W. Grijpma, *Biomaterials,* **2009,**30, 3801.

[25]. F.P.W. Melchels, K. Bertoldi, R. Gabbrielli, A.H. Velders, J. Feijen, D.W. Grijpma, *Biomaterials,* **2010**, 31, 6909.

[26]. A.Ronca, D.W. Grijpma, L.Ambrosio, *Chapter 4 of the thesis*

[27]. L. Yubao*, J. De Wijn, C.P.A.T. Klein, S. Van De Meer, K De Groot, *Journal of Material Science: Materials in Medicine*, **1994**, 5, 252.

[28]. J.B. Park, R.S. Lakes, *Biomaterials: an introduction*, **1992**, 192

[29]. F.P.W. Melchels, J. Feijen, D.W. Grijpma, *Bioamterials*, **2010**, 31, 6121

[30]. J.W. Lee, G. Ahn, D.S. Kim, D.W. Cho, *Microelectron Eng,* **2009**, 86, 1465.

[31]. V.K. Popov, A.V. Evseev, A.L. Ivanov, V.V. Roginski, A.I. Volozhin, S.M. Howdle, *Journal of material Science: Mat. In Med.,* **2004,** 15, 123.

[32]. C.M. Murphy, M.G. Haugh, F.J. O'Brien, *Biomaterials,* **2010,** 31, 461.

[33]. C.M. Murphy, M.G. Haugh, F.J. O'Brien, *Bioamterials,* **2003,** 31, 461.

[34]. K. Kim, D. Dean, A.G. Mikos, J.P. Fisher, *Biomacromolecules,***2009**, 10, 1810, *J Biomed Mater Res A* **2008,** 85, 777.

[35]. S.J. Hollister, R.D. Maddox, J.M. Taboas, *Biomaterials,* **2002**, 23, 4095.

[36]. F.M. Klenke, Y. Liu, H. Yuan, E.B. Hunziker, K.A. Siebenrock W. Hofstetter,

[37]. K. P. Menard, *Dynamic mechanical analysis :a practical introduction,* **1999**, CRC Press, Chapter 3.

[38]. S.C. Marks Jr, P.R. Odgren, Principles of bone biology. 2nd ed, San Diego: Academic Press, **2002**, 3.

APPENDIX 1

Dynamical mechanical analysis

DMA can be simply described as *applying an oscillating force to a sample and analyzing the material's response to that force* (Figure A.1). From this, one calculates properties like the tendency to flow (called viscosity) from the phase lag and the stiffness (modulus) from the sample recovery[1]. These properties are often described as the ability to lose energy as heat (damping) and the ability to recover from deformation (elasticity).DMA is a very suitable technique for investigating the viscoelastic properties of polymeric materials in a wide range of temperatures and frequencies[2]. Furthermore, DMA measures the dynamic response of a particular polymeric system, being specially adequate to evaluate the performance of biomaterials when working under the cyclic solicitations generated by the human body physiological movements[2][3].

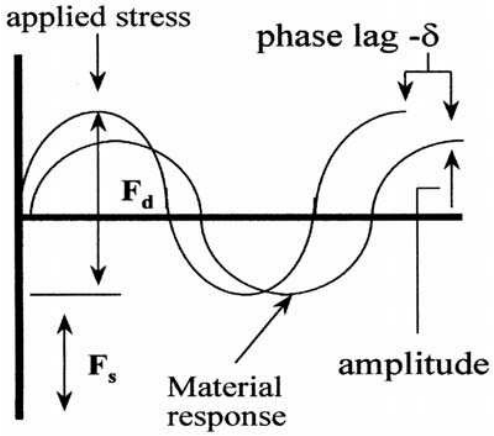

Fig. A.1: The DMA supplies an oscillatory force, causing a sinusoidal stress to be applied to the sample, which generates a sinusoidal strain[3].

The applied force is called stress and is denoted by the Greek letter, σ . When subjected to a stress, a material will exhibit a deformation or strain, γ . Most of us working with materials are used to seeing stress–strain curves as shown in Figure A.2. These data have traditionally been obtained from mechanical tensile testing at a fixed temperature.

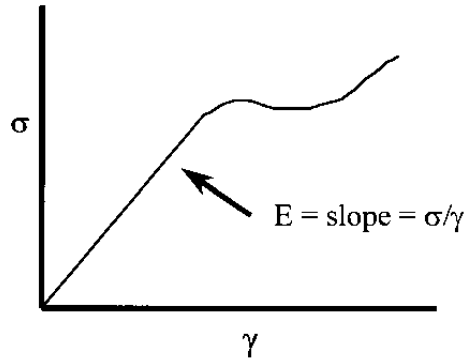

Fig. A.2: Stress–strain curves relate force to deformation [3].

The slope of the line gives the relationship of stress to strain and is a measure of the material's stiffness, the modulus. The modulus is dependent on the temperature and the applied stress. The modulus indicates how well a material will work in specific application in the real world. In DMA, a complex modulus(*E**), an elastic modulus (*E*'), and an imaginary (loss) modulus (*E"*) [1] are calculated from the material response to the sine wave. These different moduli allow better characterization of the material, because we can now examine the ability of the material to return or store energy (*E*'), to its ability to lose energy (*E*''), and the ratio of these effects (tan delta), which is called damping[4].

Applying a dynamic stress to a sample

If we take a sample at constant load and start sinusoidally oscillating the applied stress (Figure A.3), the sample will deform sinusoidally. This will be reproducible if we keep the material within its linear viscoelastic region. For any one point on the curve, we can determine the stress applied as:

$\sigma = \sigma_0 \sin(\omega t)$

where σ is the stress at time *t,* σ_0 is the maximum stress, ω is the frequency of oscillation, and *t* is the time. The resulting strain wave shape will depend on how much viscous behavior the sample has as well as how much elastic behavior. We can look at the two extremes of the materials behavior, elastic and viscous, to give us the limiting extremes that will sum to give us the strain wave. Let's start by considering the material at the Hookean region. The strain at any time can be written as:

$$\varepsilon(t) = E\sigma_0 \sin(\omega t)$$

where ε(*t*) is the strain at anytime *t, E* is the modulus, σ_0 is the maximum stress at the peak of the sine wave, and ω is the frequency. Since in the **linear region** σ and ε are linearly related by *E,* we can also write that:

$$\varepsilon(t) = \varepsilon_0 \sin(\omega t)$$

where ε_0 is the strain at maximum stress.

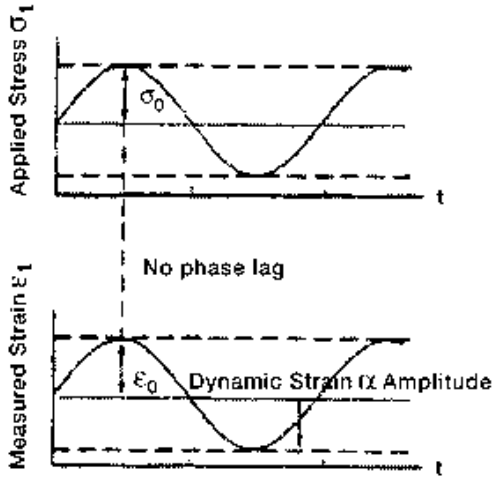

Fig. A.3: When a sample is subjected to a sinusoidal oscillating stress, it responses in a similar strain wave provided the material stays within its elastic limits[3].

The viscous limit was expressed as the stress being proportional to the strain rate, which is the first derivative of the strain.

$$\varepsilon(t) = \eta \frac{d\sigma}{dt} = \eta\omega\sigma_0 \cos(\omega t)$$

$$\varepsilon(t) = \eta\omega\sigma_0 \sin(\omega t + \pi/2)$$

$$\varepsilon(t) = \omega\varepsilon_0 \cos(\omega t) = \omega\varepsilon_0 \sin(\omega t + \pi/2)$$

where η is the viscosity. This behaviour is shown in Figure A.5,

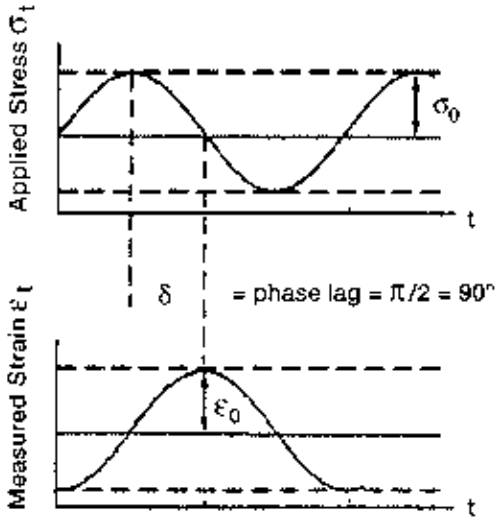

Fig. A.4: out of phase response of a viscous material

Now let's take the behaviour of the material that lies between these two limits.

$$\varepsilon(t) = \varepsilon_0 \sin(\omega t + \delta)$$

The difference between the applied stress and the resultant strain is an angle, δ, that varies in a range between 0°(elastic material) and 90°(viscous material). This behaviour is shown in figure A.4 (c).

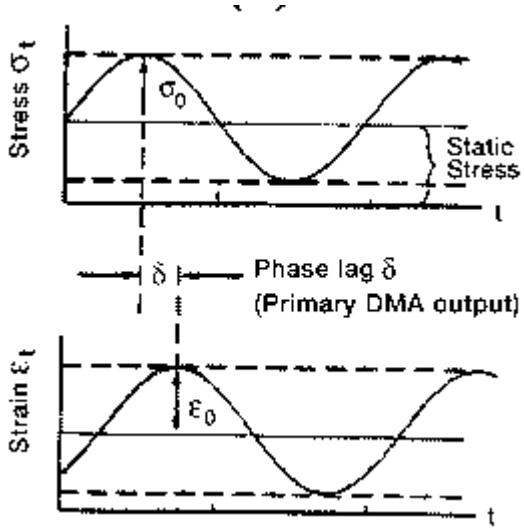

Figure A.5:viscoelastic material falls in between the elastic and viscous material

Last formula can be rewritten in this way using trigonometry:

$$\varepsilon(t) = \varepsilon_0[\sin(\omega t)\cos\delta + \cos(\omega t)\sin\delta]$$

We can now break this equation into the in-phase and out-phase strains that corresponds to curves like those in figure A.3 and A.4, respectively.

$$\varepsilon^{'} = \varepsilon_0 \sin(\delta)$$

$$\varepsilon^{''} = \varepsilon_0 \cos(\delta)$$

And the sum of these two component gives the complex strain on the sample

$$\varepsilon^{*} = \varepsilon^{'} + i\varepsilon^{''}$$

Basically this approach allows us to divide a single modulus into two terms, one related to the storage energy and another related to the loss energy.

Calculating dynamic properties

A material subject to a sinusoidal stress is characterized by a certain value of strain at the peak of the sine wave and an angle defining the lag between the stress sine and the strain sine wave[4]. We can first calculate the storage or elastic modulus, *E*'. This value is a measure of how elastic the material is and ideally is equivalent to Young's modulus. E' is calculated as follows [3]:

$$E' = (\sigma_0 / \varepsilon_0)\cos\delta = (f_0 / bk)\cos\delta$$

Where δ is the phase angle, b is the sample geometry terms, f_0 is the force applied at the peak of the sine wave, and k is the sample displacement at peak.

The loss modulus E", also called the viscous or imaginary modulus is calculated from the phase lag between the two sine waves as:

$$E'' = (\sigma_0 / \varepsilon_0)\sin\delta = (f_0 / bk)\sin\delta$$

The tangent of the phase angle is one of the most basic properties measured. Some earlier instruments only recorded phase angle, and consequently the early literature uses the tan *d* as the measure for many properties. This property is also called the damping, and is an indicator of how efficiently the material loses energy to molecular rearrangements and internal friction. It is also the ratio of the loss to the storage modulus and therefore is independent of geometry effects. It is defined as:

$$\tan(\delta) = E''/E' = \varepsilon^{''}/\varepsilon^{'}$$

Because it is independent of geometry, tan(δ) can be used as a check on the possibility of measurement errors in a test. For example, if the sample size is changed and the forces are not adjusted to keep the stresses the same, the *E*' and *E*" will be different but the tan(δ) will be unchanged. A change in modulus with no change in the tan(δ) should

lead one to check the applied stresses to see if they are different. Once we have calculated the basic properties all the other properties are calculated from them [5].

References

[1]. N. McCrum, B. Williams, and G. Read, *Anelastic and Dielectric Effects in Polymeric,* **1991** *Solids, Dover, New York.*

[2]. A. Gloria, F. Causa, R. De Santis, P.A. Netti, L. Ambrosio, *J Mater Sci: Mater Med,* **2007,** 18, 2159.

[3]. K.P. Menard, *Dynamic Mechanical Analysis*, **1999**, CRC Press

[4]. S. N. Nazhat, R. Joseph, M. Wang, R. Smith, K. E. Tanner, W. Bonfield, *Journal Of Materials Science: Materials In Medicine*, **2000**, 11, 621.

[5]. J. F. Mano, C. M. Vaz, S. C. Mendes, R. L. Reis, A. M. Cunha, *Journal Of Materials Science: Materials In Medicine,* **1999**, 10, 857.

APPENDIX 2

Poly(D,L-lactide) oligomers synthesis.

Poly(D,L-lactide) (PDLLA) is a rigid, amorphous biodegradable polyester typically made by ring-opening polymerization of its cyclic diester dimer, lactide [1].

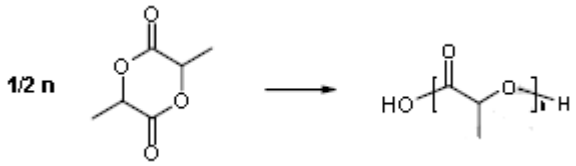

Fig. A.1: Ring-opening polymerization reaction of D,L-Lactide

A large variety of organometallic compounds have been studied as possible catalysts for the synthesis of polylactide. Tin(II)bis-2-ethylhexanoic acid (stannous octoate or SnOct2) is a frequently used because it leads to high yields, high molecular weights and it is FDA (food and drug administration) approved [2].

Fig. A.2: Tin(II)bis-2-ethylhexanoic acid (stannous octoate or SnOct2) is one of the mostly frequently used catalyst in ring-opening polymerization

Often an alcohol is used as a co-initiator and the initiator/co-initiator complex is then the true initiator of the polymerization process . Mono and bi-functional alcohols yield linear polymers, while co-initiators with more than two alcohol groups give star-shaped polymers.

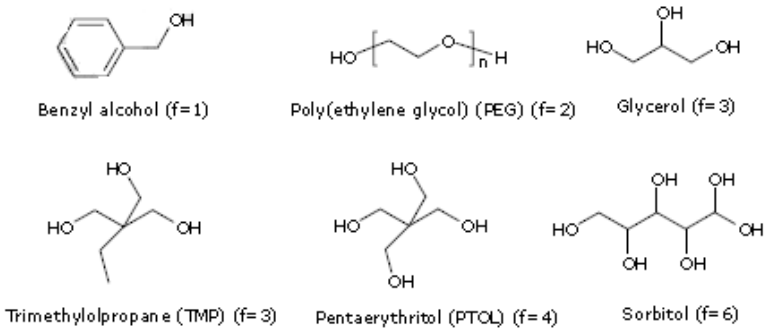

Fig. A.3 : Co-initiators with different functionalities

The ring opening polymerization is thought to follow the coordination-insertion mechanism [2]. The three-step coordination-insertion mechanism for the ROP of cyclic esters was first formulated in 1971 by Dittrich and Schulz [3]. The mechanism for the Sn(Oct)2-catalyzed ROP has been the subject of much more controversy. Recent investigations [4][5] have allowed for the characterization of several intermediate tin complexes and strongly support a coordination-insertion mechanism rather than a cationic or activated-monomer mechanism [6]. Penczek and co-workers suggest that when $SnOct^2$ is mixed with an alcohol an initiating complex is formed prior to polymerization The tin alkoxide complex thus formed then initiates the polymerization (Fig.4).

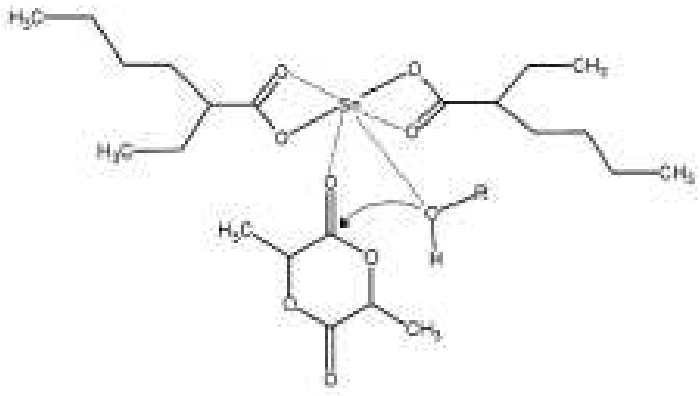

Fig. A.4: Tin Alkoxide Complex Initiated Polymerization of Lactones

The methyl group on the alpha carbon of polylactide causes chirality at this carbon, and thus D, L and DL isomers are possible. Poly-L-lactide (PLLA) is made from L-lactide and poly-D-lactide (PDLA) is made from D-lactide, while poly-D,L-lactide (PDLLA) is made from DL-lactide which is a racemic mixture of the D and L isomers. The meso form has both the D and L configuration on the same dimer molecule (Fig.5).

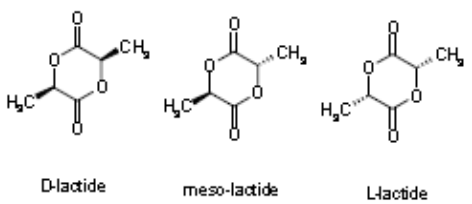

Fig. A.5: The three different configuration of lactide.

PDLLA ia a completely amorphous polymer characterized by a glass transition temperature of approximately 55°C, and an elasticity modulus close to 3 GPa . It is one of the few biodegradable polymers with mechanical properties that approach those of the bone [1]. Because of its lack of crystallinity, PDLLA has a much lower tensile strength and modulus of elasticity than PLLA. The lack of crystallinity also causes PDLLA to degrade faster than PLLA. To make oligomers suitable for photo-initiated crosslinking, they have to be functionalized with crosslinkable entities; most often carbon-carbon double bonds. PDLLA networks can be formed by (photo-initiated) radical polymerization of polylactide oligomers end-functionalised with an unsaturated moiety such as methacrylate [7], acrylate [8] or fumarate [9]. Methacrylate is the end-group that has been most frequently used to functionalize oligomers. Davis et al.[10] have functionalized D,L-lactide and ε-caprolactone based oligomers in this way:

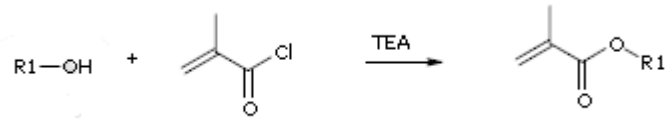

Fig. A.6: the reaction of an hydroxyl group with methacryloyl chloride

The percent methacrylation varied from 70 to 100 %.

References

[1]. S.F. Yang, K.F. Leong, Z. H. Du, C. K. Chua, *Tissue Engineering*, **2001,** 7, 679.

[2]. Odile Dechy-Cabaret, Blanca Martin-Vaca, and Didier Bourissou, *Chem. Rev*. **2004,** 104, 6147

[3]. Dittrich, W.; Schulz, R. C. *Angew. Makromol. Chem.* **1971**, *15*, 109.

[4]. Kricheldorf, H. R. Kreiser-Saunders, I. Stricker, A. *Macromolecules,* **2000**, 33, 702.

[5]. Kowalski, A. Duda, A. Penczek, S. *Macromolecules,* **2000**, 33, 7359.

[6]. Nijenhuis, A. J. Grijpma, D. W. Pennings, A. J. *MacromoleculesI,* **1992**, 25, 6419.

[7]. Storey RF, Warren SC, Allison CJ, Wiggins JS, Puckett AD, *Polymer*, **1993**, 34, 4365.

[8]. Sawhney AS, Pathak CP, Hubbell, *Macromolecules,* **1993,** 26, 2795.

[9]. Grijpma DW, Hou QP, Feijen J, *Biomaterials,* **2005**, 26, 2795.

[10]. Davis, K.A., J.A. Burdick, and K.S. Anseth, *Biomaterials*, **2003**. 24(14), 2485.

Summary

Tissue engineering is set to revolutionize the treatment of patients and contribute significantly to life sciences in the next millennium. It is based on the concept that cells seeded onto 3D bioresorbable scaffolds can recreate native tissues under suitable *in vitro* and *in vivo* conditions. General requirements involve scaffold morphology in terms of pore size and pore inteconnectivity which assure cell growth and the transport flow of nutrients and metabolic waste. Moreover the control of surface also enable a suitable cell attachment and promote cell differentiation and proliferation. Furthermore, the biocompatible degradation of the scaffold material has to proceed appropriately and in sync with the formation of tissue. In this thesis, the implementation and optimization of new interesting techniques for the realization of 3-Dimensional scaffolds was investigated to develop systems able to elicit favourable tissue response. First part of the thesis has been focused on the realization of bioactive composite scaffold obtained with different preparation techniques like salt leaching in combination with phase inversion. The PCL/HA scaffolds fabricated by the PI/SL (phase inversion/salt leaching) method (**Chapter 3**) showed a bimodal porosity, interconnected macropores (100–200 mm) were created by the leaching of the NaCl particles, and smaller, closed pores (10–45 mm) were created by the controlled solvent removal via non-solvent exchange. This method promotes more efficient exposure of HAP at the surface of polymer/bioceramics composite scaffold as confirmed by Sem images. Moreover presence of HAP enhances mechanical properties with an optimal response under compression in the case of 20% of HAP ceramic phase, while morphology and thermal properties seem to be unaffected. Cellular response and biological activity of the scaffold were evaluated *in vitro* by culturing the scaffolds with human sinovium-derived MSCs for 2 weeks. It was found that PCL scaffold obtained with PI/SL techniques supportes the seeding and proliferation of MSCs. In particular the presence of HAP encourages the differentiation process through the osteoblast phenotype. However, requrements of porosity, biocompatibility and biodegradability are often in conflict with the needful of adequate mechanical properties which can match those of the tissues at the site of implantation. Noteworthy, the measured compressive moduli of the prepared scaffolds is rather low compared to that of human bone. This is due to the highly porous structure of the

fabricated scaffolds and the poor mechanical properties of the PCL itself, independently upon the HAP reinforcement.

The definition of composite systems characterized by tailored degradation properties, coupled with a controlled decay of mechanical response, may guarantee the achievement of the long-term success of a tissue engineered construct. Three biodegradable scaffolds based on a PCL and HYAFF11® matrix, with tailored chemical and physical properties, were developed by combining a filament winding technique with a phase inversion/salt leaching method (**Chapter 4**). The combined use of SEM and computer microtomography (mCT), investigation demonstrated the contribution of single composite phases to the basic morphological features. The integration of biodegradable PLA fibers into the polymer matrix guarantees a mechanical response which is ideal for maintaining the spaces required for cellular in-growth and matrix production. Furthermore, the addition of bioactive calcium phosphates particles, generates needle-like HAP crystals which interact with the packed fbers into the PCL matrix. This interaction dramatically improves the mechanical response in compression, up to an order of magnitude. The further presence of an interconnected macroporous structure with pore size able to promote cell seeding and proliferation, combined with suitable mechanical features, concurs to define a composite scaffold to be used as a candidate for bone tissue engineering. A preliminary *in vivo* test on fibres reinforced scaffold in three different configuration, performed from Orthopaedic Institute Rizzoli of Bologna (Italy), confirm the good biocompatibility and the positive bioactive response of substrates to the biological environment. In order to overcome the main limit of the salt leaching technique on precisely controlling pore size, pore geometry, and spatial distribution of pores the use of stereolithography (**Chapter 5**) methods has been explored to accurately prepare tissue engineering scaffolds with a controlled architecture of pores by computer aided modelling. The synthesis of macromers is also the main factor to impact the physical properties of the final network. PDLLA 2- armed macromers of molecular weight of 3.0 kDa have shown to be processable by stereolithography. A *non reactive* diluent (NMP) is used to decrease resin viscosity during the fabrication process, and is extracted from the network afterwards. the choice of photo-initiator depends primarly on the used light source and solubility in the resin. A concentration of photo-initiator as used here (2-4 wt%) ensure high reactivities during

the fabrication process. A dye was shown to be essential for accurate fabrication by stereolithography. In this context, the use of 0.2 wt% of orange dye limits the penetration depth of the light, so thin layers with a controlled thickness can be cured. Porous scaffolds were designed with computer software using the PDLLA-based resin. The modelling by mathematical equations (the Schwartz, the Diamond and the Double Gyroid architecture) assures an excellent reproduction of the design, with pore size and porosities suitable for (bone) tissue engineering. In particular Double Gyroid architecture showed great values of porosity and high permeability due to great pore interconnection. The mechanical properties response in compression shows really good elastic modulus and mechanical strength, even if the scaffold shows a typical brittle behaviour. Moreover it was shown that the open accessible architecture has improved cell seedability in fact hMSCs readily adhere and proliferate on scaffold surface. Besides the aforementioned PDLLA, a PDLLA/nano-hydroxyapatite composite resin has been synthesised and used in stereolithography (**Chapter 6**). The stereolithography resin was a homogeneous dispersion that showed no settling of nano-HAP particles. The fabricated composite structure were shown to have a high hydroxyapatite content at the surface as SEM images reveal and show increasing mechanical properties with the amount of nano-HAP used. In addition preliminary biological evaluation with hMSCs show higher value of ALP activity for the composite scaffolds if compared with the pure PDLLA. In summary, compared with the scaffold produced by the conventional method, the PDLLA/nano-HAP composite scaffold fabricated by stereolithography exhibited superior mechanical properties and good *in vitro* bioactivity. These findings suggest that they may be suitable for bone implants. In the future, further structure will be realized in order to reach the best compromise between mechanical and morphological properties using new mathematical equation.

We can conclude that different scaffolds obtained by stereolithography technique show good and predictable internal architecture with a précis control of pore size, pore geometry, spatial distribution of pores and construction of internal chamber, meanwhile scaffolds obtained with conventional *phase inversion/salt leaching* technique is able to produce highly porous structure with tailored chemical and physical properties. Finally the possibility to use, for the first time, a composite resin of PDLLA and nano-HAP in

stereolithography technique opens great challenge in scaffolds design for bone tissue engineering.